1 vol P

70-01331

NATIONAL AERONAUTICS AND SPACE ADMINISTRATION
Washington, D. C.

NASA Grant NGL 44-012-006

THE EVALUATION OF REFLECTOR ANTENNAS

John H. Davis

Technical Report No. NGL-006-70-1
31 May 1970

Submitted by

Electrical Engineering Research Laboratory
MILLIMETER WAVE SCIENCES
The University of Texas at Austin
Austin, Texas

NATIONAL AERONAUTICS AND SPACE ADMINISTRATION
Washington, D. C.

NASA Grant NGL 44-012-006

THE EVALUATION OF REFLECTOR ANTENNAS

John H. Davis

Technical Report No. NGL-006-70-1
31 May 1970

Submitted by

Electrical Engineering Research Laboratory
MILLIMETER WAVE SCIENCES

The University of Texas at Austin
Austin, Texas

Preface

This report is concerned with both the theory and details associated with the evaluation of large reflector antennas. The work reported herein was motivated by this Laboratory's need to both understand and improve the performance of the 16-foot radio telescope at the Millimeter Wave Observatory, Mt. Locke. Indeed, the heart of this report, the chapters on astigmatism, gain measurements, and the case study of the 16-foot antenna, describe the fundamental properties of the 16-foot antenna, both before and after improvements.

The earlier Technical Report on the evaluation of the 16-foot antenna, TR No. NGL-006-69-1, "Calibration Program for the 16-Foot Antenna," by J. R. Cogdell, was by its own admission preliminary and incomplete. The present report, taken as a sequel, presents the complete picture of the antenna properties. The whole picture is, we feel, very pleasing: the antenna surely ranks with the best in its peer group.

This report is based upon a dissertation submitted to the Graduate School of The University of Texas at Austin in partial fulfillment of Ph. D. degree requirements.

The author wishes to acknowledge the commitment and support of his supervising professor, Dr. J. R. Cogdell. Thanks also are due to Mr. Archie M. Croom for his able technical assistance with the experiments reported herein.

This work is sponsored by the National Aeronautics and Space Administration under NASA Grant NGL 44-012-006.

Abstract

This report concerns the evaluation of large reflector antennas. The major findings include defining the effects of primary reflector asitgmatism and its quantitative measurement through diffraction pattern measurements. A method is also presented which reveals the frequency dependence of antenna efficiency.

Several basic problems are addressed. One is the focusing of reflector antennas and the interpretation of reflector errors from the antenna pattern. The second topic is the investigation of the effects of primary reflector astigmatism. Evidence is presented that several of the largest reflector antennas have astigmatism in their primary reflector. The third topic offers a method with which the antenna efficiency at one frequency can be inferred from the measured antenna efficiency at another frequency. The method given here is much less restrictive than the Ruze method and bounds the effects of measurement errors.

TABLE OF CONTENTS

LIST OF FIGURES

LIST OF TABLES

Chapter I

Introduction

This paper concerns the evaluation of large reflector antennas. The major findings include the effects of primary reflector astigmatism and its quantitative measurement. A method is also presented which provides new insight into the frequency dependence of the antenna efficiency.

The size and precision of reflector antenna systems have greatly increased over the last twenty years. Today, the largest reflector antennas are used in radar, space communications, and radio and radar astronomy. Large, highly precise antennas are required for these applications because the received signals are relatively weak.

When reflector antennas began to appear in the late nineteen-forties, there was no theory available to dictate the required precision of manufacture of such antennas. The criterion which had always been used for optical reflectors was that the reflector[1] must be within $\lambda/8$ of the required shape. However, different criteria are used to judge antennas than are used to judge optical instruments, so a reassessment of the problem was in order.

John Ruze addressed this problem in his doctoral thesis[2]. His theory is now the accepted standard in the field of reflector antenna evaluation and design. Probably the most widely used part of his theory is the frequency dependence of the antenna gain which it predicts.

The Ruze theory is basically a statistical theory and thus is based on certain mathematical assumptions. These assumptions specify the behavior of an antenna by implication. Only recently have antenna engineers come to realize that the Ruze theory is sometimes inadequate to describe all of the performance characteristics of large antennas.

The Millimeter Wave Sciences Laboratory at The University of Texas at Austin operates a 16-foot radio telescope. This instrument is used in observations of radio sources, especially the planets at frequencies up to 140 GHz. It was first located in Austin and worked well at 95 GHz.[3] In the winter of 1966/67 it was installed on Mount Locke near Fort Davis, Texas to take advantage of the better meteorological conditions there. However, soon after it was installed on Mount Locke it was determined that the performance of the antenna fell considerably short of what was expected. At 95 GHz no satisfactory focus position could be found, and the beamwidths were always broad in at least one of the principle planes. In addition, one sidelobe appeared at a level of -7 dB when the antenna was adjusted for maximum gain. This paper comes largely from efforts the laboratory has made to improve the antenna performance.

This dissertation addresses several basic problems. One is the interpretation of the reflector errors from the antenna pattern. The second major topic is the diagnosis of primary reflector astigmatism and its measurement. The third topic concerns the dependence of the

antenna efficiency on frequency and offers new insight into this problem as well as some useful quantitative results.

Chapter II is a tutorial discussion of the aperture field method of reflector analysis. The important underlying ideas of the method are discussed with an emphasis on geometric optics. The Fourier transform relations between the aperture fields and the far zone fields are then presented. This chapter may be skipped without harming the continuity of the presentation.

Chapter III is a critical review of the current literature on antenna tolerance theory. Particular emphasis is given to the Ruze statistical theory, which is widely used by antenna engineers today. In addition, the interpretation of antenna patterns is discussed.

Chapter IV is the presentation of a reflector astigmatism model. Several model properties are presented which relate to the far zone radiation pattern. These properties are useful in determining whether astigmatism is present in a given antenna and also in measuring it quantitatively. Evidence is presented through one of these properties that astigmatism appears in at least two other large reflector antennas.

Chapter V gives a method of inferring antenna efficiency at one frequency from a measured efficiency at another frequency. If the measurement frequency is the higher of the two, the error bars on the inferred efficiency are usually less than the measurement error bars. Thus, a single antenna efficiency measurement usually serves to define the efficiency at all lower frequencies. This method is then extended so

that two antenna efficiency measurements can be used to infer the efficiency at the third frequency. The proofs for these two methods are given in Appendix B.

Chapter VI is a report of the latest work done in the calibration program for The University of Texas 16-foot antenna. It provides a concrete example of the use of the astigmatic phase error model in Chapter III. A careful efficiency measurement at 134 GHz is reported. The efficiency of the antenna at other frequencies of interest is then inferred from a method given in Chapter V.

Chapter II

Analysis of Reflector Antennas

A. Introduction

At microwave frequencies and above, wavelengths become so short that conventional array antennas become impractical. However, short wavelength is a desirable feature for reflector antennas, so reflectors are more widely used at shorter wavelengths. A reflector antenna system, which consists of a small antenna and a reflector, is a simple device that focuses electromagnetic radiation in a particular direction. The purpose of the small antenna, called a feed, is to launch a wave in the direction of the reflector, as shown in Figure 1. The feed usually exhibits a broad radiation pattern. At the reflector the shape and direction of the waves from the feed are transformed. In particular, they are focused so that the radiation of the system is much more concentrated.

The following section states the general philosophy behind the aperture field method of reflector analysis. This is followed by a discussion of geometric optics. In the final section the Fourier transform relations between the far zone fields and the aperture fields are presented.

B. The Aperture Field Method

One might analyze a reflector antenna as a boundary value problem. However, this is a general mathematical method that yields little insight into the actual operation of the antenna. Engineers have traditionally used what is called the "aperture field method"[4] for analyzing reflector antennas.

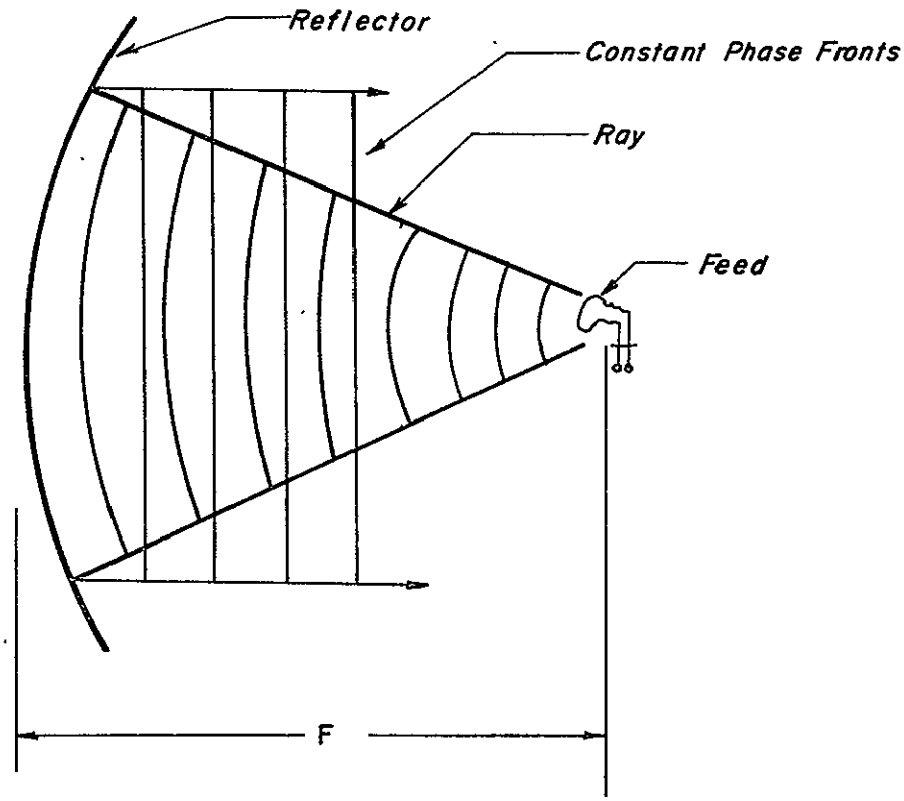

A REFLECTOR ANTENNA

Fig. 1

This approach is no less rigorous than the boundary value problem approach, at least in principle. However, the aperture field method yields a great deal of insight into the operation of a reflector antenna.

The aperture field method may be thought of as a solution to the boundary value problem with an infinite sum of partial solutions. One begins by calculating the fields that would be produced by the feed in free space. However, the feed is not in free space. Its fields propagate to the reflector where they set up currents and secondary fields. These secondary fields in turn affect the feed, so the solution for its fields and currents must be modified. This effect is called feed reaction. The perturbation caused by the feed reaction then affects the reflector currents and fields. This iterative procedure could be continued until sufficient accuracy were attained.

At first glance this procedure might seem more complicated than the general boundary value approach. However one can usually ignore the feed reaction in the case of a prime focus antenna. In addition, the feed reaction is of only minor importance in a Cassegrain fed antenna.

The neglect of the feed reaction can be seen for a prime focus instrument from simple power considerations. Suppose the feed radiates power P_r as shown in Figure 1. The Pointing vector decreases according to the $1/r^2$ law until the wave strikes the reflector. As will be shown later the reflector will columate this power into a plane wave. The power density of the reflected wave on the axis is thus $\frac{D_f}{4\pi F^2} P_r$ where D_f is the directivity of the feed and F is the feed to reflector distance. The fraction of the radiated power absorbed by the feed will be approximately $\left(\frac{A_f}{\lambda F}\right)^2$,

where A_f is the effective area of the feed. For ordinary feed dimensions and distances F this ratio is less than 10^{-4}.

Since the feed reaction is ordinarily so small the analysis of a large reflector antenna is a simple two step procedure. The first step is to analyze the feed as an antenna in feed space. The second step is to calculate the secondary fields from the reflector treating the feed fields as sources. The analysis and design of feeds is an art in itself, and has been discussed extensively[5],[6],[7]. Feeds will be given a minimum of attention in this paper.

There have been two approaches to calculating the secondary fields of the reflector. One method, discussed by Silver[8], calculates the secondary fields from the currents induced in the reflector. In the other method, Silver[9], assumes the waves which are incident from the feed bounce off the reflector according to geometric optics. The far fields may then be calculated using an equivalence theorem. Both of these methods give essentially the same results. The latter viewpoint is the one that will be followed here.

C. Geometric Optics

The geometric optics approach is a simple way of determining the result of a wave striking a reflector. This method takes advantage of the fact that reflectors are typically hundreds of wavelengths across. The wave launched by the feed may be considered a scalar wave of the form[10]

$$\Phi(r) = E(r)\, e^{-j\Psi(r)}. \qquad (1)$$

The function Φ must satisfy the wave equation

$$\nabla^2 \Phi + k^2 \Phi = 0. \tag{2}$$

If one substitutes Equation (1) into Equation (2) he obtains the equation

$$|\nabla \Psi|^2 = k^2 + \frac{\nabla^2 E}{E} . \tag{3}$$

In order to gain some insight into the implications of Equation (3), suppose the y and z derivations are zero. Then Equation (3) may be rewritten

$$\left|\frac{\partial}{\partial(x/\lambda)} \Psi\right|^2 = (2\pi)^2 + \frac{1}{E} \frac{\partial^2}{\partial(x/\lambda)^2} (\Psi). \tag{4}$$

From Equation (4) one can see that for k^2 to dominate the right hand side of Equation (3) the per unit change in amplitude grading must be small on a wavelength scale.

This condition is readily satisfied near the reflector of a large reflector antenna. This obtains because the amplitude is determined by the feed gain function which is a broad slowly changing function. It typically changes by a factor of three from the center to the edge of the reflector, but this is over a distance of several hundred wavelengths.

From this discussion one can see that the k^2 term in Equation (3) dominates in the region near the reflector. In this case the phase change of Ψ comes solely from the distance traveled. Thus the waves behave as plane waves in the vicinity of the reflector. Consequently the waves striking the reflector are reflected with their angle of incidence and reflection equal. One calls this kind of wave propagation geometric or ray optics.

D. The Fourier Transform Relations

Geometric optics applies to the local regions near the reflector, but as the waves travel away from the antenna they must suffer diffraction. Thus, geometric optics applies only in the region near the reflector.

Silver[11] makes use of an equivalence theorem to account for the diffraction phenomena that must occur for any electromagnetic antenna. The theorem requires one to draw a closed surface around the antenna. On this surface one places electric and magnetic charges and currents to account for the sources inside. In this case the sources are the fields produced by the antenna. The uniqueness theorem, then, tells us that the fields calculated from these "equivalent" sources will be the same as those calculated by analyzing the antenna as a boundary value problem.

The surface for the equivalence theorem is traditionally drawn in a particular way. Part of it is a plane perpendicular to the axis of the antenna. This plane is called the "aperture plane." The surface is then closed around the back of the antenna.

The equivalent sources that are placed on the surface are calculated from the fields that can be calculated by geometric optics. A slight problem arises in treating the fields near the edge of the reflector. In this region the amplitude of the fields are changing rapidly and hence do not obey geometric optics. Silver's[12] solution to this problem is to let the geometric optics fields continue on to the edge of the antenna where they end on a line charge in the aperture plane. This convention simplifies the mathematical expressions because it makes the aperture plane electrically charge neutral.[13]

In any case the error caused by edge diffraction is small.

Under Silver's convention there are no charges or currents on the equivalent source surface except for the aperture plane. Thus the part of the surface outside the aperture plane can be ignored. In practice the electric and magnetic equivalent charges and currents are not calculated. This intermediate step is eliminated and the far zone electric field is written directly in terms of the electric field in the aperture.

This relatively simple relationship may be written as[14]

$$\underline{E}_{ff}(\underline{a}_r) = -j\frac{k}{4\pi}\frac{e^{-jkr}}{r}\,\underline{a}_r \times \left[(\underline{a}_z + \underline{a}_r) \times \int_{\underline{x}} \underline{E}(\underline{x})\, e^{jkL(\underline{x})}\, e^{jk\underline{a}_r \cdot \underline{x}}\, d\underline{x}\right] \tag{5}$$

In this equation $\underline{E}_{ff}(\underline{a}_r)$ is the far zone electric field at a field point in the direction of the unit vector, $\underline{a}_r$, k is the wavenumber which is $2\pi/\lambda$, r is the distance to the far field point, $\underline{a}_z$ is the unit normal to the aperture plane, $\underline{E}(\underline{x})$ is the magnitude of the electric field in the aperture plane, and $kL(\underline{x})$ is the phase of the electric field in the aperture. These quantities are shown pictorially in Figure 2. Throughout this paper integrals will be assumed to be infinite over the whole plane, with $E(\underline{x})$ falling to zero for $\underline{x}$ outside the reflector area. This convention has the advantage that the integral in Equation (5) can be thought of as the Fourier inverse transform. In addition, linear polarization in the x_1 direction will always be assumed. This is really no loss in generality since the analysis can be done twice if linear polarization cannot be assumed. Thus Equation (5) becomes

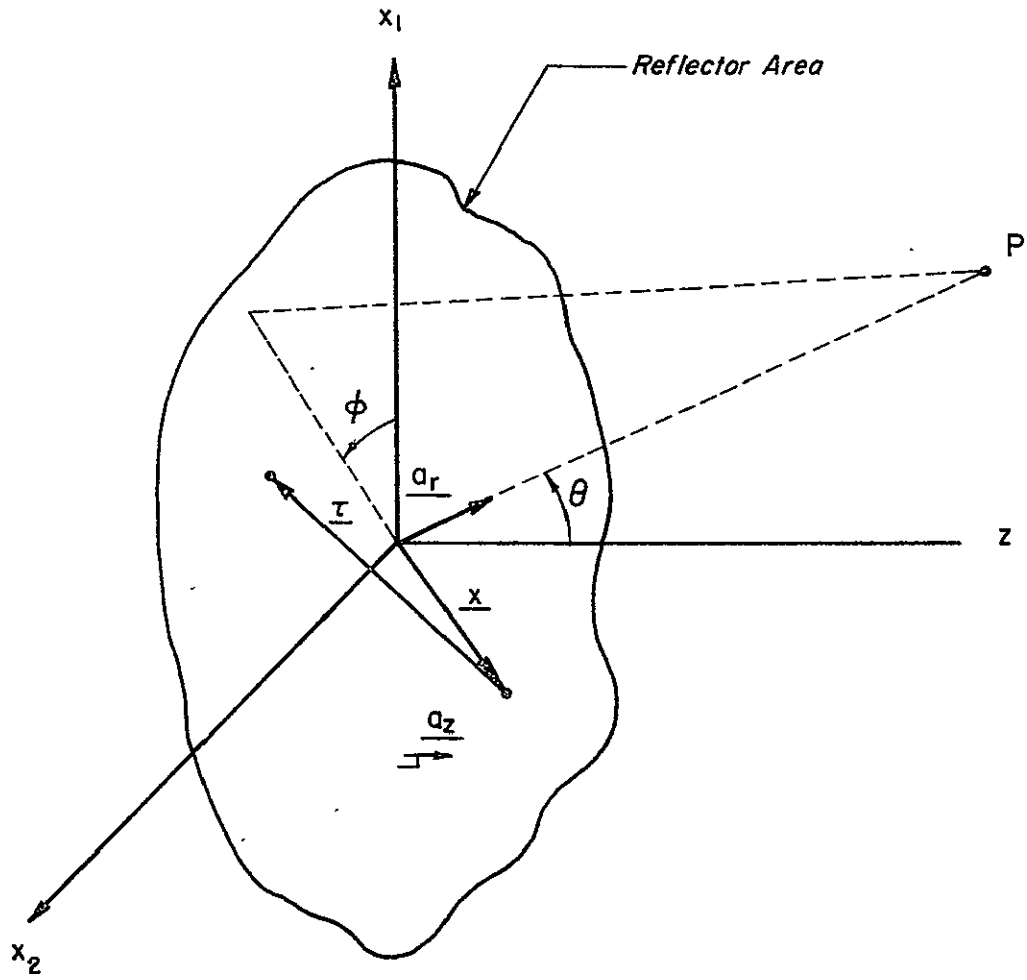

GEOMETRY OF THE APERTURE FIELD METHOD

Fig. 2

$$E_{ff}(\underline{a}_r) = -j\frac{k}{4\pi}\frac{e^{-jkr}}{r}\,\underline{a}_r \times \left[(\underline{a}_z + \underline{a}_r) \times \underline{a}_{x_1}\right] \int_{\underline{x}} E(\underline{x})\, e^{jkL(\underline{x})}\, e^{jk\underline{a}_r \cdot \underline{x}}\, d\underline{x}. \tag{6}$$

For large antennas Equation (6) can be simplified since the vector expression is very nearly $-2\underline{a}_{x_1}$ near the axis. Thus, the far electric field has the same polarization as the aperture fields near the axis. The vector dot product in Equation (6) can be expanded into a scalar dot product. Let us define the angular components in the x_1 and x_2 direction to be u_1 and u_2 with

$$\sin u_1 = \cos\varphi \sin\theta$$

$$\sin u_2 = \sin\varphi \sin\theta.$$

Now the dot product becomes

$$\underline{a}_r \cdot \underline{x} = \sin u_1 x_1 + \sin u_2 x_2.$$

The angles θ and φ are shown in Figure 2. The angular components u_1 and u_2 are almost always so small that sin (u) can be replaced by its argument.

With these simplifications the gain can be written as

$$G(\underline{u}) = \frac{\eta k^2}{4\pi z_o P_{in}} \left| \int_{\underline{x}} E(\underline{x})\, e^{jkL(\underline{x})}\, e^{jk\underline{u} \cdot \underline{x}}\, d\underline{x} \right|^2, \tag{7}$$

where P_{in} is the antenna input power and z_o is the characteristic impedance of free space. This equation states that the far zone gain is the square of the Fourier transform of the aperture electric field. Equation (7) can also be rewritten in the correlation integral form:

$$G(\underline{u}) = \frac{k^2}{4\pi z_o P_{in}} \int_{\underline{\tau}} A(\underline{\tau})\, e^{-jk\underline{u} \cdot \underline{\tau}}\, d\underline{\tau}, \tag{8}$$

where

$$A(\underline{\tau}) = \int_{\underline{x}} E(\underline{x})\, E(\underline{x} + \underline{\tau})\, e^{jk\{L(\underline{x}) - L(\underline{x} + \underline{\tau})\}}\, d\underline{x}. \qquad (9)$$

Equation (8) states that the antenna gain pattern is the Fourier transform of the field autocorrelation integral, given in (9). The vector $\underline{\tau}$ is the correlation distance between two points. Figure 2 shows the vectors $\underline{x}$ and $\underline{\tau}$ in the aperture plane.

Equations (8) and (9) can be rewritten in terms of the gain of the feed. The feed gain is usually better known than the electric field on the aperture. This form is

$$G(\underline{u}) = \frac{k^2}{\pi} \int_{\tau} A(\underline{\tau})\, e^{-jk\underline{u} \cdot \underline{\tau}} \qquad (10)$$

where

$$A(\tau) = \int_{\underline{x}} T(\underline{x})\, T^*(\underline{x} + \underline{\tau})\, e^{jk\{L(\underline{x}) - L(x + \underline{\tau})\}}$$

where

$$T(\underline{x}) = \sqrt{\frac{G_f(\theta', \varphi')}{4\pi\,(f + r^2/4f)^2}}\; e^{jk\ell(\underline{x})},$$

and

$$r = |x|.$$

The angles θ' and φ' are the angles of a ray from the feed to the point $\underline{x}$ in the aperture. The phase function $\ell(\underline{x})$ is the phase error caused by the

feed system, while $L(\underline{x})$ is the phase error caused by the reflector surface.

Equations (7) and (10) are of central importance to this study. It is through these equations that the far field gain patterns will be related to phasing errors. Phase errors are expressed in the function $L(\underline{x})$ since this function represents the phase of the electric field in the aperture plane. A paraboloid reflector has the property that it transforms a spherical wave from its focus to a plane wave. Thus, if the reflector is a perfect paraboloid and the phase surface of the feed is spherical, the phase error function, $L(\underline{x})$, will be zero. However, any physical surface must suffer imperfections on some scale. These surface imperfections are the chief limitation on the performance of a reflector antenna. Various models for phase errors caused by surface imperfections will be presented in subsequent chapters. The implications of these models for the important antenna parameters such as gain, main beam efficiency, sidelobe level, and beamwidth will also be discussed.

Chapter III

A Critical Review of the Literature

There are many articles in the literature related to the limitations of reflector antennas. This literature survey will include (A) a discussion of general antenna tolerance concepts, (B) a review of two papers dealing with specific phase errors, (C) a discussion and critique of the classical statistical tolerance model, and (D) a discussion of phase errors seen in practice. Section(E) shows a useful decomposition of errors.

A. General Reflector Tolerance Theory

Bracewell[15] showed that the aperture efficiency of a perfect reflector is unity when the power from the feed is uniformly distributed over the aperture plane. In addition, he showed that any other distribution of energy produces an efficiency less than unity. Thus, the best feed pattern is one which illuminates the reflector uniformly and falls abruptly to zero outside the reflector area. In practice, of course, it is impossible to achieve such a pattern. Some of the feed power will inevitably miss the edge of the reflector. This power is called spillover. Thus, the feed designer must strike a compromise between illuminating the reflector uniformly and having too much spillover power. Ludwig[16] had defined spillover and tapering efficiencies that separate these two effects for comparison. In some receiving applications[17] the spillover is very important because it contributes to the total noise figure as well as decreasing the efficiency of the antennas.

The efficiency of a uniform phase aperture with the spillover, tapering, and blockage losses considered will be called the design efficiency in this paper. It is so called because it is fixed by the design of the feed system. The efficiency of an actual antenna system will fall short of the design efficiency because the reflector will not produce a true uniform phase front. The amount that the true efficiency falls below the design efficiency is called tolerance loss and may be expressed as a percentage loss or in decibels.

B. The Effect of Specific Phase Errors

A few authors have calculated antenna radiation patterns for specific phase error forms. However, most of the discussed phase error forms are too restricted to be used in practice.

Dragone and Hogg[18] have calculated antenna patterns for antennas with phase errors of the form;

$$L(\underline{x}) = \frac{\lambda}{2\pi} \sum_{m=0}^{M} a_m \cos(2\pi\, mr) \qquad (11)$$

where

$$r = |x|.$$

This is a circularly symmetric phase error. Of course, any circularly symmetric function $L(\underline{x})$ may be expanded in such a series since it is a Fourier decomposition.

They worked two examples which had only a single Fourier component. In both of these examples the sidelobe level was enhanced in

a single angular direction. The enhancement was also further from the main beam for larger m.

Silver[19] has investigated circularly symmetric quadratic phase errors where

$$L(\underline{x}) = \beta \frac{2\lambda}{\pi} \left(\frac{r}{D}\right)^2 .$$

The constant β is the phase error at the edge of the aperture in radians. This work was based on an asymptotic expansion derived by Spencer[20] which was later corrected by Fagot[21]. Silver showed that this kind of error causes the antenna beam to be broadened and raises the level of the near sidelobes. In Chapter III the quadratic type phase error will be considered in a much more general context. In particular it will be shown that moving the antenna feed will introduce an error much like the error given in the equation above. Thus, if an error like this were actually present in an antenna it could be substantially cancelled by merely moving the feed.

C. The Classical Statistical Model

Many of the papers on antenna tolerance theory are based on a statistical model for the phasing errors in antennas. This model was first proposed by John Ruze in his doctoral dissertation. Ruze's model requires that one postulate a large number or ensemble of antennas. Each of these antennas is assumed to be identical except for "random" errors made in manufacturing the reflector. These manufacturing errors lead to a different phase error function $L(\underline{x})$ for each antenna of the ensemble.

Thus, $L(\underline{x})$ is a two dimensional random process. In addition, Ruze assumed $L(\underline{x})$ was wide sense stationary and Gaussian with a correlation function given by

$$R_L(\underline{\tau}) = (2\epsilon)^2 \, e^{-|\underline{\tau}|^2/c^2}.$$

The parameter ϵ is interpreted to be the rms deviation of the reflector surface from a true paraboloid while c expresses the distance over which the phase errors are correlated.

Since the function $L(\underline{x})$ is a random process in this model the gain pattern, $G(\underline{u})$ is a random process. This conclusion follows from the fact that integrals of random processes, if they exist, are random variables.

The fact that $G(\underline{u})$ is a random process poses a problem since the results of the theory must be applied to a single antenna. The solution adopted by Ruze[22], Bao[23], Shifrin[24], and others is to calculate the ensemble average radiation pattern. This is accomplished by taking the statistical expectation of the gain function. In this case one is averaging $G(\underline{u})$ over all the antennas in the ensemble for each value of $\underline{u}$. The average radiation pattern may be written from Equation (10) as

$$E\,G(\underline{u}) = \frac{k^2}{\pi} \int_{\underline{\tau}} \int_{\underline{x}} E\left\{ e^{jk[L(\underline{x}) - L(\underline{x}+\underline{\tau})]} \right\} T(\underline{x})\, T(\underline{x}+\underline{\tau})\; e^{-jk\underline{u}\cdot\underline{\tau}}\, d\underline{\tau}, \tag{12}$$

where E stands for statistical expection.

In Equation (12) the expectation has been brought inside the integral. This is permissible since the integral of $T(\underline{x})$ is bounded. Taking advantage of the stationarity of $L(\underline{x})$ one can rewrite Equation (10) as

$$E\, G(\underline{u}) = \frac{k^2}{\pi} \int_{\underline{\tau}} f(\underline{\tau})\, A(\underline{\tau})\, e^{jk\underline{u} \cdot \underline{\tau}}\, d\underline{\tau} \tag{13a}$$

where

$$f(\underline{\tau}) = E\, e^{jk[L(\underline{u}) - L(\underline{\tau})]}, \tag{13b}$$

and

$$A(\underline{\tau}) = \int_{\underline{x}} T(\underline{x})\, T(\underline{x} + \underline{\tau})\, d\underline{x}. \tag{13c}$$

The function $A(\underline{\tau})$ is the autocorrelation of the aperture field and is independent of any phasing errors.

Another consequence of the stationarity of $L(\underline{x})$ is that $L(\underline{x})$ may be assumed to have zero mean. If it does not have zero mean then another random process say $L'(\underline{x})$ may be defined as

$$L'(\underline{x}) = L(\underline{x}) - m,$$

where

$$m = E\, L(\underline{x}).$$

Consequently one can easily see

$$e^{jk[L(o) - L(\tau)]} = e^{jk[L'(o) - L'(\tau)]}$$

The function $f(\underline{\tau})$ in Equation (13b) is a characteristic function.

A characteristic function of a random vector $\underline{y}$ is in general

$$f(\underline{w}) = E\, e^{j\underline{w}^t \underline{y}}.$$

If one lets the y-vector be $[L(o), L(\tau)]$ then the expression given by Equation (13b) is $f(k, -k)$. Since L is by assumption a Gaussian random process with zero mean its characteristic function is given as

$$f(\underline{w}) = e^{-1/2\underline{w}^t \underline{B}\underline{w}},$$

where $\underline{B}$ is a matrix given by $b_{ij} = Ey_i y_j$. Thus

$$\underline{B} = (2\epsilon)^2 \begin{bmatrix} 1 & e^{-|\underline{\tau}|^2/c^2} \\ e^{-|\underline{\tau}|^2/c} & 1 \end{bmatrix}.$$

This is actually the definition of a Gaussian random process given in many texts[25]. Thus, by simple manipulation one has

$$E\, e^{jk[L(\underline{o}) - L(\underline{\tau})]} = e^{-k^2[R(\underline{o}) - R(\underline{\tau})]}. \tag{14}$$

Substituting the form of $R(\underline{\tau})$ into Equation (14), Equation (13) becomes

$$E\, G(\underline{u}) = \frac{k^2}{\pi} \int_{\underline{\tau}} e^{-\left(\frac{4\pi\,\epsilon}{\lambda}\right)^2 \left[1 - e^{-|\underline{\tau}|^2/c^2}\right]} A(\underline{\tau})\, e^{-jk(\underline{u} \cdot \underline{\tau})}\, d\underline{\tau}. \tag{15}$$

Equation (15) is of fundamental importance since it is a completely general expression for the average gain pattern under the Ruze statistical

model. Most authors who have dealt with this statistical model have derived their results under some condition which restricts the parameters ϵ and c or the angular variable $\underline{u}$.

1. Small Correlation Regions

Ruze in his original work on the subject restricted himself to the case where $c \ll D$, where D is the diameter of the antenna. Ruze's result[26] may be stated as

$$E\, G(\underline{u}) = G_o(\underline{u})\, e^{-(\sigma)^2} + \left(\frac{2\pi c'}{\lambda}\right) e^{-(\sigma)^2} \sum_{n=1}^{\infty} \frac{(\sigma^2)^{2n}}{n \cdot n!}\, e^{-\frac{(\pi c \mu)^2}{n \lambda^2}} \qquad (16)$$

where;

μ = $\sin \theta$

G_o = phase error free gain

σ = $\frac{4\pi \epsilon}{\lambda}$.

The first term in Equation (15) has the same angular dependence as the phase error free or design pattern G_o. The second term is broader in angular extent. Its beamwidth is determined by the correlation distance, c.

Equation (16) is interpreted to mean that energy is taken out of the main beam of the antenna and scattered into the sidelobe regions. Figure 3 is a normalized radiation pattern graph for $c = 0.05D$ with $(4\pi \epsilon/\lambda)^2$ as a plotting parameter. Figure 3 is borrowed from Ruze.[26] As one can see from this figure, the first term in Equation (16) dominates on the axis

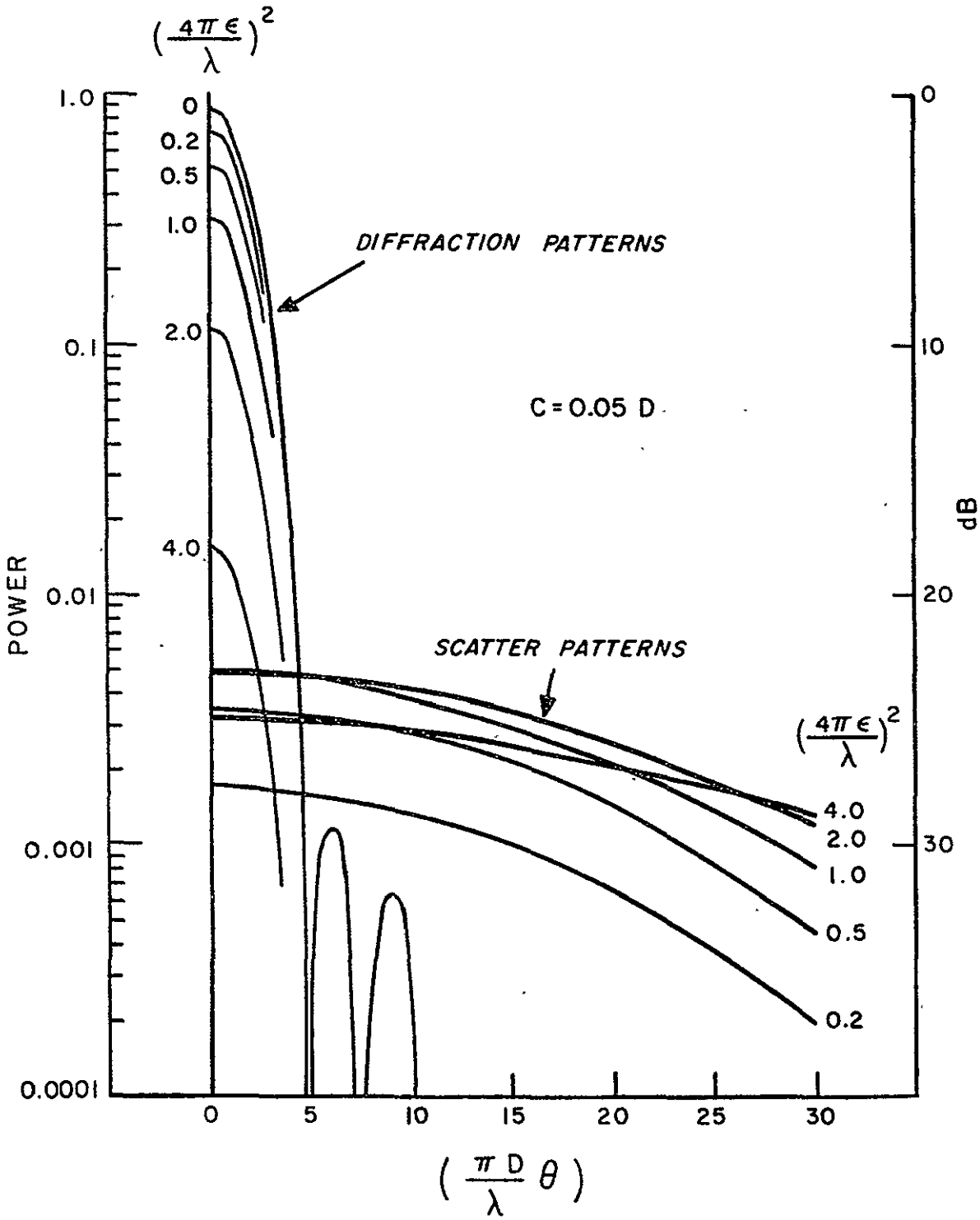
$\left(\frac{4\pi\epsilon}{\lambda}\right)^2$
1.0
0.1
0.01
0.001
0.0001
POWER
0
0.2
0.5
1.0
2.0
4.0
DIFFRACTION PATTERNS
C = 0.05 D
SCATTER PATTERNS
$\left(\frac{4\pi\epsilon}{\lambda}\right)^2$
4.0
2.0
1.0
0.5
0.2
0
10
20
30
dB
0
5
10
15
20
25
30
$\left(\frac{\pi D}{\lambda}\theta\right)$

Fig. 3

for $\epsilon << \lambda$. Thus for axial gain considerations Equation (14) is often shortened to the form

$$E \frac{G(o)}{G_o(o)} = e^{-\left(\frac{4\pi \epsilon}{\lambda}\right)^2}. \qquad (17)$$

Equation (17) is often used to extrapolate the measured peak gain of particular antennas, to different wavelengths[27],[28]. For this purpose Equation (17) is usually written in decibel form with the expectation being ignored, i.e.

$$N_t = 680 \, (\epsilon/\lambda)^2, \qquad (17a)$$

where N_t is the tolerance loss in decibels. If N_t is plotted against $(1/\lambda)^2$, a straight line should be formed if the tolerance loss follows Equation (17a). This graph has been called a Ruze diagram[29]. The usual procedure is to plot several measured values of the tolerance loss on the Ruze diagram and fit a line to the data. Then the tolerance loss is estimated by the line.

The procedure outlined above suffers from three shortcomings. First, it is a misapplication of Equation (17a). Since Equation (17a) applies to an ensemble average of antennas, the axial gain of a particular antenna cannot be expected to follow the law that Equation (17a) predicts, because the experimental outcomes of a statistical sampling scatter about the ensemble average. Secondly, Equation (17a) was derived under the assumption of a small correlation distance. As discussed in Chapter IV and pointed out by Ruze[30], errors often have large correlation distances in a practical case.

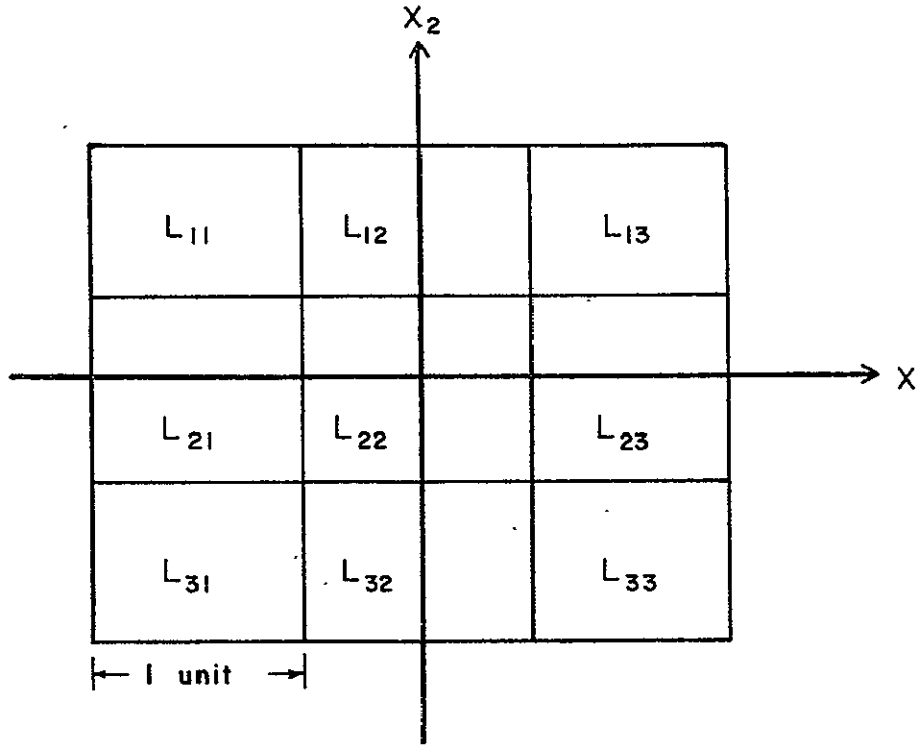

E (X) = 1 in all nine regions .

TOP VIEW OF ANTENNA

Fig. 4

The third shortcoming relates to the mathematical interpretation of the Ruze model. The experimentally measured "gain" of an antenna is always the peak gain. Thus the measured peak gain should be compared with the ensemble average of the peak gain. The average of the peak gain is greater than the peak of the average gain function given in Equation (16). This happens because the peak gain may appear off the axis for some of the sample functions of $G(\underline{u})$. The ensemble average peak gain should be written

$$\frac{k^2}{\pi} E \sup_{\underline{u}} \left\{ \int_{\underline{\tau}} \int_{\underline{x}} T(\underline{x})\, T(\underline{x}+\underline{\tau})\, e^{jk[L(\underline{x}) - L(\underline{x}+\underline{\tau})]}\, e^{-jk\underline{u}\cdot\underline{\tau}}\, d\underline{x}\, d\underline{\tau} \right\} .$$

This effect will come into play most strongly for large c. This occurs because long correlation distance errors are most likely to change the pointing of the beam.

In order to illustrate these three points an example has been constructed. The antenna for this example is a square with N^2 independent regions as shown in Figure 4. Each region in this example may be thought of as an individual reflector panel as discussed by Bao.[31] The phase in each region is given by a Gaussian random variable, L_{ij}, from a random number generator. The formula for the tolerance loss of the peak gain as a function of frequency is

$$\eta_t(f) = \sup_{x,y} \left| \frac{\sin x \sin y}{9\, x\, y} \sum_{m=1}^{N} \sum_{n=1}^{N} e^{j\frac{4\pi}{c} f L_{ij}}\, e^{j2xm}\, e^{j2yn} \right|^2 .$$

The variance of L_{ij} is chosen equal to $c/4\pi$. Thus, the antenna gain maximum (4.3 dB loss) should occur when f = 1 according to the Ruze formulation.

Figure 5 shows six experimental outcomes or sample functions on a Ruze diagram. The antenna for this example has nine independent regions. It is felt that nine is a realistic number of regions for a practical antenna. As one can see the tolerance loss does not follow any definite rule for large losses. In particular the losses deviate significantly from the line predicted by Equation (17a) in the large loss region. This is caused partly by leaving out the scattering term of Equation (16). However, it is clear that the individual sample antennas not only fail to behave as Equation (17a) predicts but fail to follow any definite law.

Figures 6 and 7 are corresponding figures for antennas with 36 and 100 independent regions respectively. It is clear that Equation (17a) gives better results as the number of independent regions on the aperture is increased, i.e. c decreased. In this case the gain integral, Equation (7), is actually an average of a large number of independent random variables. Thus, the variance of $\eta_t(f)$ becomes small by the Central Limit Theorem. In this case a particular sample function $\eta_t(f)$ should agree with the ensemble average, $E\ \eta_t(f)$.

It should be noted that small correlation distance phase errors do not guarantee that the antenna will follow the law given by Equation (17a). The assumption of Gaussian phase errors plays an important role. For example, if uniformly distributed phase errors are assumed instead of Gaussian errors, the ensemble average of the tolerance loss will increase faster than Equation (17a) predicts until the scattering term takes effect. Figure 8 shows six sample functions from an antenna with 100 correlation regions and uniformly distributed errors.

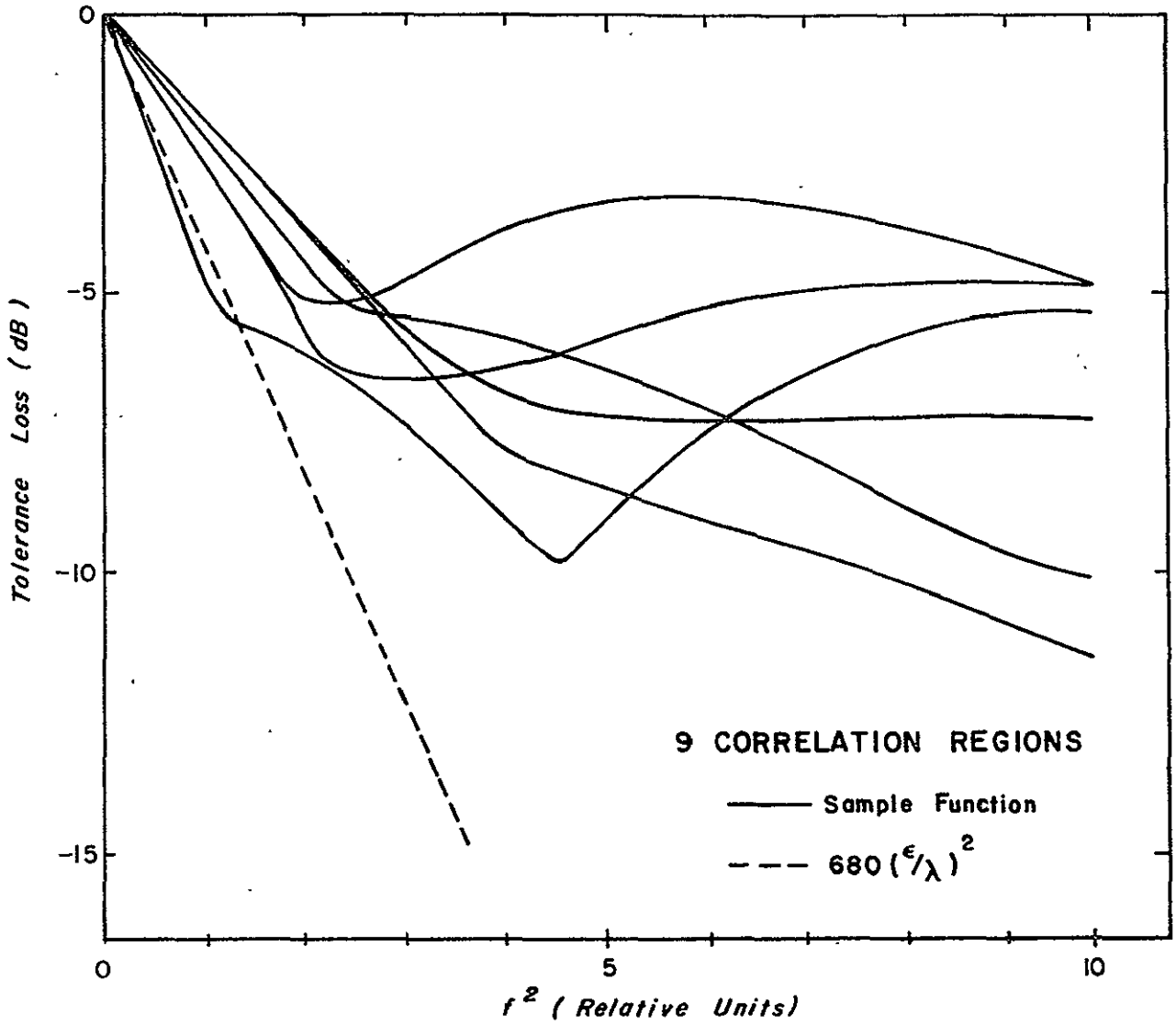
0
-5
-10
-15
Tolerance Loss (dB)
0
5
10
f 2 (Relative Units)
9 CORRELATION REGIONS
Sample Function
680 (ε/λ)2

Fig. 5

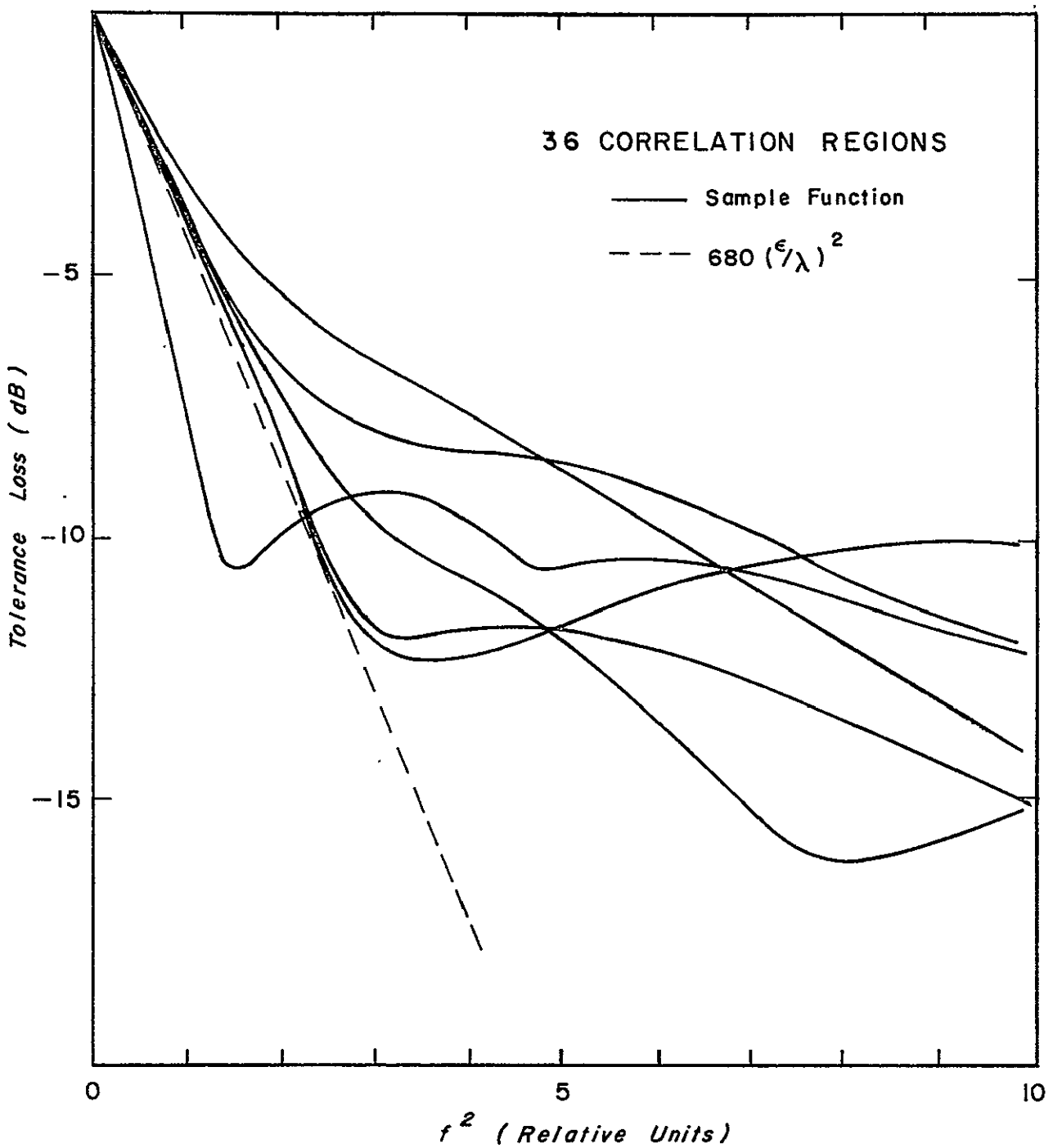
36 CORRELATION REGIONS
Sample Function
680 (ϵ/λ)²
-5
-10
-15
Tolerance Loss (dB)
0
5
10
f² (Relative Units)

Fig. 6

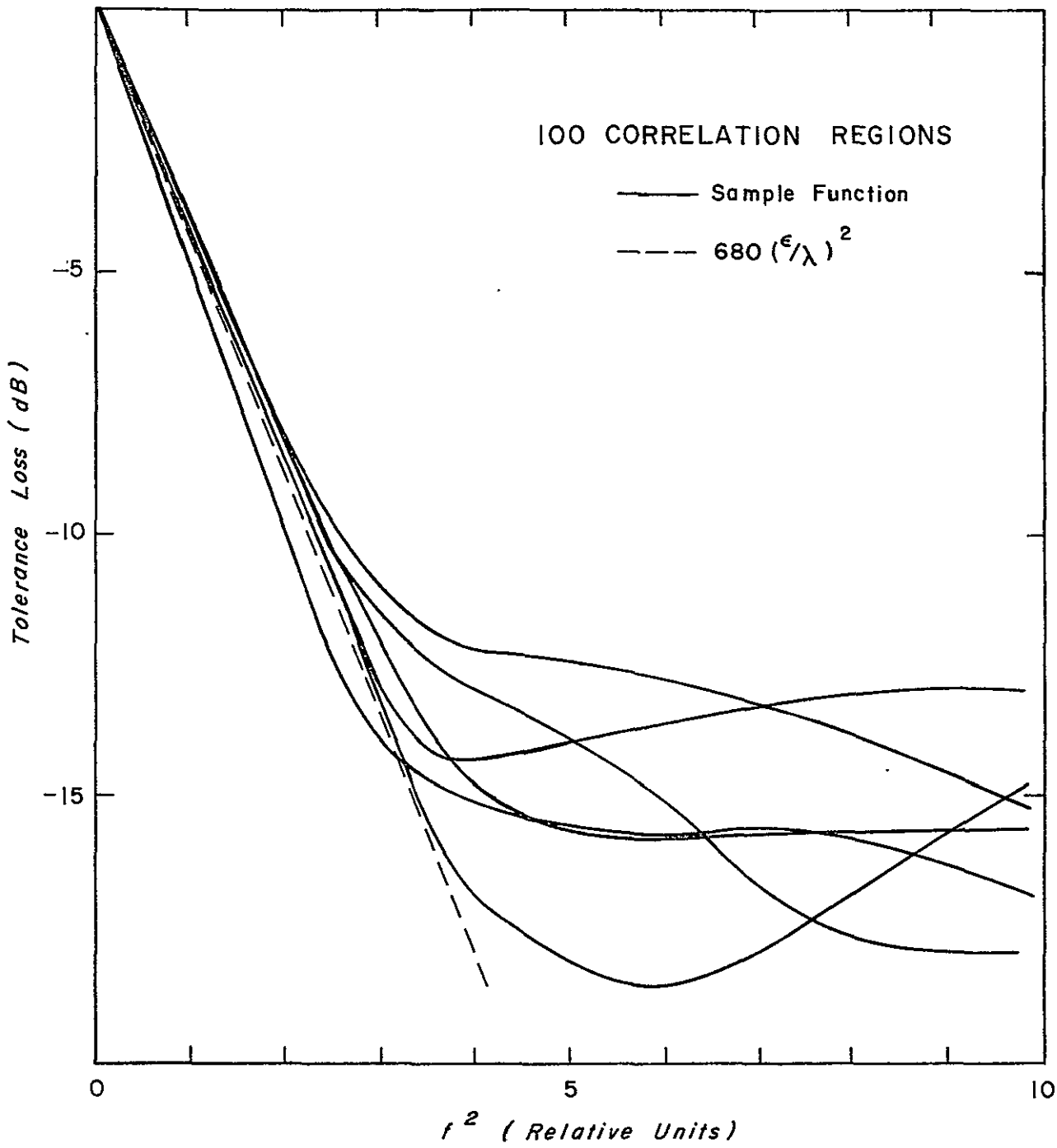
100 CORRELATION REGIONS
Sample Function
680 (ε/λ)²
-5
-10
-15
Tolerance Loss (dB)
0
5
10
f² (Relative Units)

Fig. 7

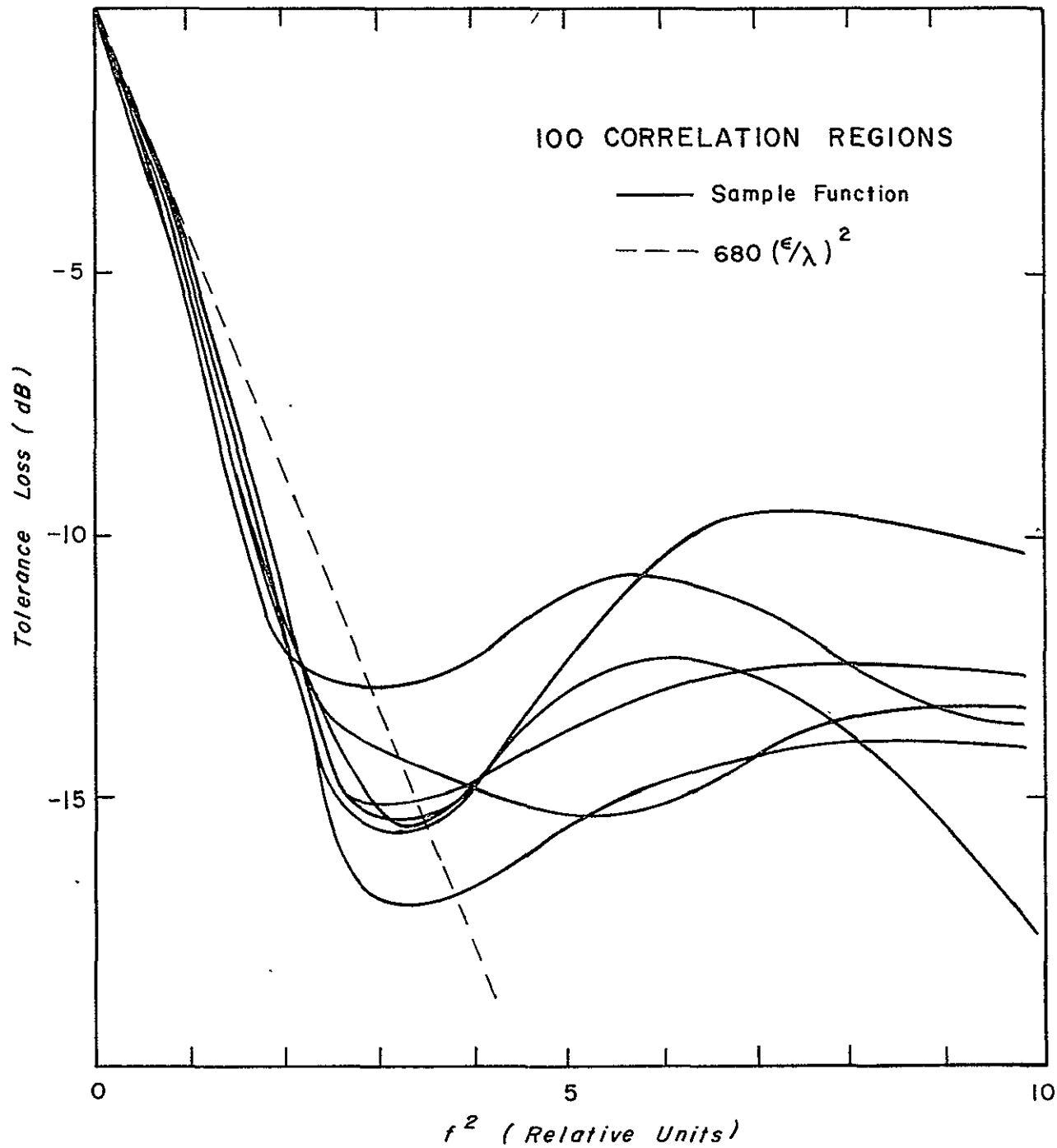
100 CORRELATION REGIONS
Sample Function
680 (ε/λ)²
-5
-10
-15
Tolerance Loss (dB)
0
5
10
f² (Relative Units)

Fig. 8

2. Larger Errors and Correlation Regions

Zucker[32] derived a form for the axial gain similar to Equation (16) where he considered larger correlation radiuses. This result may be stated as

$$E\,G(o) = e^{-\sigma^2} G_o(o) + e^{-\sigma^2} \left(\frac{2\pi c}{\lambda}\right) \sum_{n=1}^{\infty} \frac{\sigma^{2n}}{n!\, n} \left[1 - \Delta_n\right] \quad (18)$$

where all of the symbols have the same meaning as before and $\Delta_n = \frac{2c}{D\sqrt{\pi n}}$.

The parameter c must be such that

$$\left(\frac{D}{c}\right)^2 >> 2$$

In the limiting case when $c \to 0$ this form agrees with the Ruze expression given in Equation (16). This form for the axial gain has not been widely used.

Bao[33] has turned to numerical calculations to see the effects of larger c on the radiation pattern. Some of the patterns which he calculated are shown in Figure 9. For small correlation distances compared to the antenna diameter Bao's results compare favorably with Ruze. For large correlation distance phase errors the sidelobes become very indistinct and merged with the main beam. For c comparable with D the relative power became quite high at the angular position of the first sidelobes in the design pattern. In addition there begins to be considerable beam broadening. This does not happen for short correlation distance errors unless the rms phase errors are so large that the main defraction beam disappears.

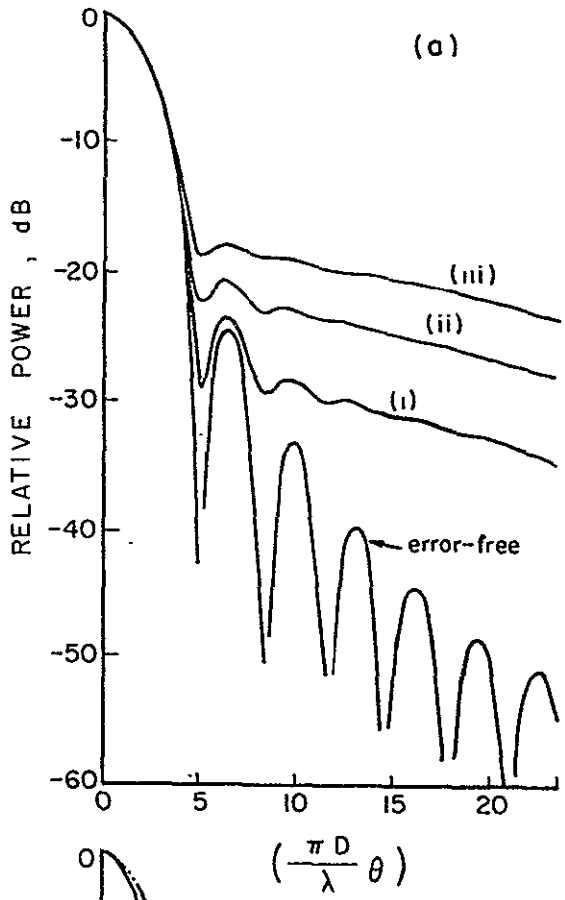

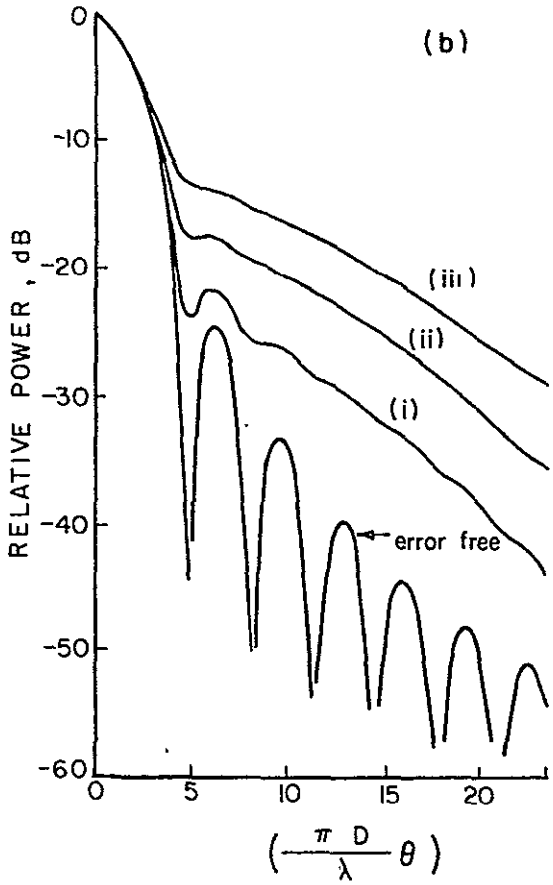

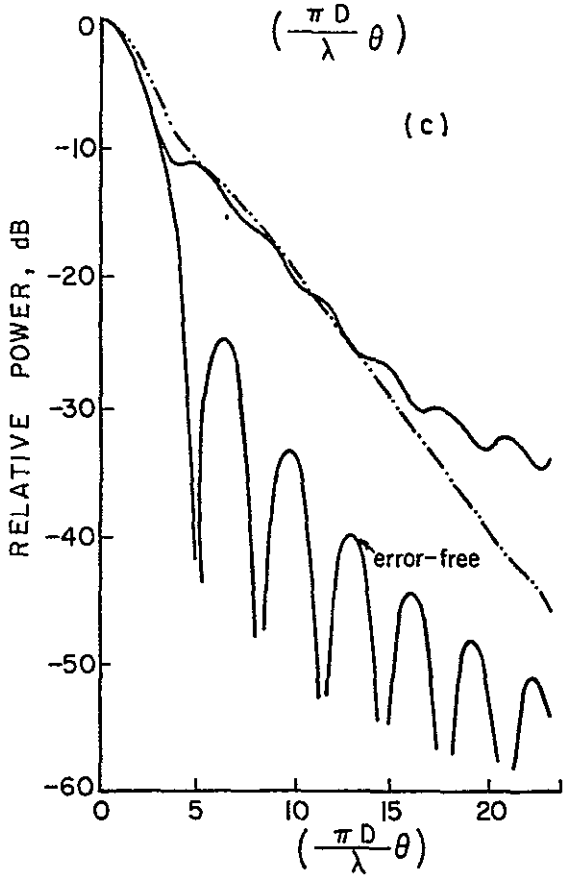

a. C = D/20 (i) $\epsilon = 0.025\lambda$

b C = D/10 { (ii) $\epsilon = 0.050\lambda$
(iii) $\epsilon = 0.075\lambda$

c C = D/5, $\epsilon = 0.075\lambda$

——— uniform

—·— tapered

ϵ is the r.m.s surface error.

C is the correlation interval.

D is the aperture diameter.

AVERAGE RADIATION PATTERNS OF CIRCULAR-APERTURE ANTENNAS WITH $f(r) = (1-r^2)$ AND $D = 360\lambda$.

Fig. 9

Scheffler[34] has given an asymptotic form of Equation (16) for large rms errors. This is

$$G(\theta) = \left(\frac{2\pi c}{\lambda}\right)^2 \frac{[1 - e^{-\sigma^2}]}{\sigma^2} e^{-\left(\frac{c\theta}{4\epsilon}\right)^2}, \qquad (19)$$

where all of the symbols have the same meaning as before. The correlation radius and rms phase error determines the beamwidth here rather than the diameter to wavelength ratio. This simply means that the level of the main defraction pattern has sunk below the level of the scattered energy. For even larger values of σ Equation (19) becomes,[35]

$$G(\theta) = \left(\frac{c}{2\epsilon}\right)^2 e^{-\left(\frac{c\theta}{4\epsilon}\right)^2}. \qquad (20)$$

Now both the peak gain and beamwidth are independent of wavelength and antenna diameter. The ratio ϵ/c has been interpreted as the average slope of the phase error function.

3. General Discussion of the Statistical Model

Many of these results can be seen in an intuitive way by considering Equation (15) as a Fourier transform. Specifically the autocorrelation function $A(\tau)$ and the design gain pattern are a Fourier transform pair. These are shown side by side at the top of Figure 10.

The effect of the Ruze model is to multiply the autocorrelation function by the function $f(\tau)$ where

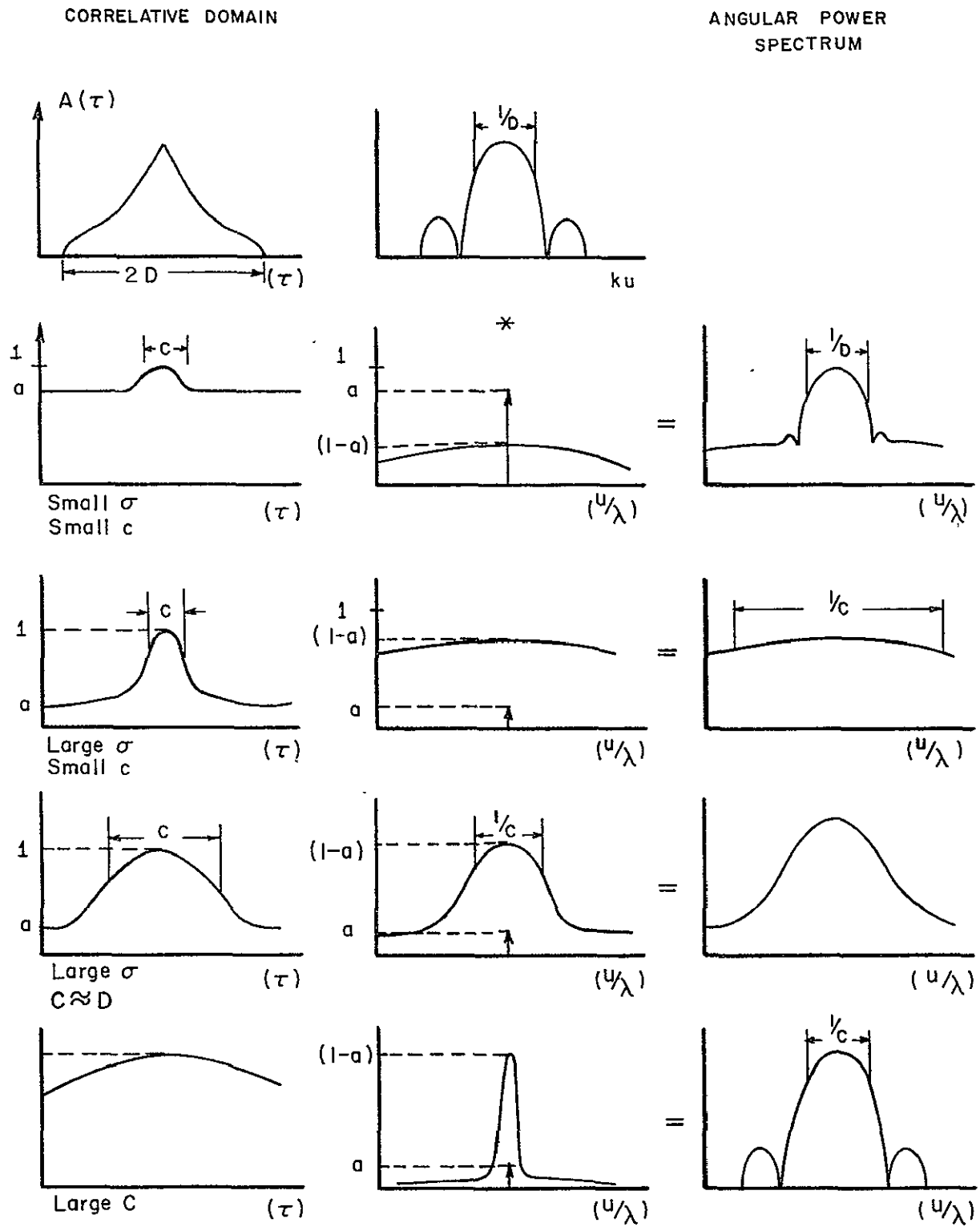

THE EFFECT OF DECORRELATION

Fig. 10

$$f(\underline{\tau}) = e^{-\sigma^2[1 - e^{-|\underline{\tau}|^2/c^2}]}.$$

This function is complicated in form, but it is almost equal to the simpler form

$$f(\underline{\tau}) = a + (1 - a)\, e^{-|\underline{\tau}|^2/c^2}. \tag{21}$$

where

$$a = e^{-\sigma^2}$$

This simpler form has the same first three taylor series terms as well as the same asymptotic value as $|\tau| \to \infty$. Actually the form given implicitly for the decorrelation of $L(\underline{x})$ by Equation (36) is just as valid as the form Ruze assumed. The advantage of this new form is that it may be easily Fourier transformed. Its transform is an impulse of heighth a plus a Gaussian of width $\sqrt{4/\pi}/c$ and height $(1 - a)\frac{\pi}{4} c^2$.

Four examples of the function $f(\underline{\tau})$ with various values of c, and ϵ are given under $A(\underline{\tau})$. Their Fourier transforms are shown to their right under $G_o(\underline{u})$. The product of $A(\underline{\tau})\, f(\underline{\tau})$ is the function actually transformed in Equation (13). However, multiplication in the correlation domain corresponds to convolution in the angular power spectrum domain. For this discussion it is easy to see the results of the convolution.

The first example is the case of small σ and small ϵ. The transform is a relatively high impulse and a broad Gaussian under the impulse. The convolution of the error free pattern with the impulse merely replicates

and reduces the error free pattern. The convolution of the pattern with the broad Gaussian essentially replicates the broad Gaussian since the pattern is nearly an impulse with respect to it. The net result is a pattern like those shown in Figure 3. It has the main diffraction beam essentially unchanged and a broad skirt in the sidelobe region. This is the case considered by Ruze.[36]

In the second example the σ is large but c is still small. In this case the main diffraction beam sinks down below the scattering level and pattern is determined entirely by c and ϵ[37].

In the third example one has large σ and c comparable with D. This is the case considered by Bao. The resulting pattern is like those of Figure 8. Here the Gaussian convolver is comparable in width to the main diffraction beam. Thus, it smears out the patterns and broadens them.

The last example is that of large σ and c larger than D. In this example both the impulse and Gaussian beam are narrow with respect to the pattern so the error free pattern is merely replicated. This case is of only academic interest since a correlation distance much larger than the antenna means that there is no phase error.

D. Phase Errors in Practice

The relationship between the characteristic function, $f(\underline{\tau})$, in the previous section and the resulting average antenna pattern is fundamental. This relationship may be stated from Equation (13) as

$$G(\underline{u}/\lambda) = \frac{k^2}{\pi} F\left[A_o(\underline{\tau})\, f(\underline{\tau})\right] \qquad (22)$$

where F represents the Fourier transform. The fact that $f(\underline{\tau})$ was derived under a statistical model and $G(\underline{u})$ was an average pattern is incidental. The function $f(\underline{\tau})$ may be defined in a completely general way as

$$f(\underline{\tau}) = \frac{\iint_{\underline{x}} T(x)\, T(x+\tau)\, e^{jk[L(x) - L(x+\tau)]}\, dx}{\int_{\underline{x}} T(x)\, T(x+\tau)\, d\underline{x}}$$

The pattern $G(\underline{u})$ is now the observed pattern of the antenna rather than an average pattern. If there were no errors on the reflector then $f(\underline{\tau})$ would be unity. If any decorrelation takes place between points $\underline{\tau}$ apart in the aperture then $f(\underline{\tau})$ falls below unity in magnitude.

Equation (22) may be rewritten as

$$G(\underline{u}/\lambda) = \frac{k^2}{\pi} F[A_o(\tau)] * F[f(\tau)]$$

where * stands for convolution. Since $f(\underline{\tau})$ represents the decorrelation of the fields on the aperture, one can classify the various kinds of decorrelation from this equation and the pattern.

The relationships shown in the previous section are still valid for this discussion if the pattern $G(\underline{u})$ is interpreted as the observed antenna pattern instead of the average pattern. If the decorrelation of the fields takes place over a distance small with respect to the diameter of the antenna, then the far zone pattern will have broad skirts. If the decorrelation takes place over a distance comparable to the diameter of the antenna, the main beam will be broadened and the sidelobe structure generally less distinct.

This latter kind of antenna pattern is the one most often reported in the evaluation of large reflector antennas. J. Schraml[38] reports that the beamwidths of the NRAO 36-foot antenna are about 10% different in the two principle planes. This effect probably comes from a long correlation radius phase error smearing out the pattern in one of the planes.

Cogdell[39] and Bathker[40] report almost identical phenomena in The University of Texas 16-foot antenna and the JPL 85-foot antenna. Both note that in one plane the pattern can be corrected by axially moving the focus. However, the pattern in the other plane is always broad.

Jacobs[41] notes that at least one of the patterns of the Aerospace Corporation 15-foot antenna is always broad. He attributes the effect to the atmospheric scintillations. However, it should be noted that the broadness of the pattern could well arise from phase errors in the reflector.

Bathker[42] gives a mechanically measured error contour map for the JPL 200 foot antenna. This map shows that the reflector is divided into six pie sections with each section having an error of the opposite sign from the two adjacent sections. This is clearly a long correlation distance error.

Thus, many of the phasing errors usually seen in practice have the characteristic in common that they cause decorrelation over distances comparable to the diameter of the antenna. This effect seems to occur

because the dominant error producing effects, such as thermal and gravity loading affect the antenna structure as a whole.

E. A Natural Decomposition of Errors

As discussed above long correlation distance errors scatter energy into the main beam and broaden it. This broadening can be used to separate the effects of long correlation distance errors from the short correlation distance "random" errors.

It might at first seem artificial to classify errors as either of long correlation distance, comparable to antenna size, or of short correlation distance, much smaller than antenna size. One tends to exclude the intermediate case through a consideration of the sources of antenna errors. In the literature the following sources of error are identified: (1) gravity loading, (2) thermal distortion, (3) initial rigging or adjustment bias, caused for example by master template error or error in optical alignment instrument, and (4) manufacturing error or residuals. The first three sources affect the entire antenna structure and hence will produce errors which are correlated over the entire antenna.

The fourth source will produce errors that tend to randomize over a small distance. In the case of a rigged antenna, in which the antenna figure is fixed by many mechanical adjustments, errors would decorrelate in a region controlled by a few adjustment bolts at most. If optical targets are placed on the surface to monitor adjustments, a similar situation would obtain. For a machined surface, errors would be determined by digitizing

residuals and deflections of the surface under the force of the machining tool. In all these instances, the correlation distance will be comparable to the microstructure of the antenna.

The tolerance loss of an antenna is defined as the ratio of the true efficiency to the design efficiency, η/η_o. Let us break the tolerance loss into two factors, i.e.

$$\frac{\eta}{\eta_o} = \eta_s \frac{\eta_\ell}{\eta_o} ,$$

where η_s is the tolerance loss from "random" errors and $\frac{\eta_\ell}{\eta_o}$ is the tolerance loss from long correlation distance errors. The parameter η_ℓ is the efficiency of the antenna if only the long correlation distance phase errors were present.

If the main lobe is modeled by a Gaussian function[43] then one can easily show that the efficiency is inversely proportional to the product of the beamwidths. This proportionality holds because the integral of the pattern must be a constant. The appropriate efficiency for this discussion is η_ℓ since it is assumed that the long correlation distance phase errors cause broadening of the beam, i.e.

$$\eta_\ell \propto \frac{1}{\theta_1 \theta_2} .$$

If there were no phase errors, then η_ℓ should become η_o, so

$$\eta_o \propto \frac{1}{\theta_1^* \theta_2^*} ,$$

where θ_1^* and θ_2^* are the design beamwidths.

The expression for the tolerance loss can now be written

$$\frac{\eta}{\eta_o} = \eta_s \frac{\theta_1^* \theta_2^*}{\theta_1 \theta_2} .$$

The parameter η_s is the loss from random errors, so it should be given by the factor derived by Ruze[44], i.e.

$$\eta_s = e^{-\left(\frac{4\pi\epsilon}{\lambda}\right)^2},$$

where ϵ is now interpreted as the short correlation distance manufacturing error. Thus, one has

$$\frac{\eta}{\eta_o} = e^{-\left(\frac{4\pi\epsilon}{\lambda}\right)^2} \frac{\theta_1^* \theta_2^*}{\theta_1 \theta_2} .$$

Rewriting this expression in decibel form, one obtains

$$N_t + 10 \log_{10}\left(\frac{\theta_1}{\theta_1^*}\right) + \log_{10}\left(\frac{\theta_2}{\theta_2^*}\right) = 680 \left(\frac{\epsilon}{\lambda}\right)^2 , \qquad (23)$$

where N_t is the total tolerance loss in decibels.

If one plots the left hand side of Equation (23) against f^2, then one should sense the losses caused by the short correlation distance manufacturing errors. The graph which has been described is plotted in Figure 11 for The University of Texas 16-foot antenna. The value of ϵ obtained is .07 mm which compares favorably with the value of .06 mm that the manufacturer quoted. This later value was measured relative to a template under ideal conditions when the antenna was being constructed.

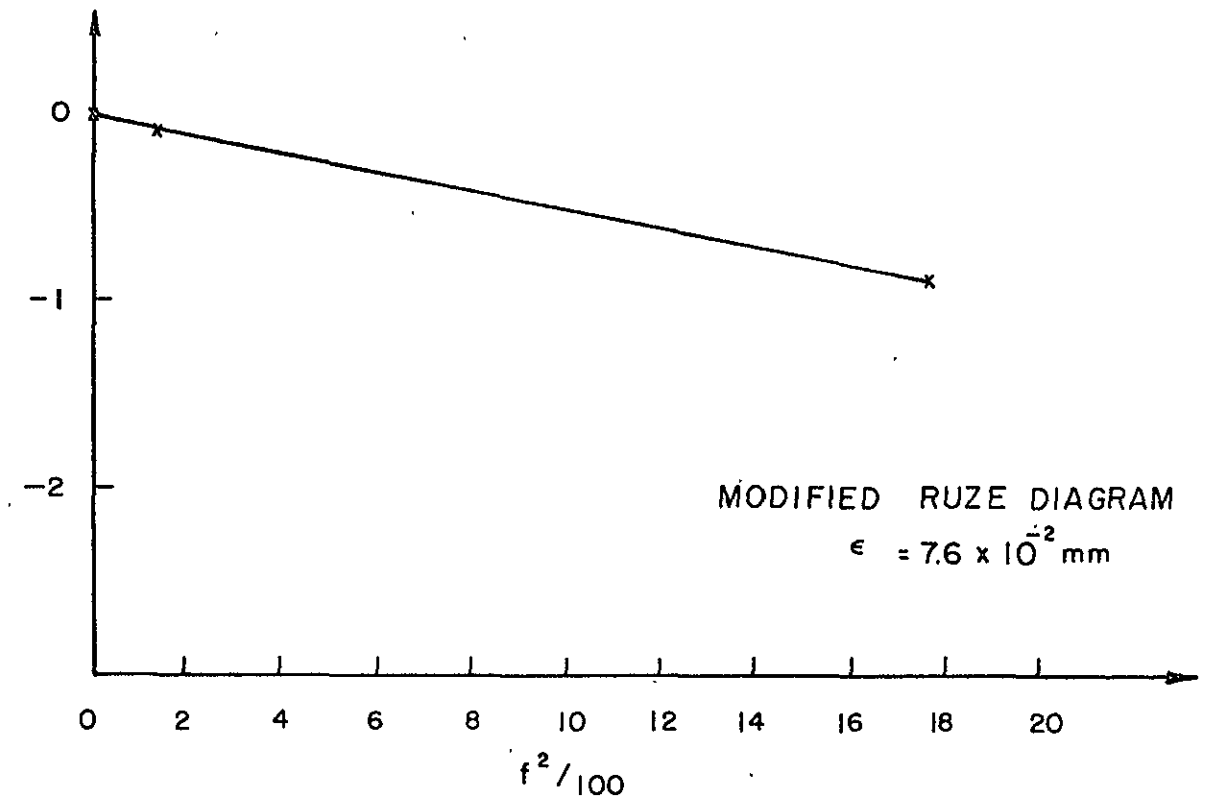
0
-1
-2
MODIFIED RUZE DIAGRAM
$\epsilon = 7.6 \times 10^{-2}$ mm
0
2
4
6
8
10
12
14
16
18
20
$f^2/100$

Fig. 11

Chapter IV

An Astigmatic Phase Error Model

A. Introduction

The dominant phase errors in reflector antennas are often errors which have a large correlation distance. Direct surface measurement by optical or mechanical methods usually reveal only a few correction regions on the reflector[45],[46]. In addition, antennas with significant tolerance loss usually have broad beamwidths and high sidelobe levels.[47],[48] In Chapter III it was pointed out that broad beamwidths and high sidelobes are evidence for large correlation radius errors.

Often the phase errors in a reflector antenna system vary with the antenna pointing[49],[50]. This effect is thought to arise from gravity. The gravity vector loads the antenna backup structure in different ways depending upon the orientation of the antenna structure. One might expect gravity loading to effect the structure as a whole and thus produce slow systematic errors. Such errors have been borne out by a structural analysis done with a digital computer on the Haystack antenna.[51] The calculated error was in the form of a four leaf clover with opposite leaves having the same sign error. The purpose of this chapter is to give a realistic model to this four-leaf-clover-type phase error, which is called astigmatism in optics. Several properties of the antenna pattern of an astigmatic reflector will be shown. In addition special emphasis will be given to determining the model parameters from experimental data. Both pattern range measurements and astronomical measurements will be considered.

Astigmatism is a well known phenomenon in optics. However, different parameters are of interest in antenna theory than in optics. Most antenna systems have only a single detector at the focus, as opposed to a photographic plate which is actually an array of detectors. An object must be observed in such a system by scanning the beam through it. Thus, the parameters of interest for an antenna system are the gain and the beam-width. In the case of an optical telescope one is interested in the extension of a star image caused by the astigmatism.

B. The Model

The model that will be considered is a model for phase errors in the aperture plane. This model may be stated as

$$L_r(\underline{x}) = \sum_{n=0}^{2} \sum_{m=0}^{2} a_{mn} \frac{x_1^n x_2^m}{R_o^{m+n}} . \qquad (24)$$

The symbol L_r means a phase error caused by the reflector. The coefficients a_{mn} are model parameters and have units of length of phase error at the edge of the aperture. This expression may be thought of as a Taylor's series expansion of the actual phase error function. All the terms of less than third order are included.

Only the second order coefficients of Equation (24) are significant to the far zone gain pattern. The coefficient a_{00} does not appear in the expression for the far field radiation pattern while a_{01} and a_{10} represent linear phase gradings. As shown in Chapter II, the far zone electric field

is the Fourier transform of the aperture electric field. Thus, the linear phase grading on the aperture represents translation of the beam in angle space.[52] However, antenna properties such as peak gain, efficiency, main beam efficiency, beamwidths, and sidelobe levels remain the same when the beam is translated. Thus translation of the beam is unimportant and will be ignored.

C. Phase Errors Introduced by Moving the Feed

The position of the feed is one of the fundamental parameters of a reflector antenna system. The feed position affects the phase front that will appear in the aperture plane. Thus, all of the important antenna parameters depend significantly on the feed position.

The absolute position of the feed is seldom accurately known. More often, however, one has available a method of moving and measuring the feed position on an incremental basis. In the following an expression will be derived for the phase error caused by such an incremental displacement of the feed.

Let the feed be moved in a coordinate system (A, B, C) as shown in Figure 12. The origin of this coordinate system is taken to be at the focus, but the final result would be unchanged so long as the origin were anywhere in the region of the focus. The length of a ray from the feed to the aperture plane is approximately

$$L_f(\underline{x}) = \frac{D^2}{16F} - \frac{1}{4f} r^2 + \sqrt{(x_1 - A)^2 + (x_2 - B)^2 + (F + C - \frac{1}{4f} r^2)^2},$$

where

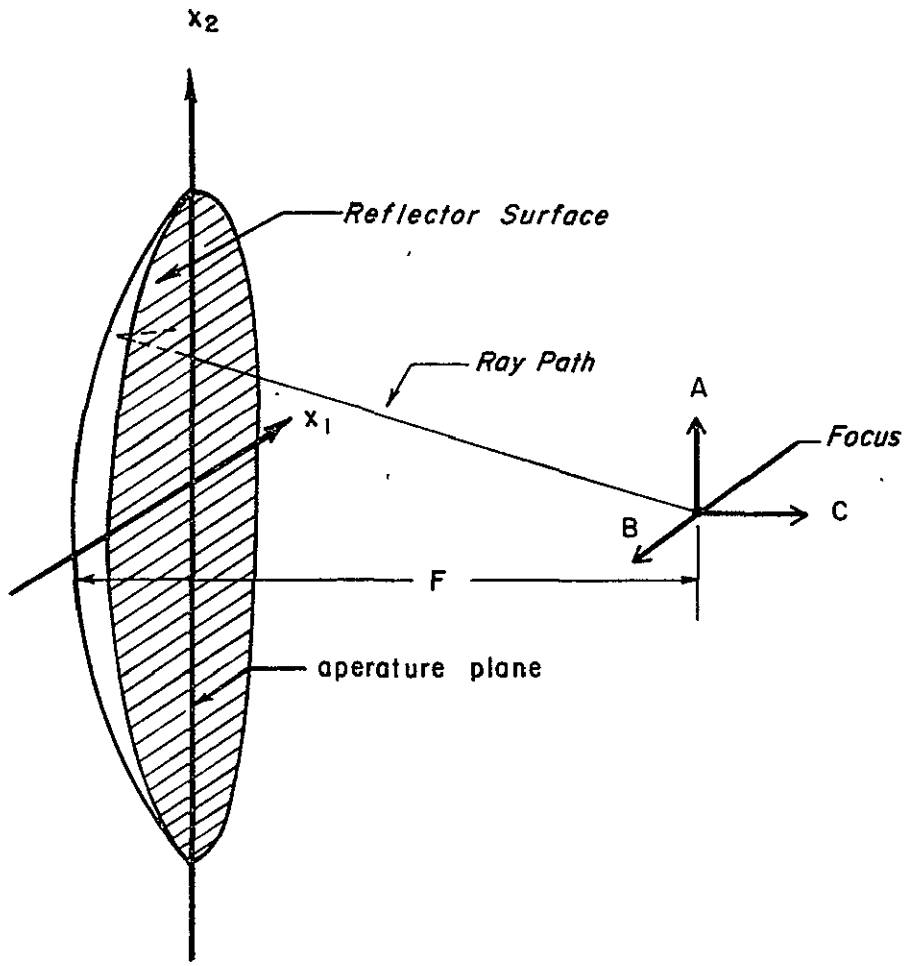

RAY PATH FROM FOCUS TO APERTURE PLANE

Fig. 12

$$r^2 = x_1^2 + x_2^2 .$$

For the discussion of this model lateral focus movement will be ignored, so A and B will be set to zero. However, it must be pointed out that lateral focus corrections should be an important part of any focusing procedure. Lateral focusing will be discussed as it relates to this model in the next section.

Assuming $C \ll F$ and using the binomial expansion of the square root one can show that

$$L_f(\underline{x}) = - c\frac{5}{4}\left(\frac{r}{2F}\right)^2 + c\frac{5}{4}\left(\frac{r}{2F}\right)^4 + \ldots ,$$

where all of the constant terms have been neglected. The quadratic term is by far the dominant term here. For $F/D = 0.5$ the quartic term is only 1/4 of the quadratic term at the edge of the aperture. In the interior of the aperture where the field intensity is greater the quartic term vanishes comparatively. Thus, only the quadratic term will be retained in this discussion. This assumption is consistent with the dropping of the third and higher order terms from the reflector error function.

D. Total Phase Error

The total phase error is the sum of the error caused by moving the focus and the error arising from the reflector. This may be written

$$L(\underline{x}) = L_f(\underline{x}) + L_r(\underline{x}).$$

Substituting the appropriate expressions for L_f and L_r, one has

$$L(\underline{x}) = \left[a_{20} x_1^2 + a_{11} x_1 x_2 + a_{02} x_2^2 + C \frac{5}{64(F/D)^2} (x_1^2 + x_2^2) \right] / R_o^2 .$$

The constants a_{20}, a_{02}, and C are redundant so it will prove convenient to eliminate one of them. Let the new set of constants be α, β, Γ where

$$L(\underline{x}) = \left[\alpha x_1^2 + \beta x_1 x_2 - \alpha x_2^2 + \Gamma K (x_1^2 + x_2^2) \right] / R_o^2 \qquad (25)$$

where

$$\alpha = \frac{a_{20} - a_{02}}{2}$$

$$\Gamma = C + \frac{a_{20} + a_{02}}{2K}$$

$$\beta = a_{11},$$

and $$K = \frac{5}{64} \left(\frac{D}{F} \right)^2 .$$

The constants α and β depend only upon reflector errors while Γ is directly proportional to the focus position. Γ also depends on the reflector errors. However since the reflector errors do not change Γ can be thought of as the focus position variable.

An interesting special case of Equation (25), given by Silver[53], has been discussed in Chapter III. He considered a quadratic reflector error of the form

$$L(\underline{x}) = Cr^2$$

where C is a constant.

Thus in Equation (24) $a_{02} = a_{20}$ and $a_{11} = 0$. The phase error given by Equation (25) can now be made identically zero by moving the feed so that

$L = 0$. Thus, since this kind of phase error can be corrected by simply moving the focus position, the quadratic reflector error given by Silver is degenerate. Of course, it should be kept in mind that moving the feed introduces higher than second order phase terms.

E. Model Properties

As discussed in Chapter III phase errors most often cause decorrelation over distances comparable to the diameter of the antenna. Hence, the astigmatic phase error model which has been discussed has a certain intuitive appeal. In this section several model properties concerning the far zone radiation pattern will be given. Through these properties, one can determine whether this model is a reasonable representation of the phase error function.

In order to state some of these properties in their most general form, the concept of an antenna pattern contour map must be introduced. A contour map is a two dimensional representation of the radiation pattern of an antenna. It has two rectangular coordinates u_1 and u_2 which correspond to angular directions u_1 and u_2. Lines are drawn in these coordinates which describe the locus of a specific pattern level.

For this discussion it will prove convenient to define two symmetry concepts. One is symmetry about a line through the origin at an angle φ. The angle φ is an angle measured counterclockwise from the u_1 coordinate. Symmetry about this line means that the mirror image of a locus on one side of the line appears on the other side of the line. Another concept that

must be defined is symmetry of the map about the origin. This will mean that all of the contour loci are symmetric about the origin and that the gain function is even, i. e.

$$G(\underline{u}) = G(-\underline{u}).$$

These five properties may be thought of as symmetry properties of the far zone pattern. Some symmetries can be seen at any focus position while others require focus movement. The proofs of these properties are given in Appendix A.

The first two properties are symmetries which can be seen at any feed position. The first of these may be stated as follows:

Property 1. If the illumination function $E(\underline{x})$ is symmetric about the origin, i. e. $E(\underline{x}) = E(-\underline{x})$, then any contour map is symmetric about the origin for all feed positions and reflector errors. That is

$$G(\underline{u}) = G(-\underline{u}), \text{ for all } \alpha, \beta, \text{ and } \Gamma.$$

This property also implies that a pattern cut taken in any direction will be symmetric.

The condition $E(\underline{x}) = E(-\underline{x})$ is a very mild one. It is difficult to imagine any feed system for which the illumination function would not be even, since most feed systems are symmetrically constructed.

Figure 13 is an example of a contour map of the pattern of a reflector with astigmatism. This figure illustrates property 1 holds in the finest detail. Figure 13 and several figures that follow in this chapter were calculated in a digital computer with a program that will be discussed in

Appendix A. The illumination function is the illumination of a horn feed of dimensions $1.25\lambda \times 0.9\lambda$ on a paraboloid with an $F/D = 0.5$.

The converse of this simple property is perhaps more useful, since if the contour map is not symmetric the model does not hold. In an actual antenna evaluation, of course, one does not expect property 1 to hold with arbitrary accuracy.

Pattern asymmetries can sometimes be corrected by moving the feed laterally. It is easy to show that the pattern assymmetry is caused by an odd phase error function, that is a phase error such that

$$L(\underline{x}) = -L(-\underline{x}).$$

Moving the feed laterally produces an incremental phase error that also has the odd property. This incremental phase error can sometimes be used to cancel the odd error in the reflector. The focus position can be moved laterally until the level of the first two sidelobes are equal in each of the two principle planes.[54] It is easy to show that the feed should be moved in the direction of the lower sidelobe. For example, if the lower sidelobe is East of the main beam, then the feed should be moved East.

If the patterns are still asymmetric after the sidelobe levels are made equal then there is a large odd phase error. In this case the astigmatic phase error model is clearly inappropriate.

The second property shows that the contour map should be symmetric about two perpendicular lines. Property 2 may be stated as follows:

Property 2. If the illumination function $E(\underline{x})$ is only a function of r, the

the radius from the center of the aperture, then a contour map of the pattern is symmetric about the lines

$$\tan 2\varphi = \frac{-\beta}{2\alpha}$$

for all feed positions.

Property 2 gives a further fact that can be used to determine whether a given reflector has astigmatism. If the property is satisfied then the relationship between α and β is easy to establish. One need only plot a contour map of the antenna and draw the φ direction on it. Then a linear relationship between α and β is established by the equation given above.

Figures 13 and 14 illustrate this property. In the first case the φ directions are aligned with the axes. In Figure 14, however, the φ direction is inclined to the axis by about $-9°$. As one can see property 2 is not rigorously satisfied in Figure 14. This occurs because the illumination function is not quite circularly symmetric. The illumination, however, is chosen to be realistic. It is the illumination produced by the horn feed discussed above.

Property 3 shows that the radiation pattern produced by a phase error of α and β for some Γ is the same radiation pattern that would be produced by $-\alpha$, $-\beta$, and $-\Gamma$. Property 3 may be stated as follows:

Property 3. If the illumination function $E(\underline{x})$ is symmetric about the origin, i.e. $E(\underline{x}) = E(-\underline{x})$, then the gain is an even function of α, β, and Γ taken together. That is

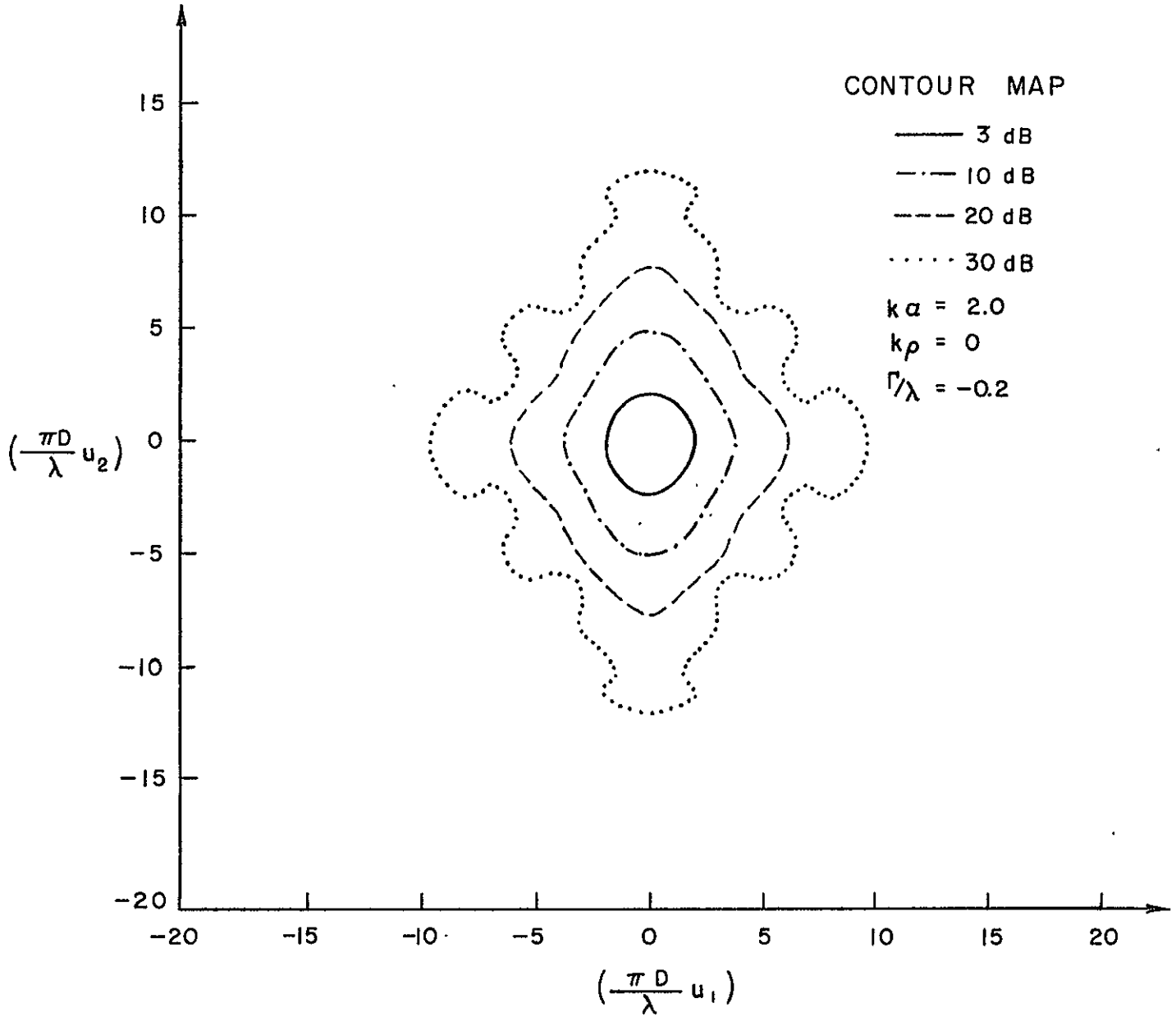
CONTOUR MAP
3 dB
10 dB
20 dB
30 dB
kα = 2.0
kρ = 0
Γ/λ = −0.2
15
10
5
0
−5
−10
−15
−20
(πD/λ u2)
−20
−15
−10
−5
0
5
10
15
20
(πD/λ u1)

Fig. 13

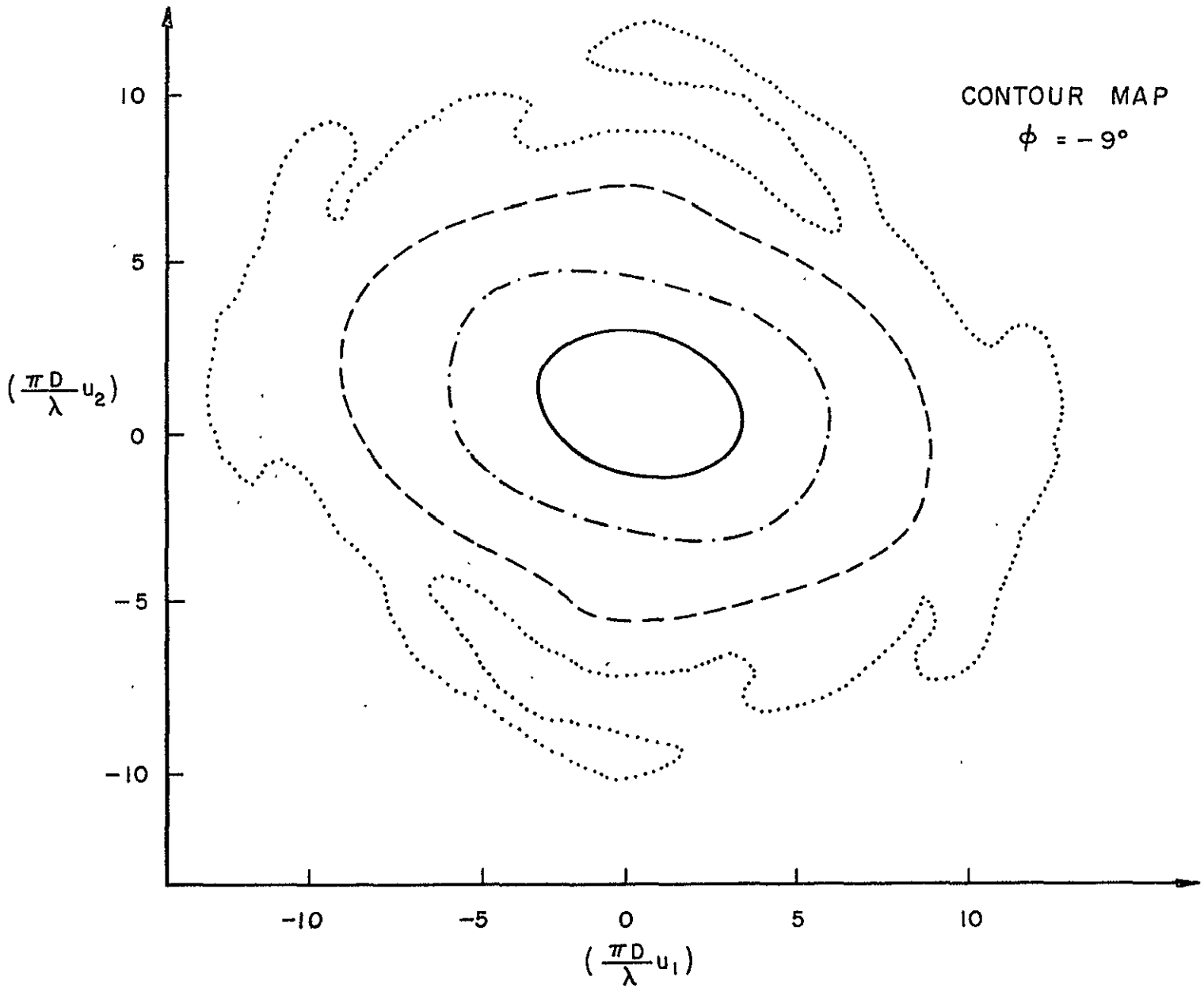
CONTOUR MAP
$\phi = -9°$
10
5
0
−5
−10
$(\frac{\pi D}{\lambda} u_2)$
−10
−5
0
5
10
$(\frac{\pi D}{\lambda} u_1)$

Fig. 14

$$G(u_1, u_2, \alpha, \beta, \Gamma) = G(u_1, u_2, -\alpha, -\beta, -\Gamma).$$

Figures 13 and 15 illustrate this property. These two contour maps are identical while Figure 13 was calculated with the negative of the parameters used in Figure 15.

In a subsequent section a technique will be presented that predicts the model parameters by matching the predicted radiation pattern of this model to the observed pattern. Property 3 makes the results of any such technique ambiguous. Specifically, it is impossible by this method alone to determine whether a certain reflector error α and β or its negative $-\alpha$ and $-\beta$ is present in the reflector.

Property 4 states that changing the sign of the reflector errors α and β exchanges the role of the patterns taken in the φ direction. The u_1 pattern becomes the u_2 pattern and the u_2 pattern becomes the u_1 pattern. Property 4 may be stated as follows:

Property 4. If the illumination function $E(\underline{x})$ is only a function of r, then the angular coordinates which are aligned with the φ direction, $\tan 2\varphi = \frac{-\beta}{2\alpha}$, exchange roles when α and β change sign. That is

$$G(u_1', u_2', \alpha, \beta, \Gamma) = G(u_2', u_1', -\alpha, -\beta, \Gamma)$$

where

$$\begin{bmatrix} u_1' \\ u_2' \end{bmatrix} = \begin{bmatrix} \cos\varphi & -\sin\varphi \\ \sin\varphi & \cos\varphi \end{bmatrix} \begin{bmatrix} u_1 \\ u_2 \end{bmatrix}$$

This property will be useful in a subsequent section.

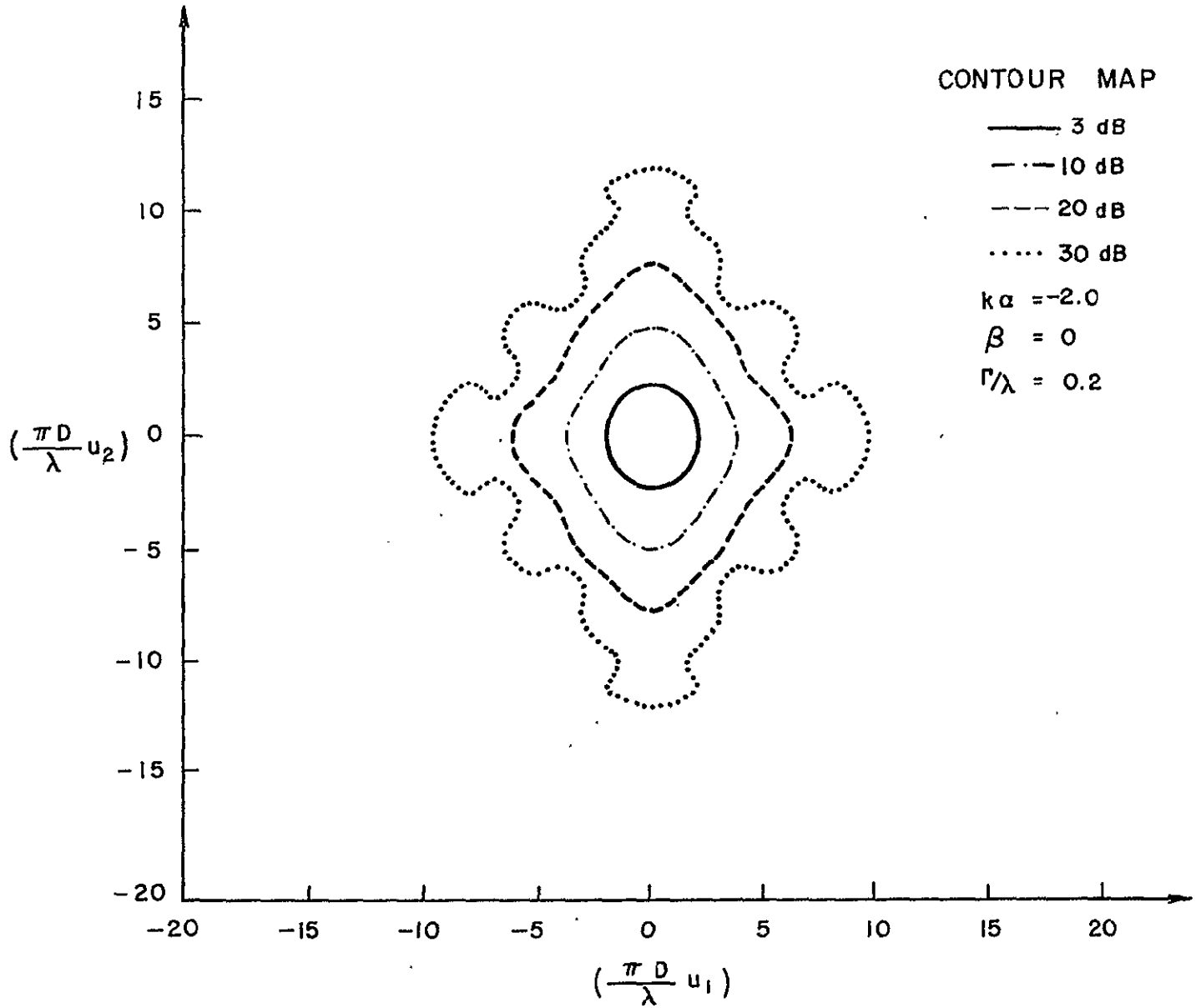
CONTOUR MAP
3 dB
10 dB
20 dB
30 dB
kα =-2.0
β = 0
Γ/λ = 0.2
15
10
5
0
-5
-10
-15
-20
-20
-15
-10
-5
0
5
10
15
20
(πD/λ u2)
(πD/λ u1)

Fig. 15

Property 5 gives the most detectable consequence of primary reflector astigmatism. It may be stated as follows:

Property 5. If the illumination function $E(\underline{x})$ is only a function of r, then the angular coordinates which are aligned with the β direction, $\tan 2\varphi = \frac{-\beta}{2\alpha}$, change roles when Γ changes sign. That is

$$G(u_1', u_2', \alpha, \beta, \Gamma) = G(u_2', u_1', \alpha, \beta, -\Gamma)$$

where

$$\begin{bmatrix} u_1' \\ u_2' \end{bmatrix} = \begin{bmatrix} \cos\varphi & -\sin\varphi \\ \sin\varphi & \cos\varphi \end{bmatrix} \begin{bmatrix} u_1 \\ u_2 \end{bmatrix} .$$

One immediately correlary of property 5 is that the axis gain is an even function of Γ/λ. The axis gain is the case where $u_1 = u_2 = 0$. Figure 16 shows the axis gain plotted against Γ with α as a plotting parameter ($\beta = 0$). This graph shows that the axis gain suffers little when α is small, but deteriorates rapidly as α is increased. The axial gain is also much less sensitive to the feed position when α is large.

Property 5 also requires the radiation patterns in the φ directions to exchange roles when Γ changes sign. This is perhaps the most striking quality of the model. As the feed is moved from $-\Gamma$ to Γ, the u_1' coordinate should become the u_2' coordinate, and the u_2' pattern should become the u_1' coordinate. Figures 15 and 17 illustrate this behavior. The illumination function for these maps was calculated for a horn feed as mentioned above, so the illumination is not quite circularly symmetric. That property 5 is not satisfied exactly can be seen in the 30 dB contour.

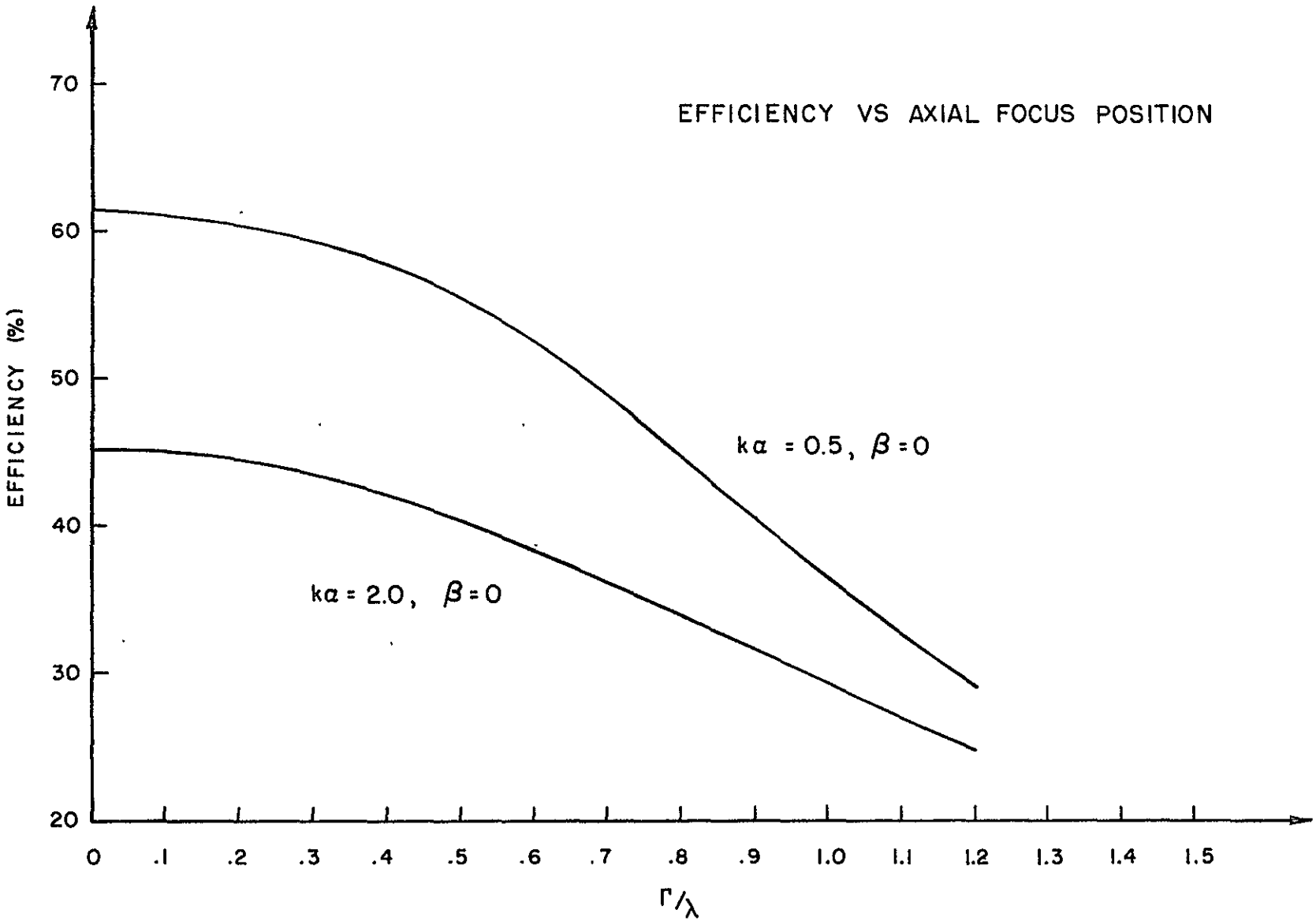
EFFICIENCY VS AXIAL FOCUS POSITION
EFFICIENCY (%)
70
60
50
40
30
20
kα = 0.5, β = 0
kα = 2.0, β = 0
0
.1
.2
.3
.4
.5
.6
.7
.8
.9
1.0
1.1
1.2
1.3
1.4
1.5
r/λ

Fig. 16

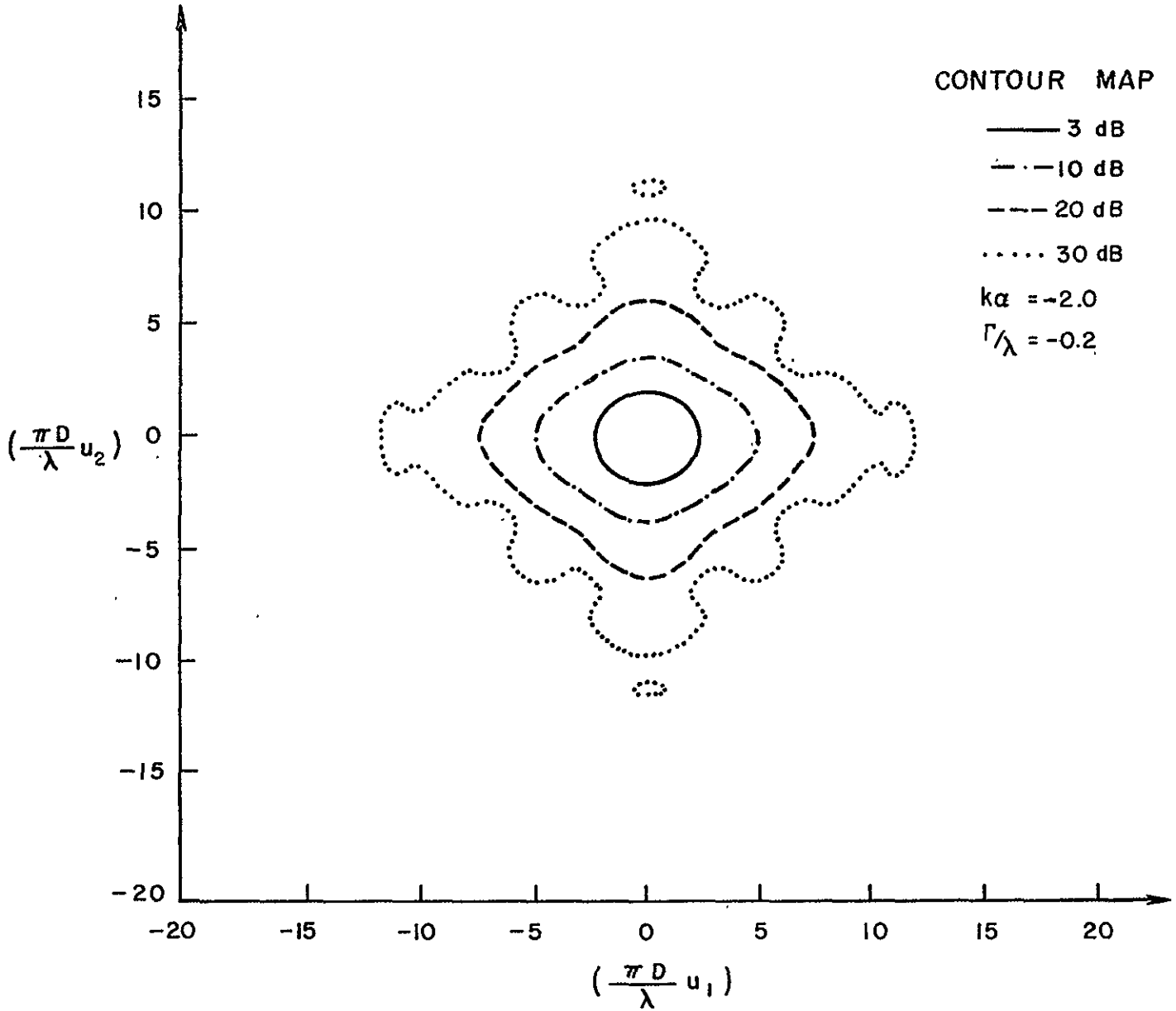
CONTOUR MAP
3 dB
10 dB
20 dB
30 dB
kα = -2.0
Γ/λ = -0.2
15
10
5
0
-5
-10
-15
-20
(πD/λ u2)
-20
-15
-10
-5
0
5
10
15
20
(πD/λ u1)

Fig. 17

Suppose the u_1' pattern is broad while the u_2' pattern is narrow at some focus position. Then there should be another focus position where the u_2' pattern is broad while the u_1' pattern is narrow. Figures 18 and 19 illustrate this fact. Figure 18 shows the principle cuts of the pattern with $k\alpha = 2$, $\beta = 0$, and $\Gamma/\lambda = +0.2$, while Figure 19 shows the pattern cuts with $k\alpha = 2$, $\beta = 0$, and $\Gamma/\lambda = -0.2$. The u_1 pattern of Figure 18 is the u_2 pattern of Figure 19 and vice versa.

This kind of pattern behavior has been noted by several authors. Bathker in his evaluation of the JPL 85-foot Ground Antenna[55] states,

> The hyperboloid was set 0.500 in. toward the apex which approximates the high elevation angle focus for maximum gain. Figures 29 and 30 show the resultant patterns. The azimuth cut is seen to have a narrower main beam while the elevation cut is broader.... Although a corresponding hyperboloid position toward the vertex was not tried it is suspected the inverse would be true, i.e. the elevation would be nearer an optimum focus and the azimuth plane would be defocused....

Bathker later confirmed that the paraboloid had a surface error that would fit the astigmatic phase error of Equation (25) very well by making mechanical measurements of the reflector figure.

Bathker is not alone in reporting this effect. Jacobs and King[56] in reporting on the characteristics of the Aerospace 15-foot antenna state:

> ...On rare occasions only moderate beamwidth broadening in the two orthogonal patterns occurred. However, on most occasions there was modest broadening in one plane and considerable broadening in the orthogonal plane. Sometimes this large amount of broadening occurred in the declination cut, and on other occasions it occurred in the hour-angle cut. On no occasion did extensive broadening occur in both planes during one measurement period....

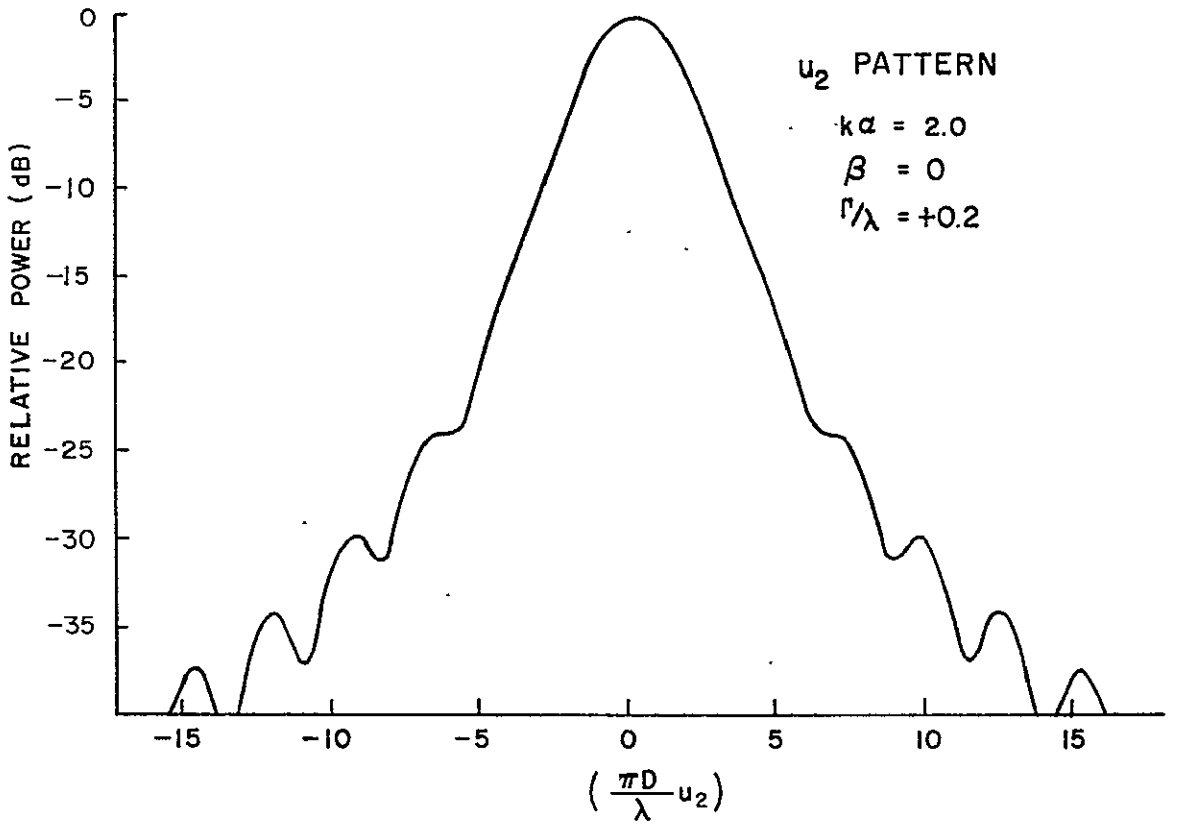
RELATIVE POWER (dB)
0
-5
-10
-15
-20
-25
-30
-35
-15
-10
-5
0
5
10
15
u_2 PATTERN
$k\alpha$ = 2.0
β = 0
Γ/λ = +0.2
$(\frac{\pi D}{\lambda} u_2)$

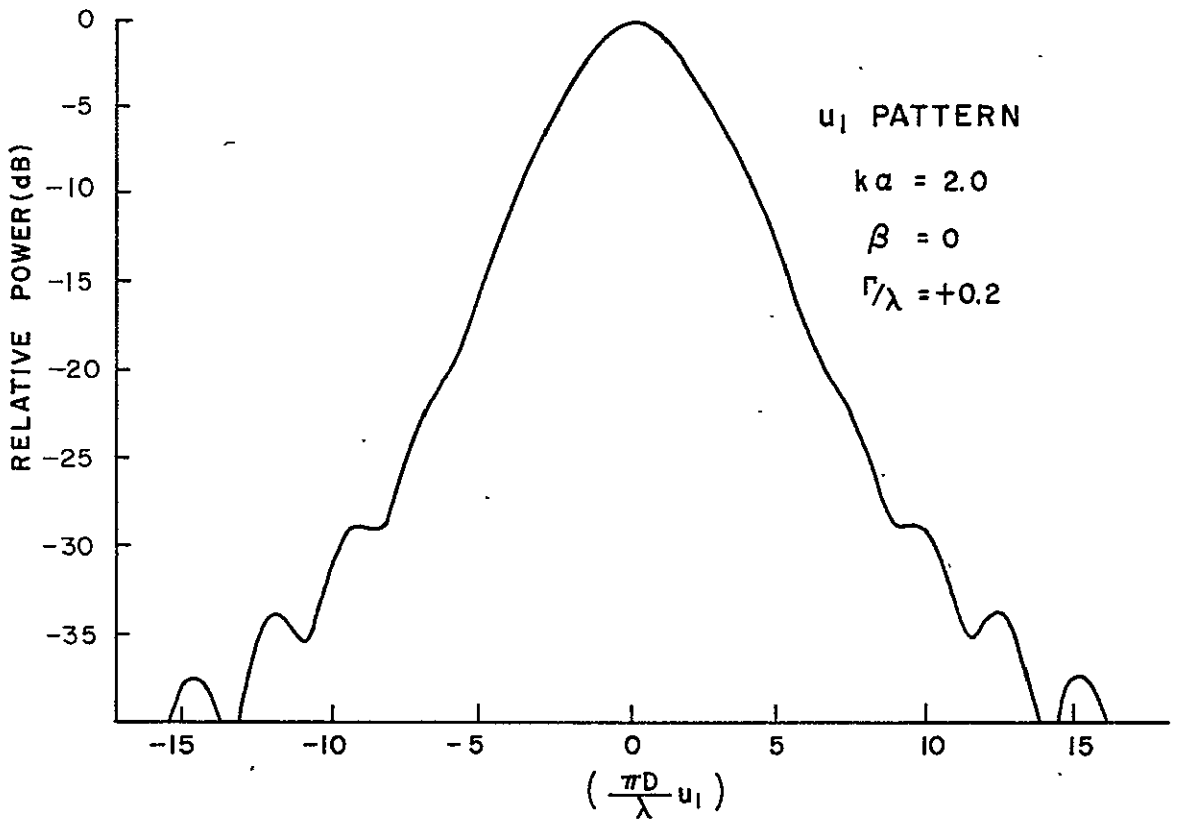
RELATIVE POWER(dB)
0
-5
-10
-15
-20
-25
-30
-35
-15
-10
-5
0
5
10
15
u_1 PATTERN
$k\alpha$ = 2.0
β = 0
Γ/λ = +0.2
$(\frac{\pi D}{\lambda} u_1)$

Fig. 18

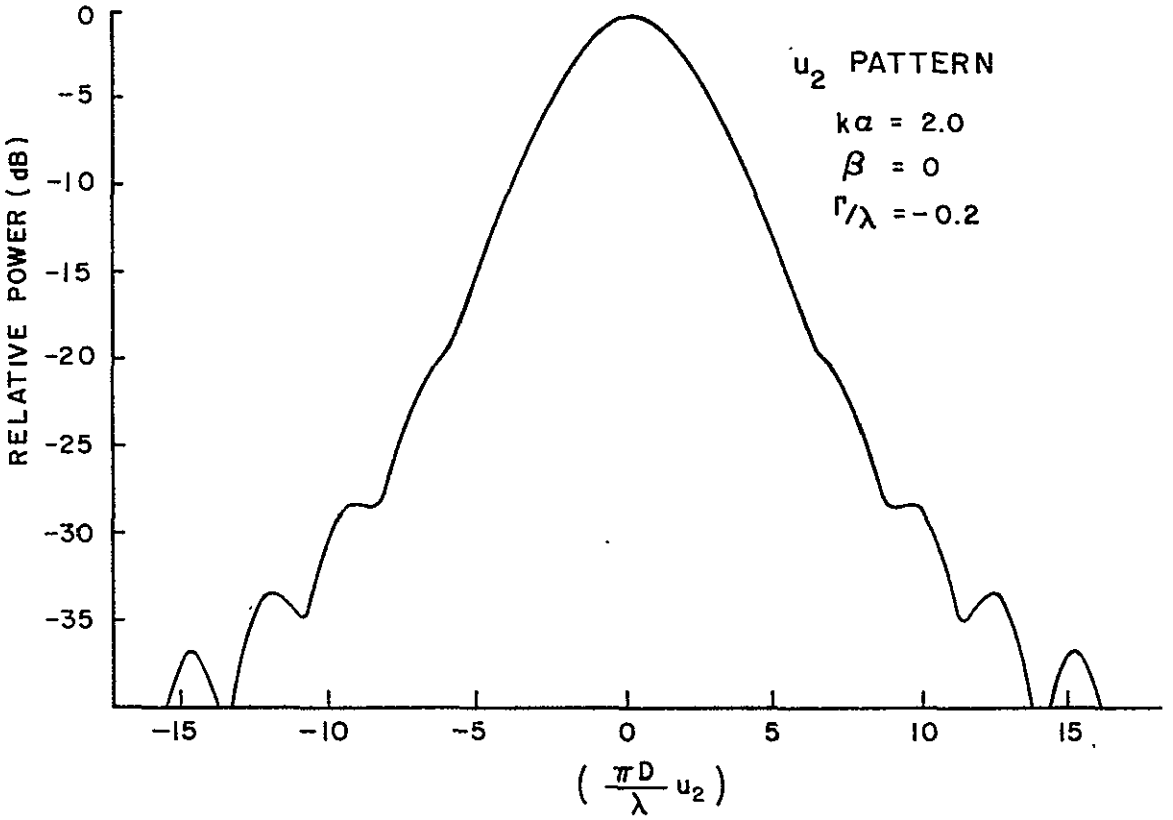
RELATIVE POWER (dB)
0
-5
-10
-15
-20
-25
-30
-35
u_2 PATTERN
$k\alpha = 2.0$
$\beta = 0$
$r/\lambda = -0.2$
-15
-10
-5
0
5
10
15
$\left(\frac{\pi D}{\lambda} u_2\right)$

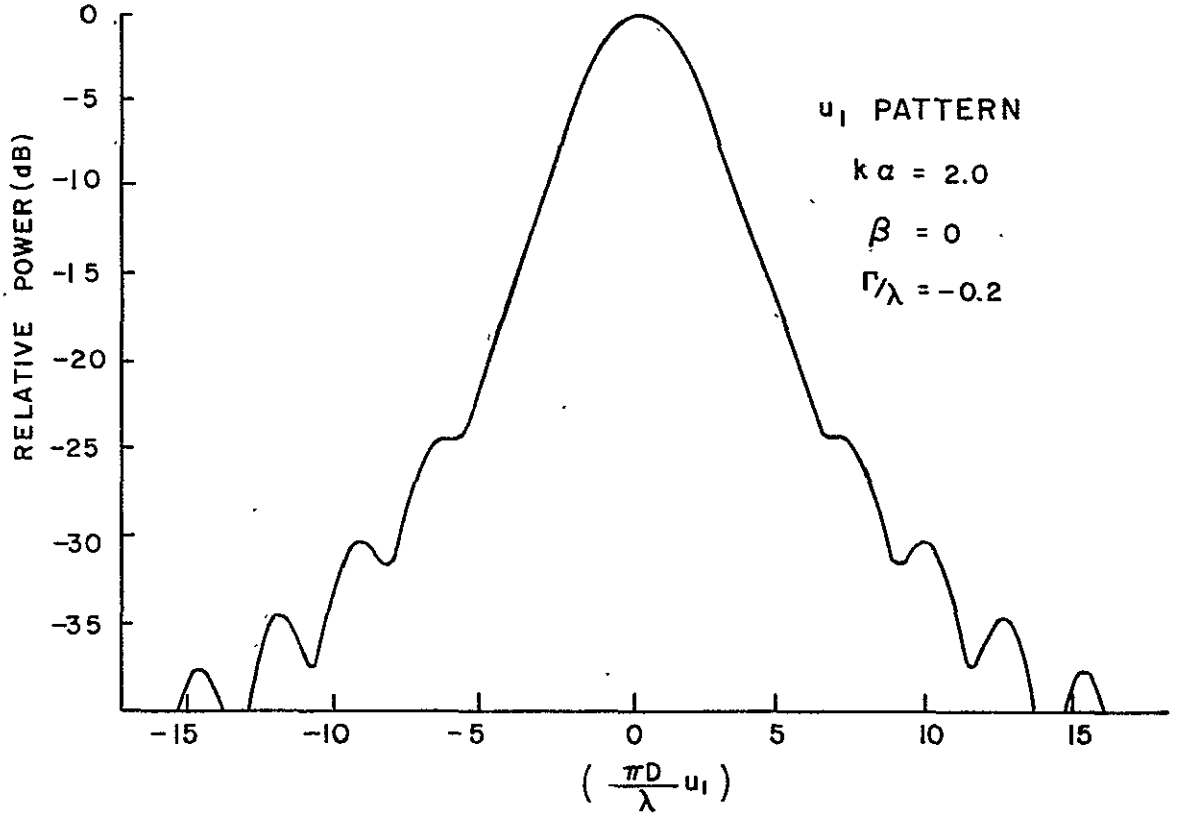
RELATIVE POWER (dB)
0
-5
-10
-15
-20
-25
-30
-35
u_1 PATTERN
$k\alpha = 2.0$
$\beta = 0$
$r/\lambda = -0.2$
-15
-10
-5
0
5
10
15
$\left(\frac{\pi D}{\lambda} u_1\right)$

Fig. 19

Jacobs and King interpreted this effect as arising from the atmosphere. However, it seems strange that the atmosphere could somehow scatter energy in the declination direction and not in the polar direction. Instead, this effect could quite possibly have come from slight movement of the secondary reflector and astigmatism in the primary reflector.

F. Measurement of Model Parameters

If adjustments are to be made based on this phase error model it is important to know the model parameters. Three methods will be given for determining these parameters. The first method depends upon the use of a pattern range facility to make a contour map and beamwidth measurements. The second is a method for measuring beamwidths astronomically by observing solar limb crossings. The third technique is a digital computer algorithm. It matches a predicted map of the antenna pattern to an observed map.

1. Pattern Range Method

The model parameters can easily be measured if a pattern range is available. The first step is finding the line of symmetry on the contour map. The line of symmetry can usually be found from a single pattern contour. A 10 dB level has been found to be convenient, because it is sensitive to the φ direction yet it is not usually complicated by sidelobes. If one identifies the symmetry directions on the contour map, then a linear relation between α and β is established by Property 2. This is

$$-2\alpha \tan 2\varphi = \beta. \tag{26}$$

It is possible that the contour map will be circular. However, at another axial focus position the eccentricity of the contour map should appear. If the contour map were circular at each axial focus position no astigmatism is present in the antenna.

The parameter α can be determined by observing the beamwidth change in the φ direction with the axial feed position. Figure 20 is a graph of the beamwidth in the φ direction vs focus position. The abscissa scale is Γ/λ. The ordinate scale is the fractional widening of the beam over the design pattern beamwidth. The plotting parameter is $k\alpha'$, where k is the wavenumber. The relation between α', α and φ is given by

$$\alpha = \alpha' \cos 2\varphi. \tag{27}$$

The parameter α' is the value α takes on when the (x_1, x_2) - coordinates are rotated so that the center term in the model, Equation (25), is eliminated.

The value of α' can be determined by plotting the observed beamwidths in the φ direction vs focus position on Figure 20. The parameter α' is then estimated by eye. This task is relatively simple because for phase errors greater than one radian at the edge of the aperture the beamwidths are very sensitive to axial focus position changes.

If the measured beamwidths match the predicted beamwidths but with the coordinate labels reversed, then the sign of α' is negative. This fact follows from Property 3.

With α' and φ determined, the parameters α and β can be calculated from Equation (27) and (26).

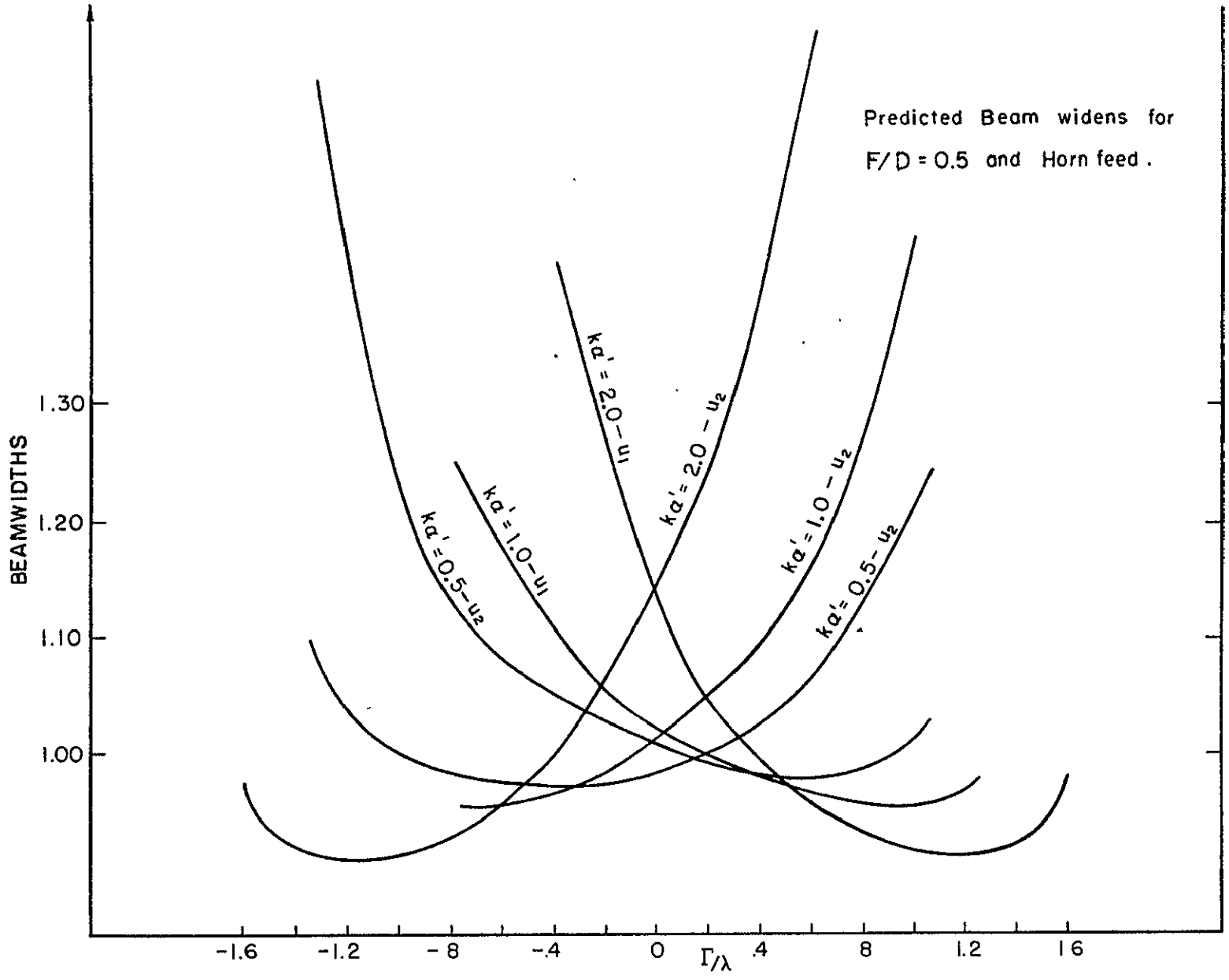
Predicted Beam widens for
F/D = 0.5 and Horn feed .
BEAMWIDTHS
1.30
1.20
1.10
1.00
-1.6
-1.2
- 8
-.4
0
.4
8
1.2
16
Γ/λ
ka' = 2.0 − u1
ka' = 2.0 − u2
ka' = 1.0 − u1
ka' = 1.0 − u2
ka' = 0.5 − u2
ka' = 0.5 − u2

Fig . 20

The parameters α and β were estimated by this method for The University of Texas 16-foot antenna as discussed in Chapter VI. A contour map was plotted and the φ direction was taken to be -18°. The φ direction beamwidths were then plotted, and the value of α' was estimated as 1.5. The values Equations (27) and (26) give for α and β are $\alpha = 1.21$ and $\beta = 1.75$. This compares favorably with $\alpha = 1.13$ and $\beta = 0.73$, given by the more objective computer minimization method. The discrepancy in β can be explained by the fact that the angle φ was clearly taken too large, see Figure 26, Chapter VI.

2. Astronomical Method

The method given above depends upon measuring the beamwidth change as a function of focus position in order to estimate the magnitude of the astigmatism. Beamwidths can also be measured astronomically if a pattern range is not available by observing solar limb crossings. This, method has been used by Jacobs and King[57] with good results. Also a solar limb crossing experiment is reported in Chapter VI. The beamwidths that were determined from this experiment compare favorably with the beamwidths measured on the pattern range.

The passing of the solar limb through the antenna beam produces a record proportional to the integral of the antenna pattern. Thus, is is expedient to choose a model for the antenna beam. Almost any model would suffice since one is interested in only the gross pattern features, so a Gaussian pattern will be chosen for analytical convenience. In the (x_1, x_2)-coordinates of Figure 21, the antenna pattern model may be written,

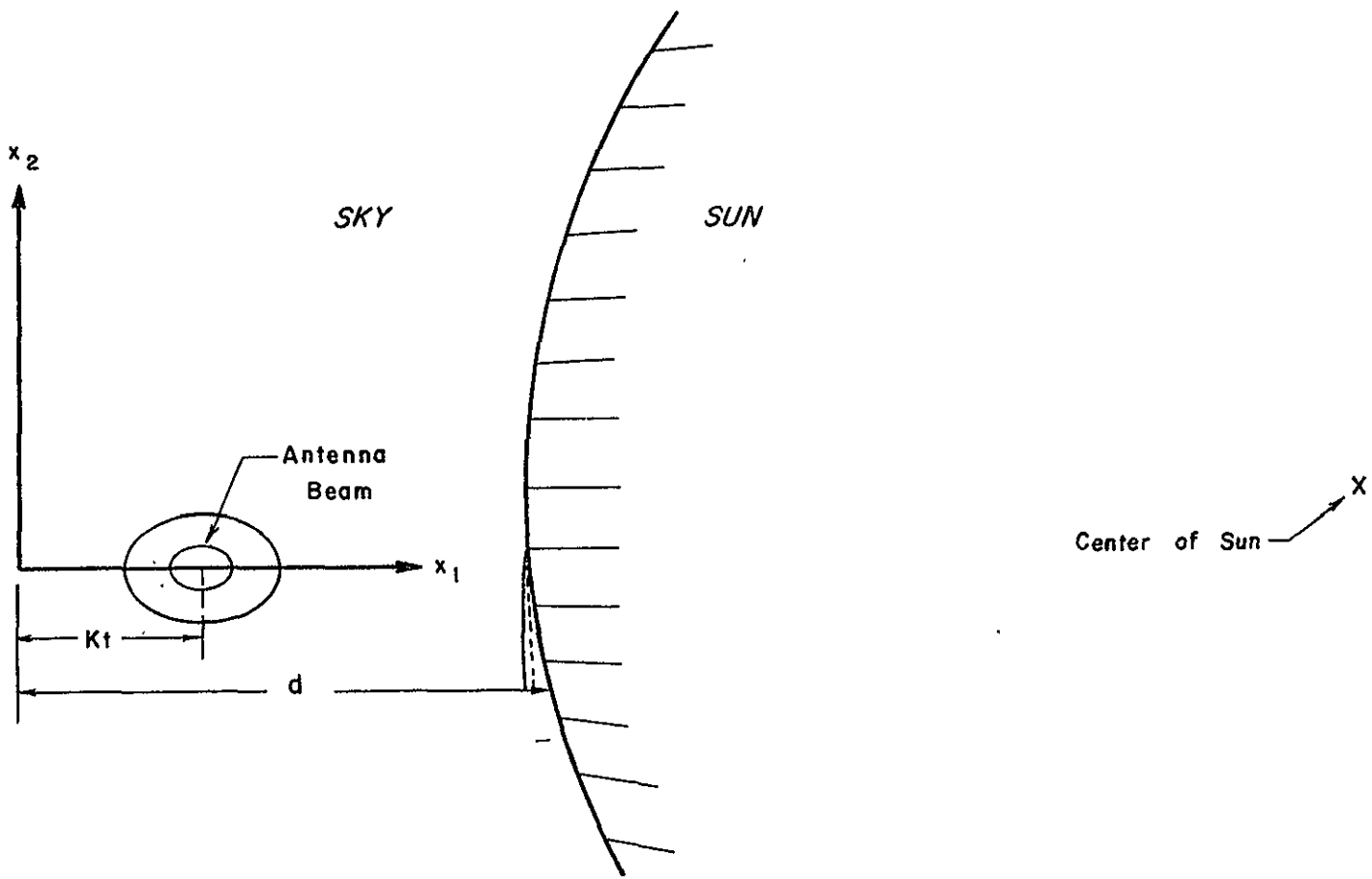

SOLAR LIMB CROSSING EXPERIMENT

Fig. 21

$$G(x_1, x_2) = G_o \, e^{-\left\{\left(\frac{x_1 - Kt}{\theta_1}\right)^2 + \left(\frac{x_2}{\theta_2}\right)^2\right\} \ln 2} \qquad (28)$$

where G_o is the peak gain, θ_1 and θ_2 are the semi-beamwidths, K is the solar rate, and t is time.

The sun is a thermal source, so the antenna smoothing equation applies. The antenna response is thus,

$$T_a = \frac{1}{4\pi} \int_{-\infty}^{\infty}\int G(x_1, x_2) \, T(x_1, x_2) \, dx_1 dx_2, \qquad (29)$$

where T_a is the antenna temperature, and $T(x_1, x_2)$ is the equivalent temperature at the point (x_1, x_2). Substituting the form given in Equation (28) for G into Equation (29) and assuming the sun has a linear edge, one obtains

$$T_a = \frac{1}{2}\left(T_{sky} + T_{sun}\right) + \frac{1}{2}\left(T_{sun} - T_{sky}\right) \operatorname{erf}\left\{\frac{(Kt - \varphi)}{\theta_1\sqrt{\ln 2}}\right\}. \qquad (30)$$

T_{sky} is the equivalent temperature of the sky, T_{sun} is the equivalent temperature of the sun, and erf(x) is the error function. Equation (30) states that the antenna temperature increases from the sky temperature to the solar temperature as the antenna beam crossed the limb of the sun. The scale of this transition is proportional to the half power beamwidth in the direction that the antenna is driven across the solar limb.

The procedure for measuring θ_1 is to let the antenna temperature during the limb crossing be the data set, i.e.

$$T_a(i),\ i = 1, 2, \ldots n.$$

Then one estimates θ_1 by minimizing the rms error between the data and Equation (30) with a digital computer.

The experiment that has been outlined gives the equivalent beamwidth in the direction the antenna crosses the solar limb. Thus, in order to obtain a contour map one must take the beamwidth in a number of directions. This will determine the φ direction just as before. One can then determine the parameters by plotting the beamwidths in the φ direction vs axial focus position.

This method is much more tedious than the pattern range method and requires the use of a digital computer. However, it does not require the availability of a pattern range. This is important because some antennas do not have a pattern range.

3. Computer Algorithm

The computer algorithm method of estimating the model parameters depends upon matching a predicted pattern map with the measured radiation pattern of the antenna. The radiation pattern of a reflector antenna is sensitive to long correlation radius phase errors in the angular region near the main beam. Thus, even with only a small dynamic range there should be little difficulty in obtaining a relatively noise free measurement of any astigmatism present.

This algorithm calculates the antenna radiation pattern using the Fast Fourier Transform method presented in Appendix A. The predicted radiation pattern can be computed to slide rule accuracy in less

than one second on the CDC 6600 computer. This high speed operation makes the iterative prediction of the model parameters possible since the predicted radiation pattern must be calculated hundreds of times in such an iterative method.

The data for this experiment is a map of the antenna pattern near the main beam digitized at an N x N grid of points. The map is normalized to unity power level on the axis. This data set may be expressed as

$$D(i,j) = G'(u_i, u_j)$$

where

$$\begin{aligned} u_i &= [i-n/2+1]\,\Delta u_1 \\ u_j &= [j-n/2+1]\,\Delta u_2. \end{aligned} \tag{31}$$

G' is the measured normalized pattern of the antenna in dB units. The normalized axis gain $G'(0,0)$ appears one point to the right and above the center of the array. The sampling intervals Δu_1 and Δu_2 should be chosen smaller than the maximum dictated by the sampling theorem[58], i.e.

$$\Delta u_1, \Delta u_2 < \frac{\lambda}{2D} \text{ radians.}$$

The sampling intervals in the two directions need not be equal.

The algorithm minimizes the objective function, F, over the four parameters a, b, α, β, Γ where

$$F = \sum_{j=1}^{n} \sum_{i=1}^{n} [D(i,j) - P(i,j)]^2$$

The predicted antenna pattern, P(i, j), is calculated by the program of Appendix A. P(i, j) is an approximation to the integral

$$P(i,j) = \frac{k^2}{\pi} \left| \int_{\underline{x}} T(x_1, x_2)\, e^{jkL(\underline{x})}\, e^{jk\underline{u} \cdot \underline{x}}\, d\underline{x} \right|^2,$$

where u_i and u_j are defined by Equation (31).

The phase error function $L(\underline{x})$ is given by

$$L(\underline{x}) = ax_1 + bx_2 + \{\alpha x_1^2 + \beta x_1 x_2 - \alpha x_2^2 + \Gamma K(x_1^2 + x_2^2)\}/R_o^2$$

The linear phase grading terms are included so that the predicted pattern can be translated to agree with the observed pattern as much as possible.

To test the method and the program, the data array was set to the pattern of a uniformly illuminated constant phase aperture. This data pattern was calculated analytically from the form given in Silver[59]. Then all of the phase error parameters were each initialized at 2/k where k is the wavenumber. All five parameters converged toward zero as expected. When the program ran out of time each parameter was less than 0.01/k.

The program was then tried with real data. The pattern map was taken by J. R. Cogdell on January 30, 1969. The results of this is shown in Figures 22 through 24. Figure 22 shows the predicted and observed radiation patterns on the same scale. Figure 23 shows the observed radiation contour map while Figure 24 shows the best fit map. The observed map shows a considerable amount of beam squint which cannot be taken

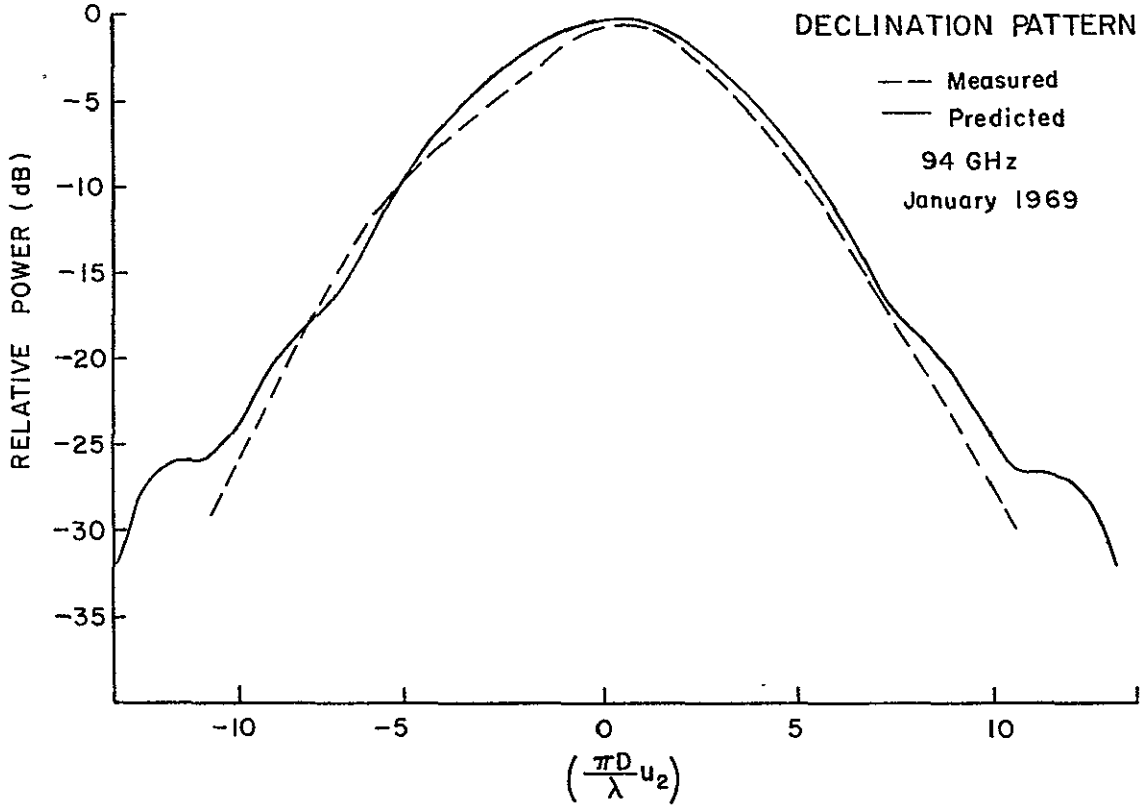
DECLINATION PATTERN
Measured
Predicted
94 GHz
January 1969
RELATIVE POWER (dB)
0
-5
-10
-15
-20
-25
-30
-35
-10
-5
0
5
10
$\left(\frac{\pi D}{\lambda} u_2\right)$

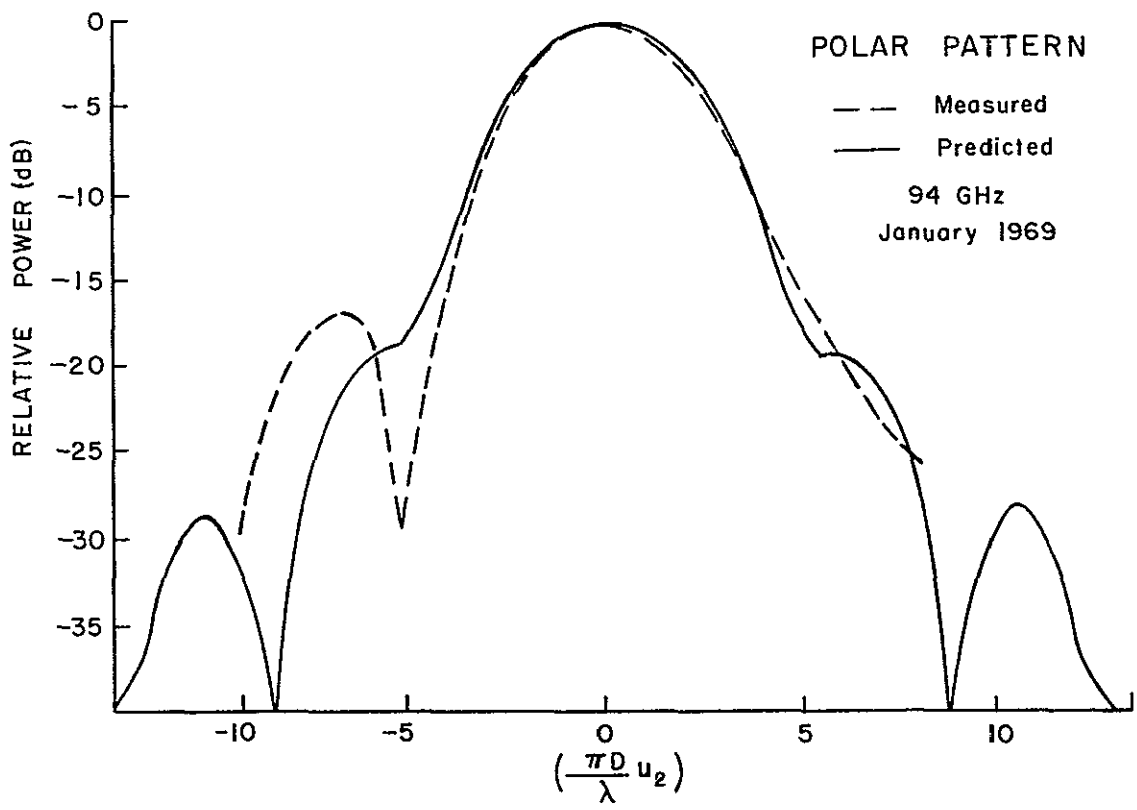
POLAR PATTERN
Measured
Predicted
94 GHz
January 1969
RELATIVE POWER (dB)
0
-5
-10
-15
-20
-25
-30
-35
-10
-5
0
5
10
$\left(\frac{\pi D}{\lambda} u_2\right)$

Fig. 22

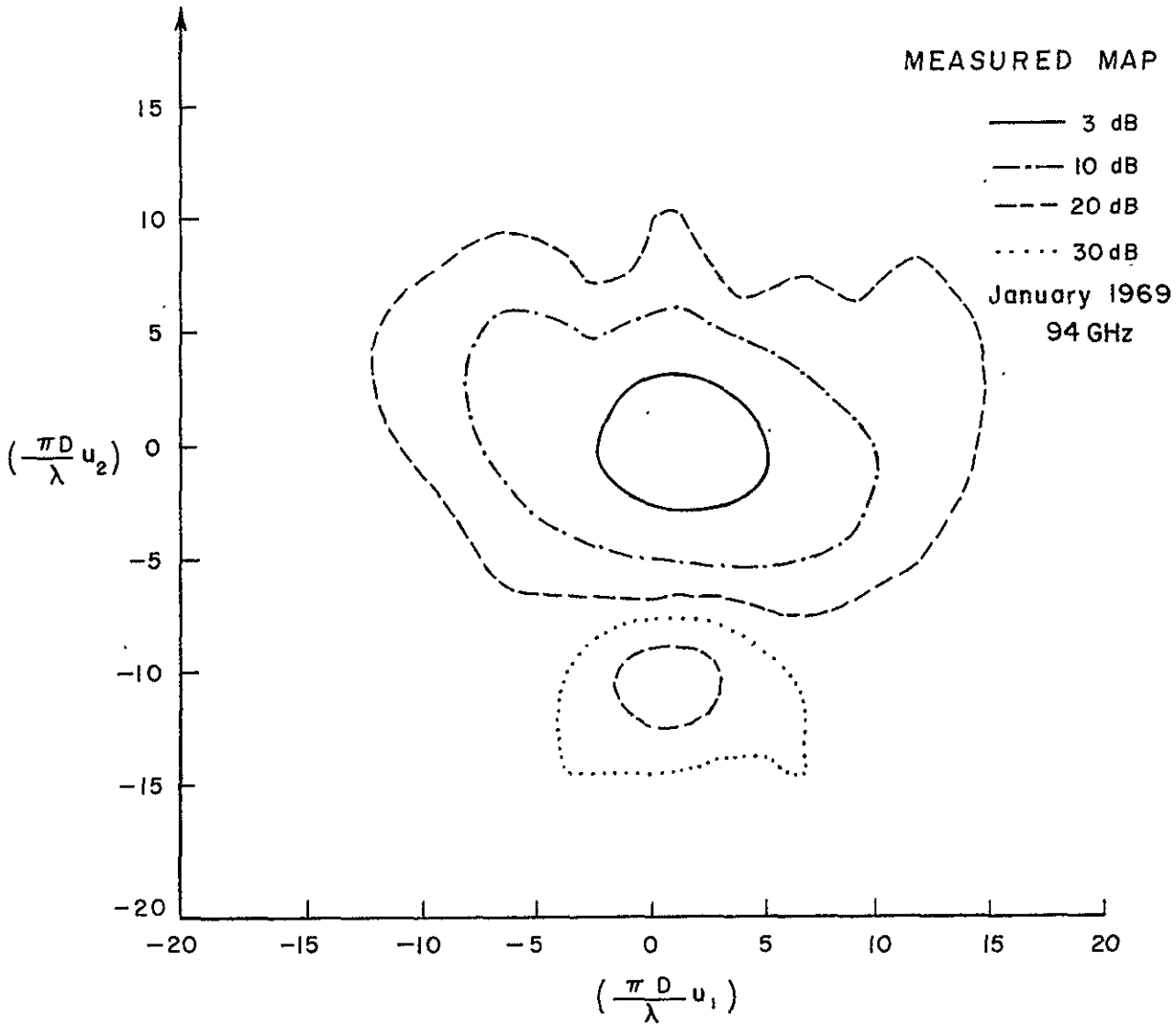
MEASURED MAP
3 dB
10 dB
20 dB
30 dB
January 1969
94 GHz
15
10
5
0
−5
−10
−15
−20
$(\frac{\pi D}{\lambda} u_2)$
−20
−15
−10
−5
0
5
10
15
20
$(\frac{\pi D}{\lambda} u_1)$

Fig. 23

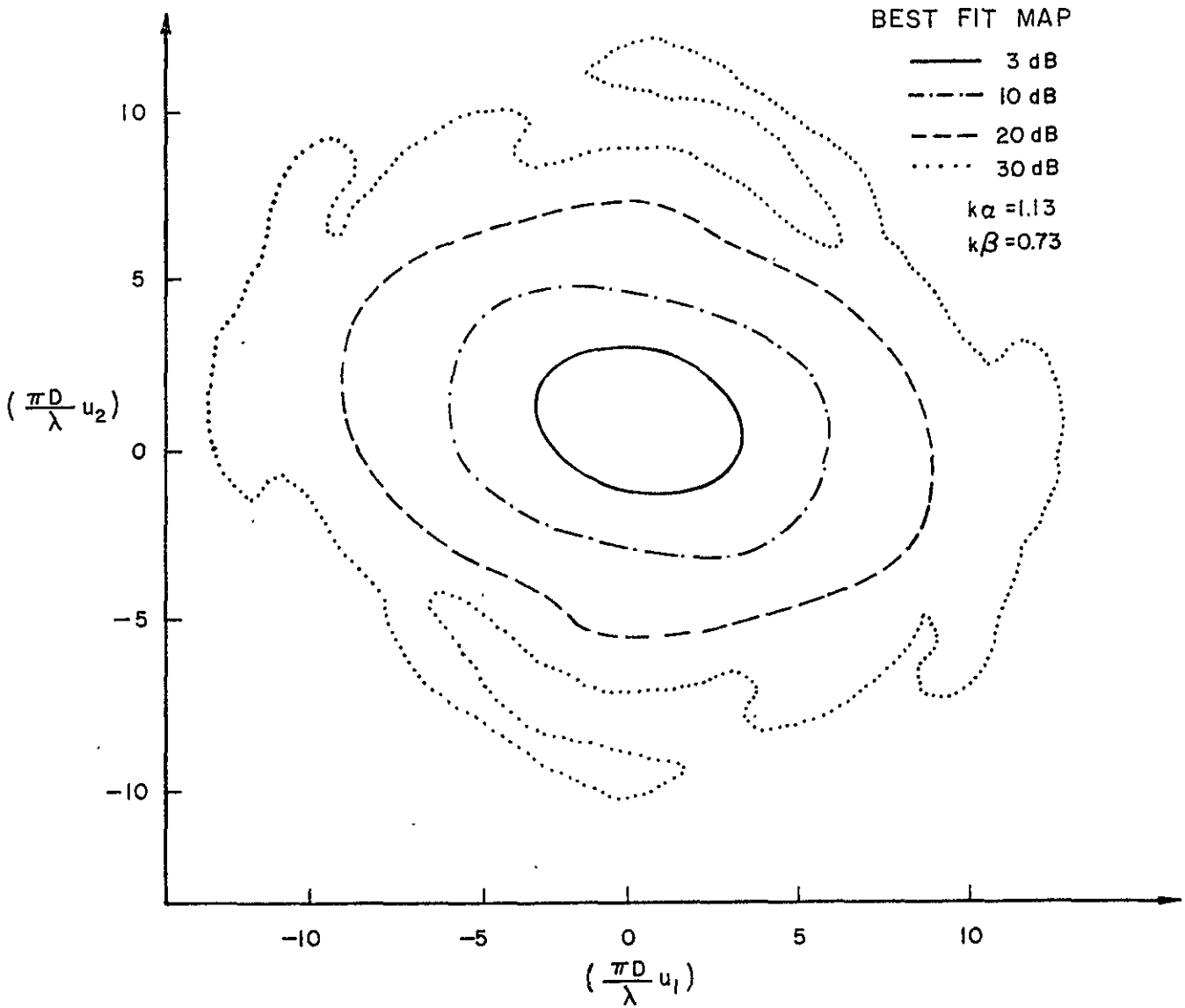
BEST FIT MAP
3 dB
10 dB
20 dB
30 dB
kα =1.13
kβ =0.73
10
5
0
−5
−10
$(\frac{\pi D}{\lambda} u_2)$
−10
−5
0
5
10
$(\frac{\pi D}{\lambda} u_1)$

Fig. 24

into account by this model. However, this kind of error can sometimes be corrected by simply moving the feed laterally.

It should be remembered, of course, that the results of this minimization procedure are ambiguous. Property 3 guarantees that the predicted pattern for α, β, and Γ will be the same as the predicted pattern for $-\alpha$, $-\beta$, and $-\Gamma$. This ambiguity can be resolved by plotting the beam-widths against feed position as shown in the previous section.

Both a conjugant gradient iterative method and a simplex method were tried with almost identical results. The conjugant gradient method, however, was somewhat faster.

The computer algorithm method for determining the model parameters is the most objective of the three methods and probably is the best. However it is also the most time consuming because of the programming effort required. In addition, it requires both a pattern range facility and a large digital computer.

G. Conclusions

An astigmatic phase error model has been presented. It has been shown that the axial feed position plays an important role in determining the character of the total phase error at the aperture plane. Five model properties have been presented with examples. Property 5 is particularly interesting since it has been seen in at least three large reflector antennas. If astigmatism is identified in the reflector then one is interested in measuring it quantitatively. Three methods are given for doing this. The first and

third methods depend upon pattern range measurements. The former is a field method; the later uses a computer minimization technique. The second method is an astronomical method which can be used if no pattern range is available.

Chapter V

Reflector Efficiency Evaluation By Frequency Scaling*

A. Introduction

The useful bandwidth of a parabolic reflector antenna is limited by the precision of its surface and the integrity of its supporting structure. Surface deviations from a true parabolic degrade performance as the frequency of operation is raised [60]. The number of antennas in which such effects have been observed over a wide range of frequencies is continually increasing.

Most applications involving reflector type antennas require only a knowledge of the antenna properties as a function of frequency. However, there is an increased class of problems where precise knowledge of antenna characteristics is required. Space communications and radio astronomy provide significant examples where large antennas are used at many frequencies. The Ruze tolerance theory [61] is currently used to predict antenna efficiency at frequencies where performance has not been evaluated by direct methods.

*A large portion of this chapter is taken from a paper of the same title submitted to the IEEE Transactions on Antennas and Propagation. This paper was co-authored by J. R. Cogdell and the author.

The Ruze tolerance model has successfully described the variation of small tolerance losses with frequency in several antenna evaluation programs [62], [63]. The wide success of this model is somewhat surprising in view of the strict statistical assumptions which underlie the theory. As duscussed in Chapter III, the model assumes that the phase fronts in the antenna aperture may be described by a two dimensional Gaussian random process. It also requires that the random process be stationary and decorrelate over distances larger than c, where c is much less than the diameter of the antenna [64].

As discussed in Chapter III, a number of large reflector antennas have been subjected to extensive mechanical error evaluations [65], [66]. The results are usually displayed in the form of error contour maps. Examination of these maps confirm the impression that errors tend to be correlated over large regions of the antenna, with the result that only a few independent correlation regions exist in the antenna surface. There are further reasons to suspect that errors should correlate over large fractions of the antenna surface. Error producing effects such as gravitational loading and thermal expansion act on the structure as a whole, producing systematic deformation in the structure. As shown in Chapter II, the tolerance loss of an antenna will not follow any precise law if there are only a few correlation regions on the aperture.

The purpose of this chapter is to describe the tolerance loss in reflector antennas as a function of frequency without the statistical assumptions.

The theory is based upon measurements and estimates of peak to peak error. The major points of the theory may be summarized as follows:

1. An efficiency measurement and error estimate at one frequency implies firm bounds on the efficiency at other frequencies. These bounds can be used with confidence because nothing about the statistics of the phase errors is assumed.
2. Measurement errors scale down with frequency. Thus, a moderately accurate measurement of the fficiency at a high frequency can be used to yield a highly accurate inferred efficiency at a lower frequency. This approach has the added advantage that gain measurements at higher frequencies are less subject to multi-path interference.

In the following section tolerance loss is discussed generally. A series form for the telerance loss is presented and discussed with reference to the Ruze theory. In the fourth section the theory of efficiency measurement by frequency scaling is presented in the form of two theorems. The first theorem gives a method for predicting the efficiency at one frequency given a measurement at another frequency with an electrically scaled-feed system. The second theorem extends the first theorem to include gain measurements at two frequencies, which are used to predict the efficiency at a third frequency. These two theorems are rigorously true only for prime-focus instruments with electrically scaled feed systems.

This assumption is required to make the illumination of the reflector the same at all the frequencies. The first theorem, however, is extended by an approximate method to cases where small changes in the illumination takes place from frequency to frequency. Cassegrain antennas are also considered by this approximate method. The use of these methods will be illustrated by published data.

B. Tolerance Loss

As shown in Chapter II, the efficiency of a reflector antenna, at a frequency f, may be expressed as

$$\eta(f) = F \int_{\underline{\tau}} B(\underline{\tau})\, d\underline{\tau}$$

where

$$B(\tau) = \int_{\underline{x}} E(\underline{x})\, E(\underline{x}+\underline{\tau})\, e^{jk\left[L(\underline{x}) - L(\underline{x}+\underline{\tau})\right]}\, d\underline{x}$$

and

$$F = \frac{\eta}{2 Z_o P_r A_g}$$

The function $E(\underline{x})$ is the magnitude of the electric field at point $\underline{x}$ in the aperture plane and is assumed known. The phase length function, $L(\underline{x})$, is usually unknown and contains the phase deviations caused by reflector defects. $B(\underline{\tau})$ is the autocorrelation function of the fields in the aperture plane. The other symbols are $\eta(f)$, the aperture efficiency as a function of frequency; $k = 2\pi f/c$; η = ohmic efficiency of the antenna, $Z_o = \sqrt{\mu_o/\epsilon_o}$;

P_r the radiated power; and A_g, the geometric antenna area. For the rigorous results it is assumed that the antenna is illuminated the same at all frequencies, such that $E(\underline{x})$ does not depend on frequency.

It is well known that the autocorrelation function $C(\tau)$ is Hermitian, i.e.,

$$C(\tau) = C^*(-\tau)$$

Thus, when the integral over τ is performed the imaginary part of the integral will vanish, and we may work simply with the real part. Hence,

$$\eta(f) = F \int_{\underline{\tau}} \int_{\underline{x}} E(\underline{x})\, E(\underline{x}+\underline{\tau}) \cos k[L(\underline{x}) - L(\underline{x}+\underline{\tau})]\, d\underline{x}\, d\underline{\tau}.$$

One can define the sequency of coefficients A_{2n} as

$$A_{2n} = \frac{(-1)^n}{(2n)!} F \int\int_{\underline{\tau}\,\underline{x}} E(\underline{x})\, E(\underline{x}+\underline{\tau}) \left\{ \frac{2\pi}{c} [L(\underline{x}) - L(\underline{x}+\underline{\tau})] \right\}^{2n} d\underline{x}\, d\underline{\tau}.$$

such that one obtains an infinite series in even powers of frequency:

$$\eta(f) = \sum_{n=0}^{\infty} f^{2n} A_{2n} \tag{32}$$

In this expansion the first term is clearly the phase error free efficiency, which can be calculated without knowledge of reflector errors. The second term will describe a loss in efficiency which is quadratic in frequency and will show the beginning effects of tolerance loss. The quartic term will be important as tolerance loss gets substantial and so forth.

Other aspects of Equation (32) should be noted. The first is that the series can be terminated after a few terms and the remainder bounded. In cases where peak phase errors are not unreasonably large the higher order terms are of rapidly decreasing importance. With one or two measurements one can estimate the important coefficients and bound the efficiency characteristics in the useful region of the antenna. This procedure will be quantified and illustrated in the final section of this paper. Spencer[67] gave a form equivalent to the first two terms of this series. He made no effort to bound the error of approximation, and did not deal with the effects of measurement errors. Equation (32) can also be related to the statistical results of Ruze[68]. The Ruze theory is applicable to the average of Equation (32) over a large number of similar antennas. The effect of the statistical assumptions is to determine all of the coefficients of the averaged equation in terms of two parameters, the rms surface deviation and the decorrelation distance.

The Ruze tolerance loss factor is of the same form as Equation (32) when expanded in a power series in frequency. The first effects of tolerance loss, which are always quadratic in frequency by Equation (32), can therefore always be fit by the Ruze factor, $e^{-(\frac{4\pi\epsilon}{\lambda})^2}$. This might explain the fact that the Ruze factor is useful in the small tolerance loss region, say less than 6 dB tolerance loss, for some value of ϵ, which is often called the "electrical tolerance." It is relevant to consider that the "electrical tolerance" is often significantly different from the measured

mechanical tolerance [69, 70, 71], while the Ruze theory requires that they be the same. Thus, our conclusion is that the wide success of the Ruze tolerance loss equation is due more to the functional form of the equation than to the validity of the model.

C. Notation

Before stating the theorems, we shall define the notation used in the two theorems. These quantities are as follows:

η_o = design efficiency (the efficiency with no phase errors)

$\eta(f)$ = true overall efficiency at f(unknown)

$\eta'(f)$ = measured overall efficiency at f

B_i = peak measurement error bar at f_i

$K(f)$ = peak-to-peak phase error at frequency f

f_m = measurement frequency

f_1 = first measuring frequency

f_2 = second measurement frequency

f_e = frequency of estimation (frequency for which efficiency estimate is desired)

$\delta(f, \underline{x})$ = phase error function = $kL(\underline{x})$

D. Theorems

Theorem 1 gives a method of predicting the gain at frequency f, based on the gain measured at another frequency, f_m, and an estimate of the peak-to-peak phase errors. The error made in estimating the gain is from two

sources. One is the error in the measurement at frequency f_m; the other is the mathematical error made in the estimation. Theorem 1 may be stated as follows:

Theorem 1

If the feed system of a prime focus reflector antenna at frequency f_e is a scale model of the feed system at f_m, and

$$|\eta'(f_m) - \eta(f_m)| \leq B$$

and

$$|\delta(f_m, \underline{x}) - \delta(f_m, \underline{y})| \leq K(f_m), \text{ all } \underline{x} \text{ and } \underline{y}$$

then the relations

$$\eta(f_e) < \eta_o - P[\eta_o - \eta'(f_m)]\left(\frac{f_e}{f_m}\right)^2 + \eta_o \sup S + P\,B\left(\frac{f_e}{f_m}\right)^2, \text{ for all } P$$

and

$$\eta(f_e) \geq \eta_o - P[\eta_o - \eta'(f_m)]\left(\frac{f_e}{f_m}\right)^2 + \eta_o \inf S - P\,B\left(\frac{f_e}{f_m}\right)^2, \text{ for all } P$$

hold true. The set S is defined as

$$S = \left\{z : z = U\left(\frac{f_e}{f_m} x\right) - P\left(\frac{f_e}{f_m}\right)^2 U(x);\ 0 \leq x \leq K(f_m)\right\}$$

The function U(x) is given by

$$U(x) = \cos(x) - 1$$

The proofs of the theorems will be given in Appendix C.

In the bounds for the efficiency given above, the terms $\eta_o \sup S$ and $\eta_o \inf S$ bound the mathematical error caused by approximating cosine

while the terms $\pm \varepsilon \left(\frac{f_e}{f_m}\right)$ result from the measurement error. The quantity P is a free parameter, so the method is most effective if the bounds are appropriately minimized or maximized over P, which is normally different for the upper and lower bounds.

In the case where $f_e < f_m$ very good results may be obtained using P = 1 for the upper bound and

$$P = \frac{U\left(\frac{f_e}{f_m} K(f_m)\right)}{U(K(f_m))} \left(\frac{f_m}{f_e}\right)^2$$

for the lower bound. In that case one has the simple expressions

$$\eta(f_e) \leq \eta_o - \frac{U\left(\frac{f_e}{f_m} K(f_m)\right)}{U(K(f_m))} [\eta_o - \eta'(f_m) - \varepsilon]$$

and

$$\eta(f_e) \geq \eta_o - \left(\frac{f_e}{f_m}\right)^2 [\eta_o - \eta'(f_m) + \varepsilon].$$

Theorem 1 may be applied to predict the efficiency of a prime-focus reflector antenna with a scaled feed system at either a higher or lower frequency, but it is most useful in the latter case. This is true since the factor $\left(\frac{f_e}{f_m}\right)^2$ scales down the measurement error in the case where f_e is less than f_m. The University of Texas 16-foot antenna is a good example. The required data is as follows: Cogdell [72]

η_o = 67.5

$\eta'(134)$ = 45% ± 5% (peak)

K(134) ≤ 2 radians.

The effieicney at several different frequencies has been calculated from the data set. The results are given in Table 1.

f_e(GHz)	$\eta(f_e)$% ± peak
15	67.15 ± .13
35	63.73 ± .67
70	60.1 ± 2.3
94	55.0 ± 3.6
100	53.6 ± 4.0

Table 1

Theorem 1 works very well so long as the peak-to-peak phase error does not get too large. For peak-to-peak phase errors above 3 radians at the measurement frequency the mathematical error of approximation increases so rapidly that the method becomes useless. It is interesting that this breakdown occurs at about 3/5 of the gain maximum frequency for a reflector governed by the Ruze model. The gain maximum occurs when the rms phase error is about 1 radian or when the peak-to-peak error is about 5 radians. Thus the theorem applies throughout what is considered the useful bandwidth of the antenna. On the other hand, the bound on the mathematical error is rather conservative since it bounds a weighted

average by its peak-to-peak value. One could actually perform the integral that this term bounds if the function L(x) were available from a STAIR program or a field measurement. Extreme accuracy would not be required since this integral represents only a small correction. If the appropriate integral were performed the method could probably be used with an efficiency measurement above the frequency of the gain maximum.

Theorem 1 may be extended to the Cassegrain antenna case by considering only the most significant terms. A rigorous result seems impossible because of amplitude and phase of the electric field on the primary reflector will inevitably be functions of frequency. The usual practice is to scale the primary feed horn and leave the subreflector unchanged [73]. We can modify Theorem 1 to apply to a Cassegrain antenna by the following procedure.

Let us define the per unit change in electric field from the measurement frequency to the estimation frequency as e(x) i.e.,

$$E(f_e, \underline{x}) = E(f_m, \underline{x}) [1 + e(\underline{x})].$$

Also let us define the phase error produced by the feed system as $\ell(f, \underline{x})$. It is important to distinguish this type of phase error from the phase errors caused by reflector surface deviations, $\delta(\underline{x})$, because $\ell(f, \underline{x})$ will not scale with frequency. Furthermore, suppose that the design efficiency which includes ℓ-type phase errors is defined as $\eta_o(f)$.

With these definitions bounds similar to the ones given in Theorem 1 are derived in Appendix C. This is done under the assumption that terms

up to third order in $e(\underline{x})$, $\ell(x)$, and $\delta(x)$ are retained. The only fourth order terms retained are $\delta^4(\underline{x})$ terms since the surface tolerance, $\delta(\underline{x})$, is small but more significant than $e(x)$ or $\ell(x)$. In addition several terms were evaluated under the Ruze statistical model *. These bounds on the efficiency are given by

$$\eta(f_e) \le \eta_o(f_e) - P\left[\eta_o(f\ ) - \eta'(f_e)\right]\left(\frac{f_e}{f_m}\right)^2 + \eta_o(f_m)\sup S + P B\left(\frac{f_e}{f_m}\right)^2$$

$$+ \left[\eta_o(f_m) - \eta_o(f_e)\right]\sigma^2(f_e), \quad \text{for all } P$$

and

$$\eta(f_e) \ge \eta_o(f_e) - P\left[\eta_o(f_m) - \eta'(f_m)\right]\left(\frac{f_e}{f_m}\right)^2 + \eta_o \inf S$$

$$-PB\left(\frac{f_e}{f_m}\right)^2 + \left[\eta_o(f_m) - \eta_o(f_e)\right]\sigma^2(f_e), \text{ for all } P$$

where $\sigma(f_e)$ is the rms phase error in the aperture plane.

As an example, suppose one wanted to estimate the efficiency of the JPL 85-foot antenna at S-band (2.388 GHz) using X-band (8.448 GHz) data. The necessary information is given by

$$\sigma(S) = 0.166 \text{ radians}^{[74]}$$

$$K(X) = 2.9 \text{ radians}^{[75]}$$

*The statistical model is used to make the problem tractable. However, it is felt that the terms on which the statistical analysis is used will always be small. In fact, the only non-zero term is $[\eta_o(f_m)-\eta_o(f_e)]\sigma^2(f_e)$, which is usually quite negligible. Thus, the method is only weakly dependent on the statistical model.

$$\eta_o(S) \quad = 63.0\%^{[76]}$$

$$\eta_o(X) \quad = 64.7\%^{[77]}$$

$$\eta'(X) \quad = 44.7 \pm 4.9\% (3\sigma)^{[78]}$$

The efficiency estimate from the above bounds is $60.4 \pm 1.4\%(3\sigma)$. This compares favorably with the measured value of $59.8 \pm 8.9\%(3\sigma)$[79].

This data assumes that the error in the measurement is a random variable. The error bars are given as a percentage. Then the number of sigma units that this percentage represents is given in parenthesis. This procedure is probably the one most commonly used for efficiency measurements. The error is usually assumed to be Gaussian so the number of sigma units represents the confidence level for the measurement. For example, a 2σ measurement means that the probability is 95% that the true value lies within the stated error bars.

The error bars, stated in this way, may be used as peak errors as required by Theorem 1 and Theorem 2. Theorem 2 will be presented in the following section. Then, the probability that the true efficiency lies between the inferred bounds is the greater than or equal to the probability that the measured efficiency lies between its error bars.

Theorem 2 is a generalization of Theorem 1. It gives a method of predicting the efficiency of a prime focus reflector antenna at frequency f_e based on measurements at two other frequencies. Here again one source of error is the error in the original measurements, but the mathematical error is considerably less since three terms of the cosine series are used.

Thus, it is possible to use a measurement well beyond the gain maximum frequency and obtain more leverage in reducing the measurement errors below gain maximum frequency.

Theorem 2

If the feed system of a prime focus reflector antenna is scaled at frequencies f_e, f_1, and f_2, and,

$$|\eta'(f_1) - \eta(f_1)| = B_1,$$

$$|\eta'(f_2) - \eta(f_2)| \le B_2,$$

$$|\delta(f_e, \underline{x}) - \delta(f_e, \underline{y})| \le K(f_e) \text{ all } \underline{x} \text{ and } \underline{y},$$

and A_2'' and A_4'' are roots of the simultaneous equations

$$\eta_o + A_2'' f_1^2 + A_4'' f_1^4 = \eta'(f_1)$$

$$\eta_o + A_2'' f_2^2 + A_4'' f_2^4 = \eta'(f_2).$$

Then,

$$\eta(f_e) \le \eta_o + P A_2'' f_e^2 + Q A_4'' f_e^4 + |F_1| B_1 + |F_2| B_2 + \eta_o \sup S, \text{ all } P \text{ and } Q$$

and

$$\eta(f_e) \ge \eta_o + P A_2'' f_e^2 + Q A_4'' f_e^4 - |F_1| B_1 - |F_2| B_2 + \eta_o \inf S, \text{ all } P \text{ and } Q,$$

where

$$S = \left\{ z : z = F_2 T\left[\frac{f_2}{f_e} u\right] - F_1 T\left[\frac{f_1}{f_e} u\right] + T[u] - (1-P) u^2/2! + (1-Q) u^4/4! ; \right.$$

$$\left. 0 \le u \le K(f_e) \right\}$$

and

$$F_1 = \frac{f_e^2 (P f_2^2 - Q f_e^2)}{f_1^2 (f_2^2 - f_1^2)}$$

$$F_2 = \frac{f_e^2 (P f_1^2 - Q f_e^2)}{f_2^2 (f_2^2 - f_1^2)}$$

The remainder function T[x] is

$$T[x] = \cos(x) - [1 - x^2/2! + x^4/4!].$$

This Theorem is useful when the peak-to-peak phasing error is large. Consider the case of The University of Texas 16-foot antenna as delivered by the contractor. It had an astigmatic phasing error as discussed in Chapter III. This will be discussed in Chapter VI. Suppose one wanted to predict the efficiency at 35 GHz based on measurement at 70 GHz and 94 GHz. The data is repeated as follows, Cogdell[80]

η_o = 65.0

$\eta'(94)$ = 44.0 ± 7% (3σ)

$\eta'(70)$ = 58.0 ± 7% (3σ)

K(94) = 4.3

With this data the predicted efficiency at 35 GHz is 61.58 ± 3.11% (3σ). The measured value is 62 ± 9% (3σ)[81]. This measurement is based on an astronomical measurement and assumes a disk temperature of 151° for Jupiter[82] at 35 GHz.

The advantage of Theorem 2 over Theorem 1 is that the mathematical error of approximation is considerably less for a given peak-to-peak phase error. Thus, the method is appropriate at higher frequencies where there is significant tolerance loss. The disadvantage of this method is that two measurements of the efficiency must be made. The method does, however, modestly improve the accuracy of the inferred efficiency.

If the measurement errors have the same sign, the errors in the inferred efficiency tend to cancel. This fact can be exploited to obtain even more accurate inferred efficiencies. Whether or not there will be common errors in both measurements depends, of course, on how the efficiency is measured. However, if the same equipment and calibration techniques are used at both measurement frequencies some errors should appear in common.

For example, in the efficiency measurement method used by Bathker[83], the uncertainty in the directivity of the standard gain horn is the dominant error. The directivity of this horn was calculated by integrating the experimentally measured pattern. If this procedure were repeated at two frequencies, the error in the horn calibration would tend to have the same sign. If the standard gain horns for the two measurements were scale models of each other, the error in horn calibration should be the same in both cases.

One possible way of dealing with the common error is to assume that the measurement errors are correlated random variables. This assumption will be avoided, however, since these measurement errors are not

random variables, as pointed out by Cogdell[84] and Ludwig[85]. If they were true random variables, repeating the measurement should increase the accuracy. However, it is known from experience and intuition that this averaging effect does not occur. Instead, errors tend to be systematic and bias the results.

Instead of assuming that the measurement errors are correlated random variables, let us define the common error to be c.

Thus,

$$\eta'(f_1) - \eta(f_1) = c + r_1$$

$$\eta'(f_2) - \eta(f_2) = c + r_2$$

where r_1 and r_2 are the remainder errors which are not common to both measurements. Bounds for the efficiency can now be derived in terms of the peak values of c, r_1, and r_2, which will be denoted by C, R_1, and R_2.

With this notation the bounds in Theorem 2 become

$$\eta(f_e) \le \eta_o + P A_2'' f_e^2 + Q A_4'' f_e^4 + |F_1| R_1 + |F_2| R_2 + |F_3| C + \eta_o \sup S,$$

all P and Q,

and

$$\eta(f_e) \ge \eta_o + P A_2'' f_e^2 + Q A_4'' f_e^4 - |F_1| R_1 - |F_2| R_2 - |F_3| C + \eta_o \inf S,$$

all P and Q,

where all of the symbols are the same as before and

$$F_3 = \left(\frac{f_e}{f_1 f_2}\right)^2 \left[P (f_1^2 + f_2^2) - Q f_e^2\right].$$

Suppose that 5% of the 7% error in the example considered before was in common. It should be emphasized that this is a hypothetical example.

η_o = 65.0%

$\eta(94)$ = 44.0%

$\eta(70)$ = 58.0%

R_1 = 2%

R_2 = 2%

C = 5%

K(94) = 4.3 radians.

The bounds at several frequencies were optimized on a digital computer. The results are shown in Table 2.

This table has two interesting features. The first is that the bounds at the measurement frequencies, 70 and 94 GHz, are much better than the original measurements. This happens because more information is used than is contained in the single measurement. The second interesting feature of this table is that Theorem 2 predicts a negative upper bound at 200 GHz. The efficiency of an antenna is always positive, so a negative upper bound is a contradiction. It simply means that the data is inconsistent. In particular, this inconsistency can be traced to the fact that the measured efficiency at 94 GHz is too far below the measured value at 70 GHz. Thus, the parameter A_4 is negative while it should be positive.

This contradiction is not surprising since there is no reason to believe that these two measurements had any errors in common. The

Frequency GHz	Lower Bound of Efficiency %	P	Q	Upper Bound of Efficiency %	P	Q
35	60.17	1.32	1.36	61.61	1.23	14.02
70	51.00	1.00	1.00	51.79	1.10	3.10
94	40.50	0.94	.52	41.73	1.09	1.70
134	18.63	0.80	.22	21.76	0.99	0.94
200	-22.03	0.58	.07	- 5.98	0.93	0.73

Table 2

dominant error in these measurement is the uncertainty in the gain of a standard gain horn. The gain for the horn was measured at 94 GHz while a calculated value was used for the 70 GHz efficiency measurement. This example makes it clear that Theorem 2 can be used to check the consistency of antenna efficiency data.

E. The Design Efficiency η_o

In the above it was assumed that the design efficiency, η_o, is not a function of frequency. In practice the design efficiency includes ohmic losses, which are proportional to the square root of the frequency. However, these effects usually are small. For example, at 100 GHz an aluminum reflector absorbs only 0.1% of the incident power. Thus, the assumed constancy of η_o with frequency will introduce negligible errors in the results.

Clearly the accurate calculation of η_o is crucial to this method of scaling. The uncertainty in η_o was not included since it is typically much less than the uncertainty in the efficiency measurement. For a prime-focus instrument with solid supporting spars η_o may be calculated within $\pm$ 0.2% see Ludwig[86], [87]. It would be a simple matter however to account for uncertainty in η_o in the error bounds.

F. Conclusion

Two methods for predicting the efficiency at frequencies different from the one at which it was measured have been presented. The first method is based on a single efficiency measurement; the second uses two measurements. It has been shown that the error made in predicting the gain at a lower frequency is often considerably less than the measurement error. In fact is possible to achieve much better gain measurements by this method than any other known to the author. In addition, the theorems offer an easy way to check the consistency of antenna efficiency data. Unlike many antenna tolerance results, the method is independent of any statistical modeling in the case of prime-focus instruments, and is only weakly dependent upon it in the case of a Cassegrain antenna.

Chapter VI

Calibration Program for the 16-Foot Antenna

In 1963 The University of Texas acquired a 16-foot reflector antenna designed to operate up to 140 GHz. It was first located in Austin, Texas, but in 1967 it was moved to Mount Locke, near Fort Davis, Texas. In Austin the antenna worked well at 95 GHz; however, after moving the antenna performance was unsatisfactory at this frequency. At 95 GHz no satisfactory focus position could be found, and the beamwidths were always broad in at least one of the principle planes. In addition, one side-lobe appeared at a level of -7 dB when the antenna was adjusted for maximum gain.

This chapter is an account of how the performance of this antenna was improved and a report of the subsequent careful evaluation. The antenna evaluation work reported here provides concrete examples of the methods presented in Chapters IV and V. In addition, this chapter is meant to be a sequel to an earlier antenna evaluation report by Cogdell[88].

The section A contains a detailed account of the measurement and correction of astigmatism in the reflector. The section B is a discussion of the patterns of the antenna. The patterns before the reflector adjustment are compared with the patterns after the adjustment. Both sets of patterns are compared with the theoretical patterns. Section C is a discussion of a careful antenna efficiency measurement at 134 GHz. A table is also presented which shows the inferred efficiencies at other frequencies of interest. Section D is a discussion of two antenna stability tests.

A. Adjustment of the Reflector

The 16-foot antenna was known to exhibit astigmatism because it satisfied all of the properties given in Chapter IV. Thus, in June of 1969 it was decided to adjust the figure of the reflector by shimming the backup structure.

The positions of the shims that were used are adjacent to the eight bolts shown in Figure 25. The shim positions were numbered as W1 through W4 and E1 through E4 as shown in Figure 25. This figure also shows a top view of the antenna and the reference coordinates in the aperture plane. The coordinates x_1 and u_1 are in the declination plane while x_2 and u_2 are in the polar plane. Driving the antenna south increases the angular coordinate u_1 while driving the antenna east increases u_2.

The adjustment was carried out by a two step procedure. The first step was making the φ direction agree with the servo coordinates; the second was reducing the magnitude of the astigmatism. The astigmatism was measured by observing the φ direction beamwidths. Thus, the φ direction was first made to correspond with the servo coordinates so that the φ direction beamwidths could be observed more easily.

In each of the two steps outlined above the quantity of interest was first measured. Then, an arbitrary adjustment was made and the quantity of interest remeasured in order to get a feeling for the scale of the change produced by the added shims. This iterative procedure was continued until satisfactory results were obtained. For the φ direction adjustment of two different shim positions excluding the original state were tried.

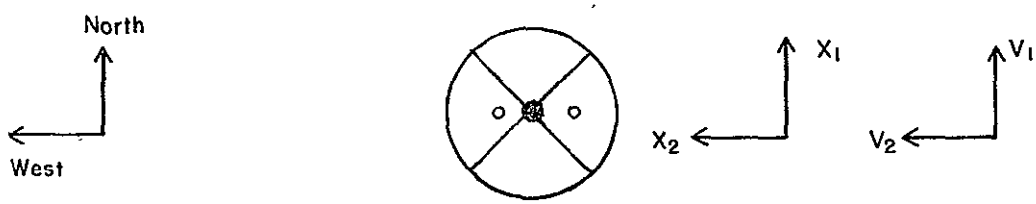

Top view of Antenna

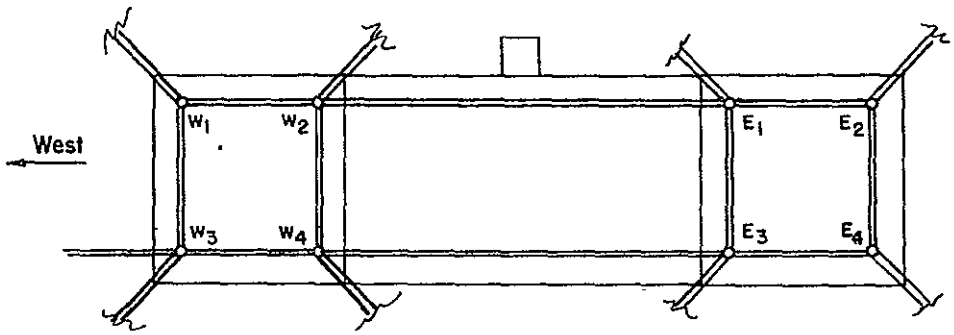

Top view of Support

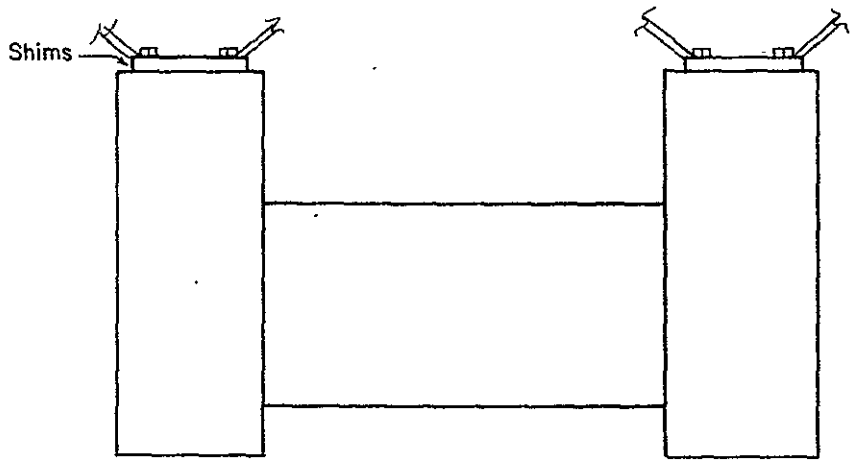

Front view of Support

ANTENNA SUPPORT STRUCTURE

Fig. 25

The magnitude of the astigmatism was luckily reduced to an insignificantly small value by the first shim change.

The initial φ-direction was known because it was calculated carefully through the computer minimization procedure discussed as an example in Chapter III. However, it was decided to plot a contour map to see whether any difficulty was encountered in inferring the symmetry direction directly from a contour map. This first contour map is shown in Figure 26. The symmetry direction that was inferred from this was $\varphi = -18°$. This compares favorably with the value of $\varphi = -9.0°$ which was obtained from the computer minimization.

In order to bring the major axis of the elipse closer to the polar direction a shim of 0!!020 was put in positions W1 and E3. Subsequently, another contour map was taken at approximately 10 dB down from the beam peak. The results of this are shown in Figure 27. The major axis of the best fitting elipse, drawn by eye, was taken to be +31°. It is apparent that the error was overcorrected with the 0!!020 shim.

Having removed the 0!!020 shim a 0!!008 shim was put under W1 and E3. This value was chosen by linear interpolation between the -18° and +31° values. The resulting contour map is shown in Figure 28. From Figure 28 it is apparent that the φ direction agrees with the servo coordinate direction, so the first step was complete.

The magnitude of the astigmatism was then measured. The polar and declination beamwidths were taken at five different feed positions.

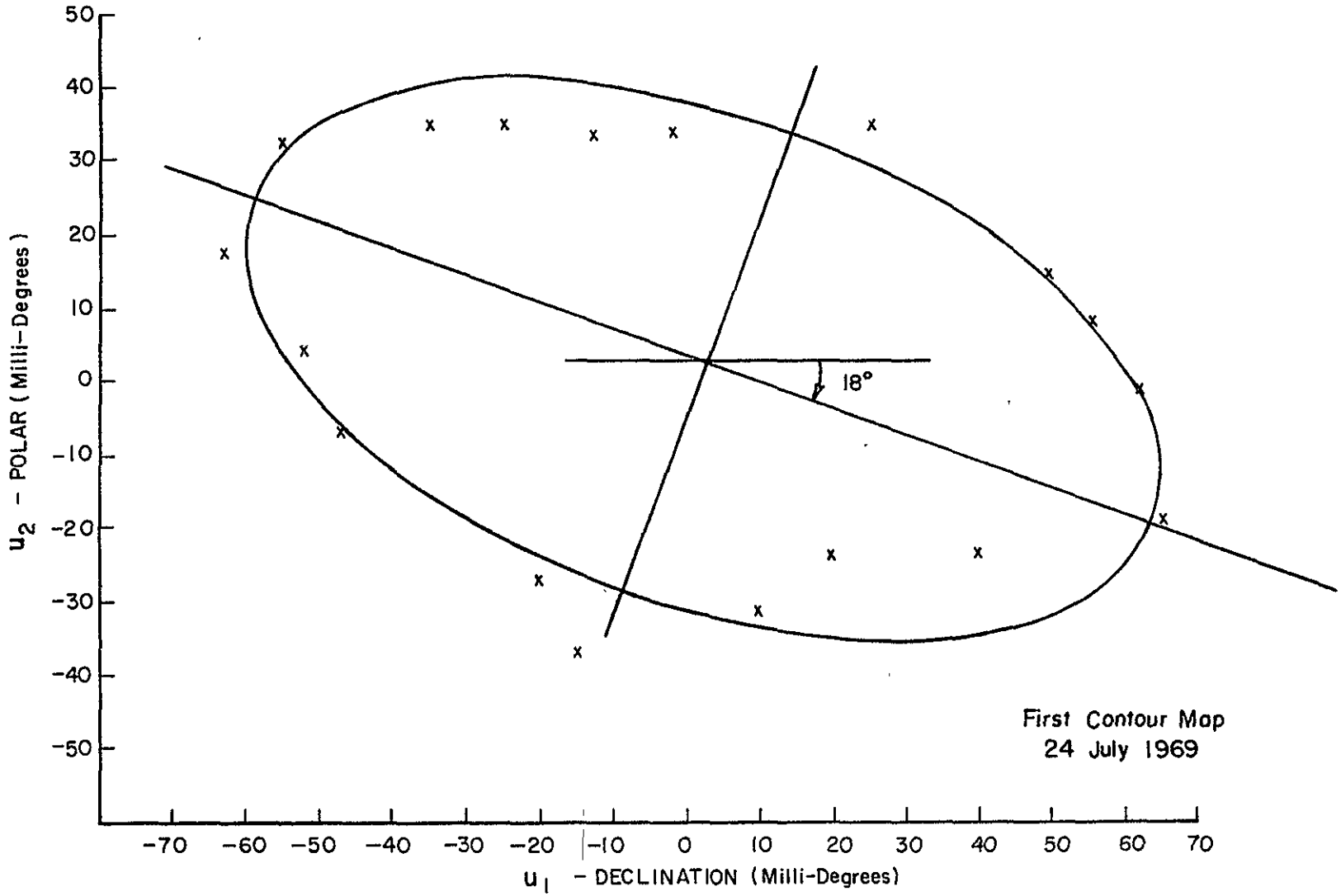
50
40
30
20
10
0
-10
-20
-30
-40
-50
u_2 - POLAR (Milli-Degrees)
18°
First Contour Map
24 July 1969
-70 -60 -50 -40 -30 -20 -10 0 10 20 30 40 50 60 70
u_1 - DECLINATION (Milli-Degrees)

Fig. 26

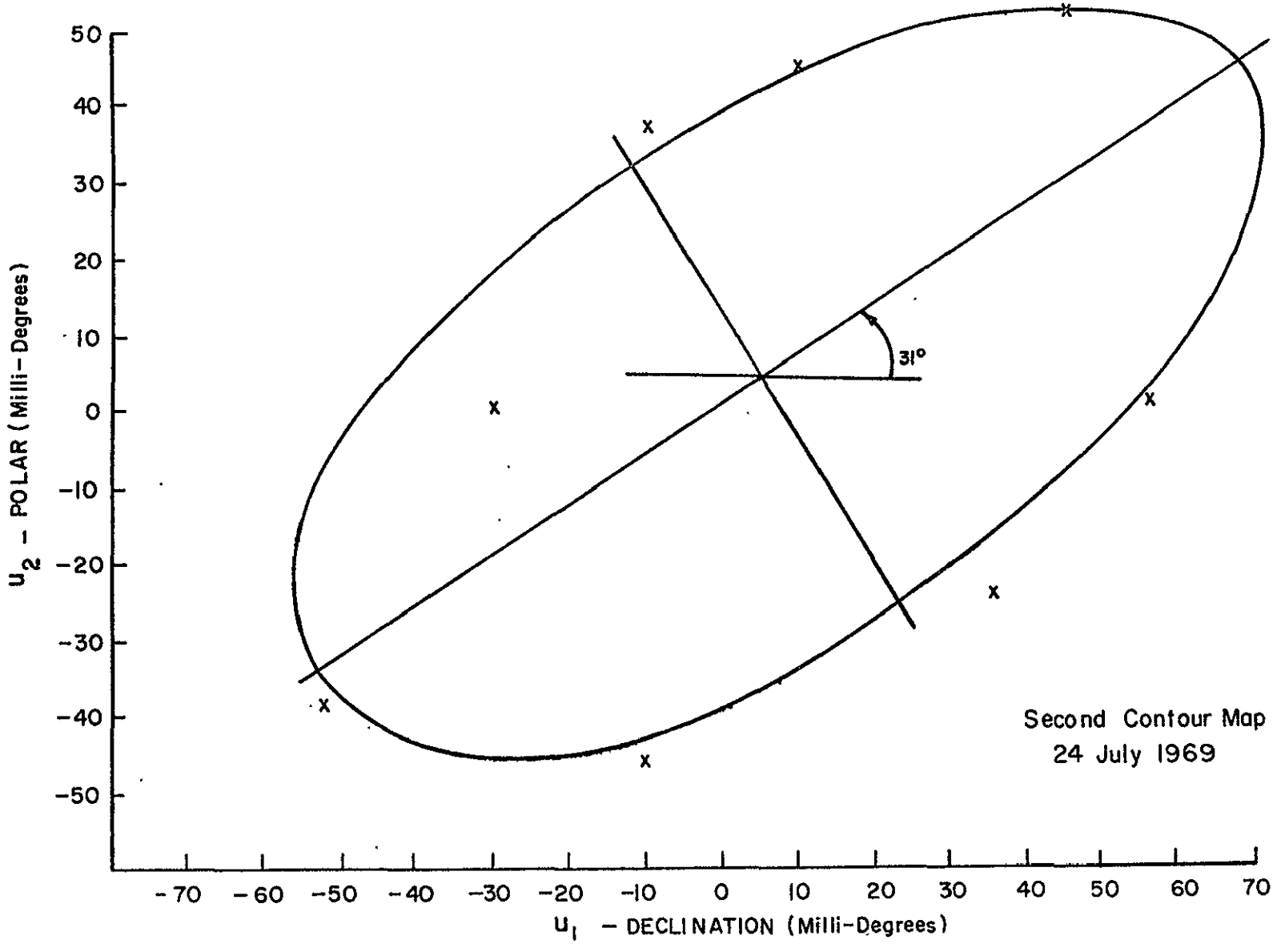
50
40
30
20
10
0
-10
-20
-30
-40
-50
u_2 - POLAR (Milli-Degrees)
31°
Second Contour Map
24 July 1969
-70 -60 -50 -40 -30 -20 -10 0 10 20 30 40 50 60 70
u_1 - DECLINATION (Milli-Degrees)

Fig. 27

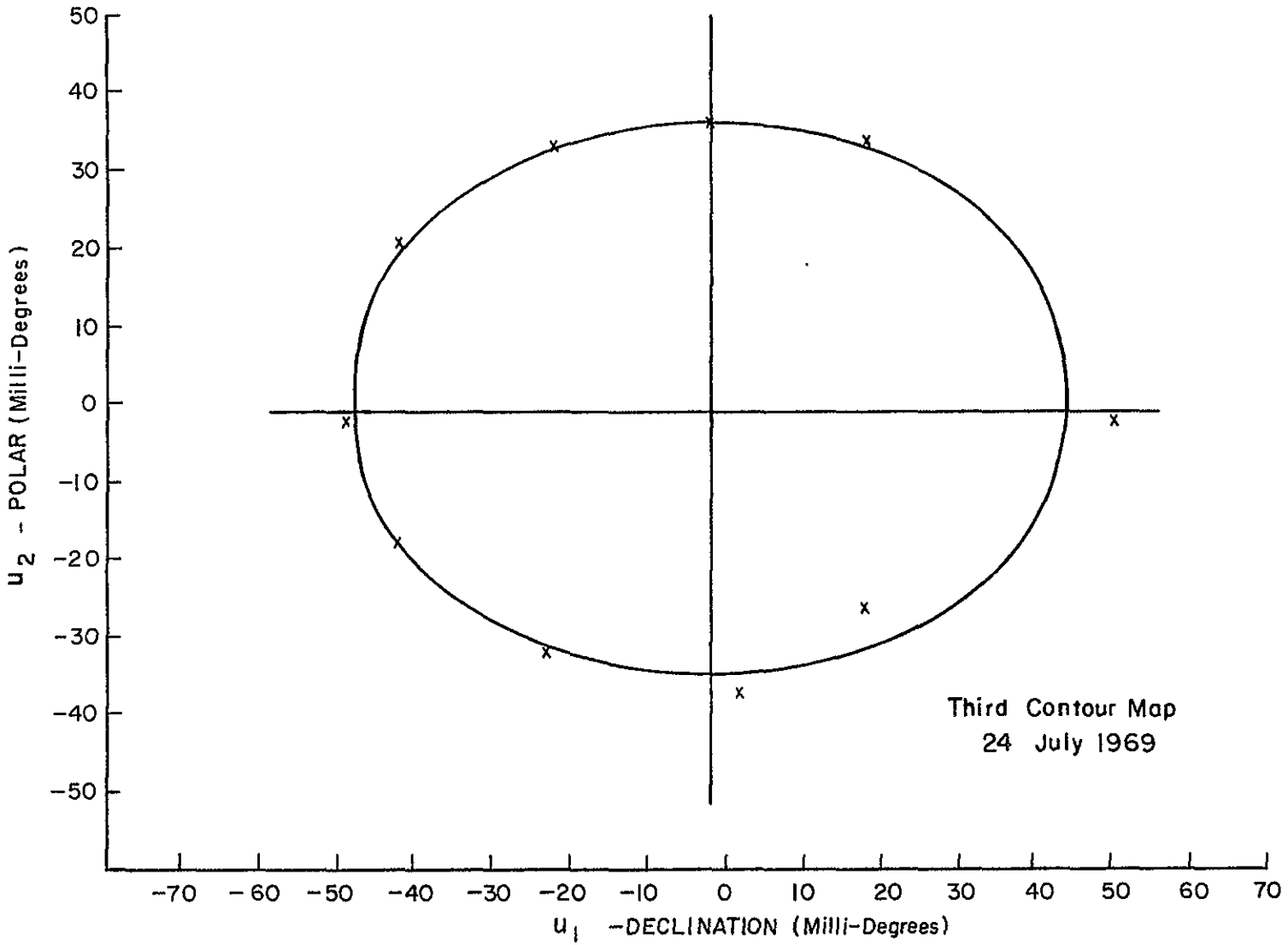
50
40
30
20
10
0
-10
-20
-30
-40
-50
u_2 - POLAR (Milli-Degrees)
-70 -60 -50 -40 -30 -20 -10 0 10 20 30 40 50 60 70
u_1 -DECLINATION (Milli-Degrees)
Third Contour Map
24 July 1969

Fig. 28

The results are shown in Figure 29. From this figure it is apparent that most of the astigmatic phase error still remains as might be expected. The error was estimated as $\alpha = 1.3$.

The action taken was to insert a shim of 0.010 under W4, W1, E2, and E3. The astigmatism was then remeasured by taking beamwidths at four different shim positions. Since the beamwidths did not change significantly it was concluded that fortunately the astigmatic phase error was substantially corrected. Figure 30 shows a contour map taken after this adjustment was completed. It shows no significant directional preference.

B. Patterns of the Antenna

The method used for taking the patterns of the antenna has been discussed in detail by Cogdell[89]. The antenna servo drives the antenna through the direction of the transmitter sight. At the same time the recording chart is marked every 0.010 degrees by a trigger placed in the servo display network.

Figure 31 shows a contour map of the error free pattern. The horn feed has the dimensions that correspond to the maximum forward gain for an antenna of F/D = 0.5. These dimensions $1.25\lambda \times 0.9\lambda$. The efficiency achieved by the feed design is 65.02%.

Figures 32 and 33 show the antenna patterns reported by Cogdell.[90] These were taken prior to the reflector surface adjustment discussed in the previous section. These figures show the design pattern or phase error free pattern drawn on the same scale. Figure 29 shows the 35 GHz pattern. It is very close to the theoretical pattern although one can see the beginnings

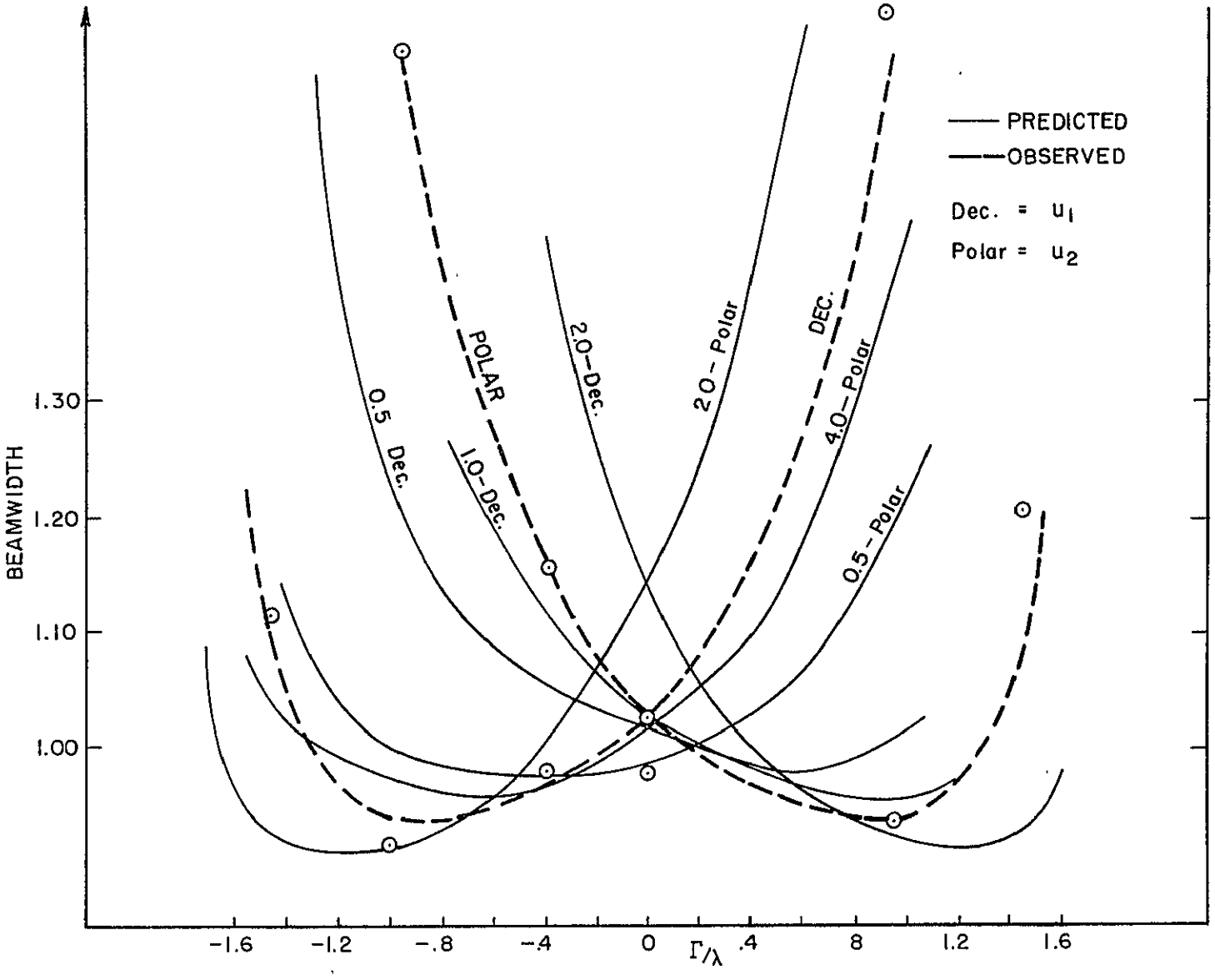

PREDICTION OF ASTIGMATISM WITH BEAM WIDTH MEASUREMENTS

Fig. 29

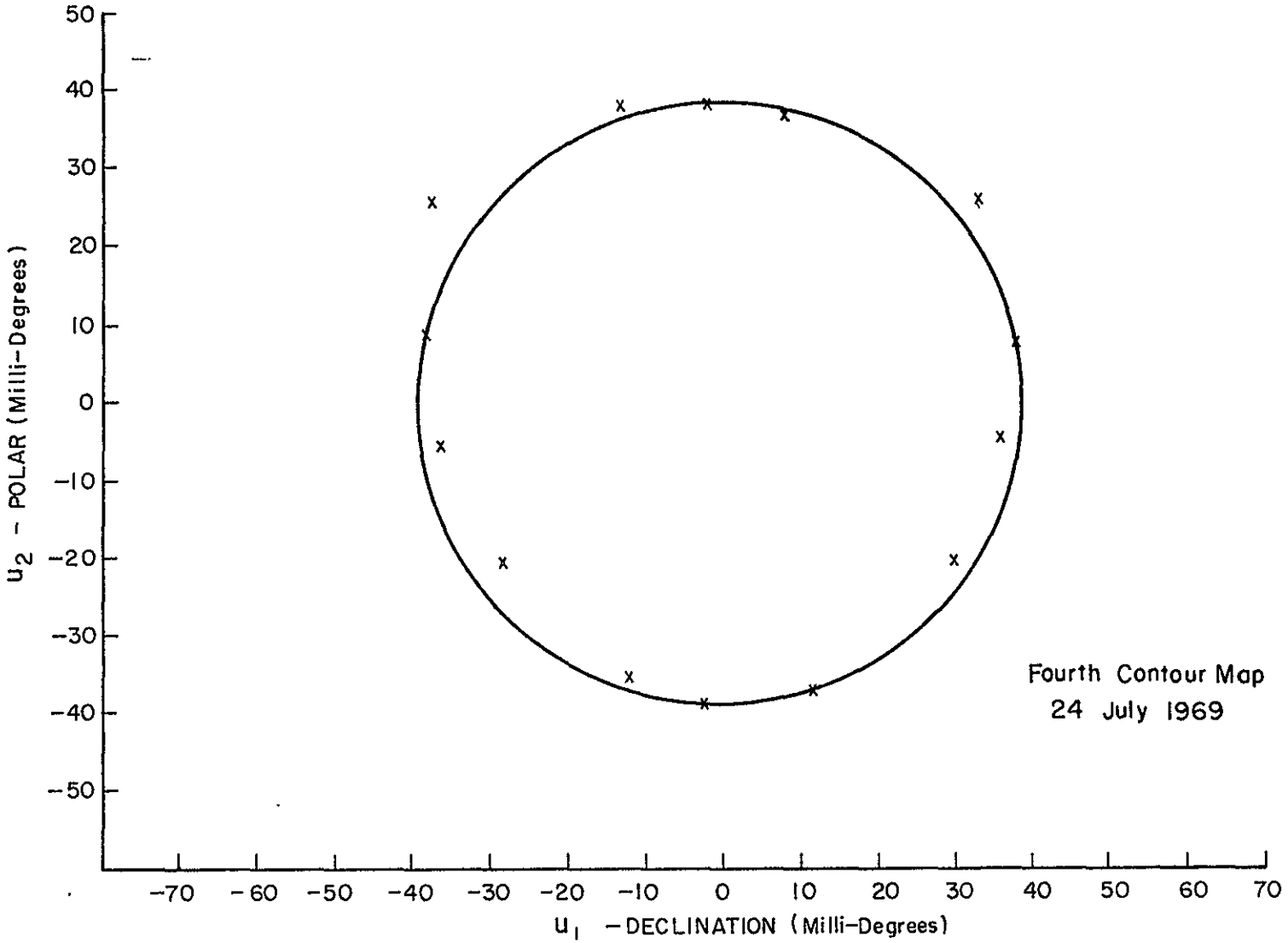
50
40
30
20
10
0
-10
-20
-30
-40
-50
u_2 - POLAR (Milli-Degrees)
-70 -60 -50 -40 -30 -20 -10 0 10 20 30 40 50 60 70
u_1 - DECLINATION (Milli-Degrees)
Fourth Contour Map
24 July 1969

Fig. 30

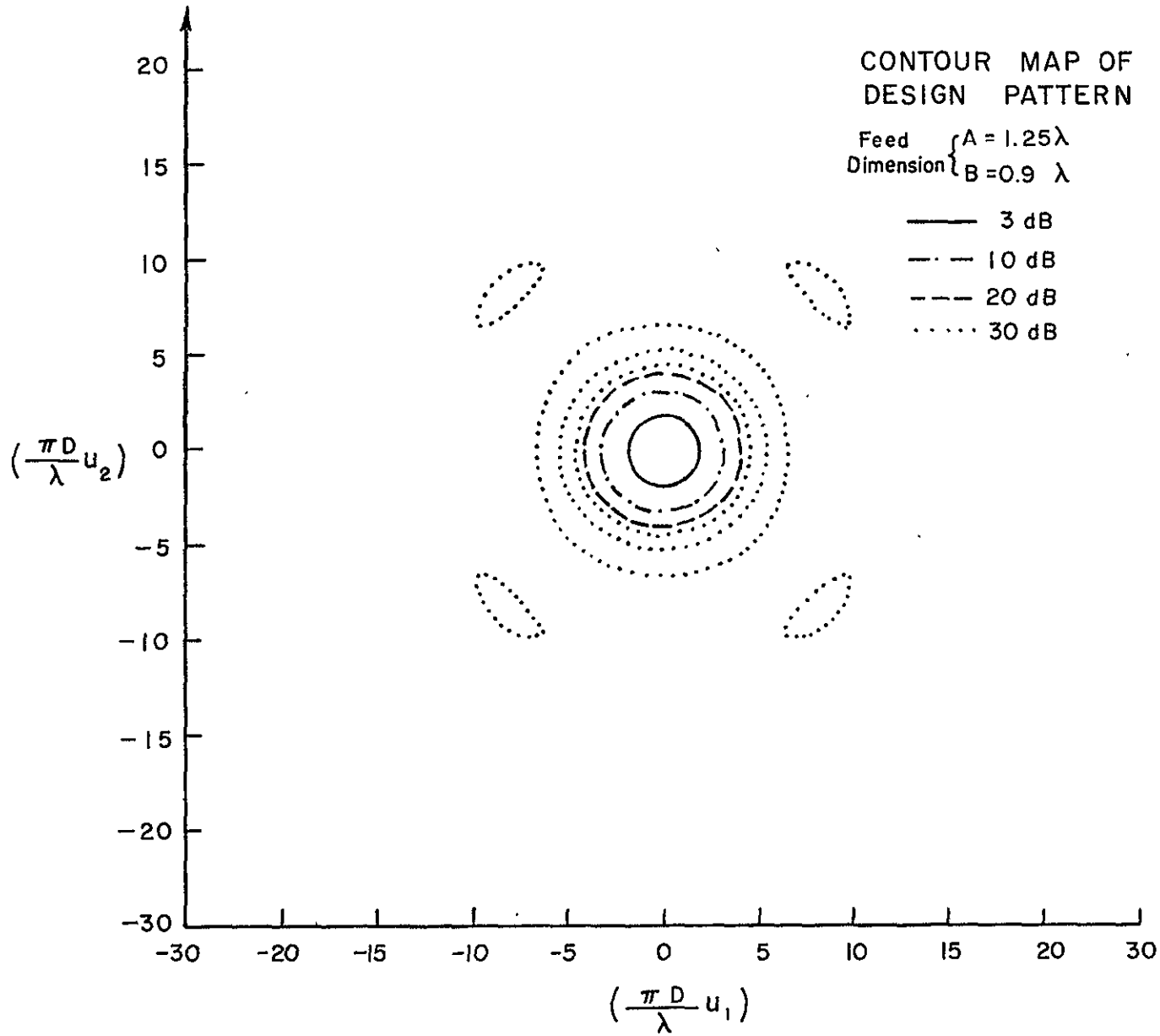
CONTOUR MAP OF
DESIGN PATTERN
Feed Dimension
A = 1.25λ
B = 0.9 λ
3 dB
10 dB
20 dB
30 dB
20
15
10
5
0
−5
−10
−15
−20
−30
(πD/λ u2)
−30 −20 −15 −10 −5 0 5 10 15 20 30
(πD/λ u1)

Fig. 31

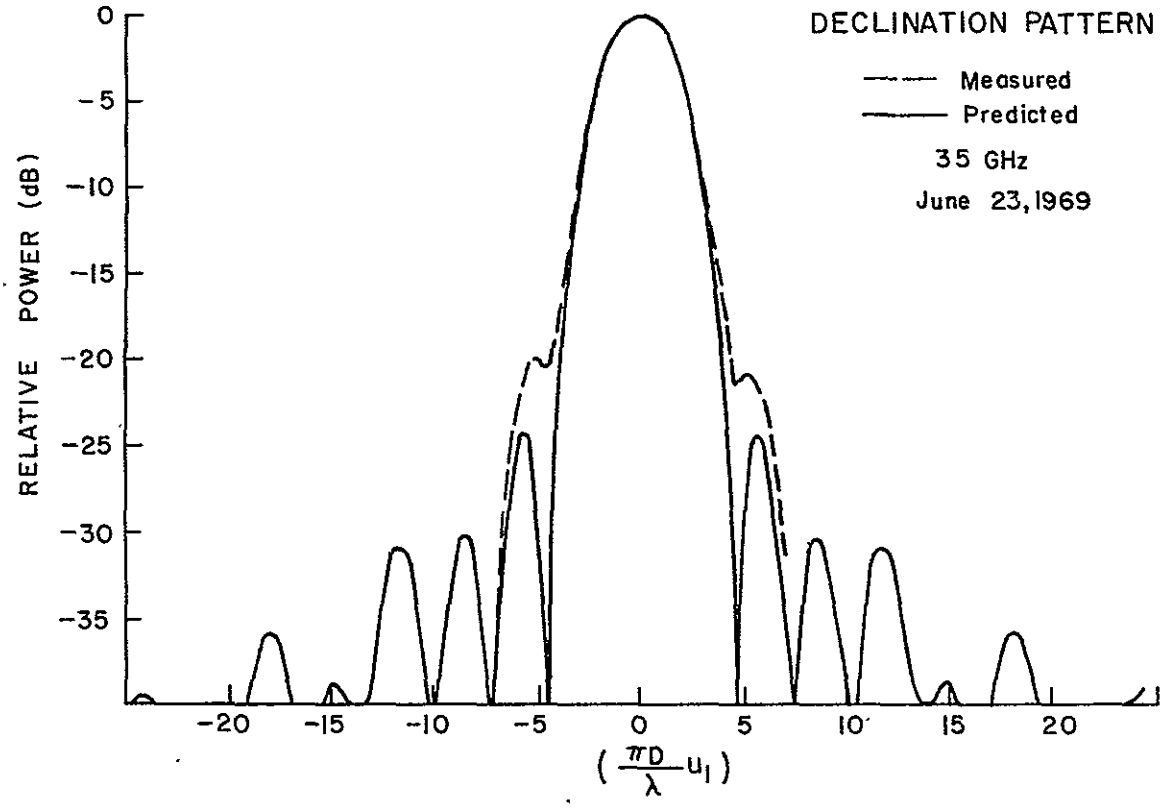
DECLINATION PATTERN
Measured
Predicted
35 GHz
June 23, 1969
RELATIVE POWER (dB)
0
-5
-10
-15
-20
-25
-30
-35
-20
-15
-10
-5
0
5
10
15
20
$(\frac{\pi D}{\lambda} u_1)$

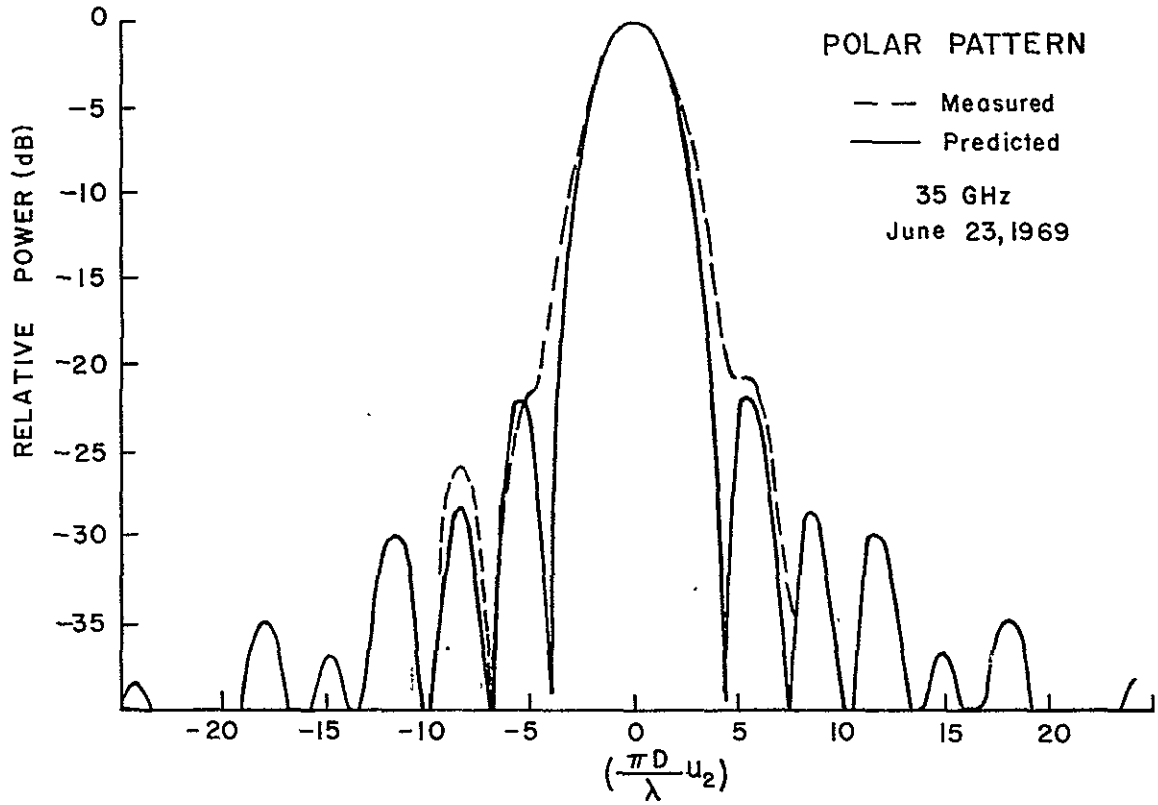
POLAR PATTERN
Measured
Predicted
35 GHz
June 23, 1969
RELATIVE POWER (dB)
0
-5
-10
-15
-20
-25
-30
-35
-20
-15
-10
-5
0
5
10
15
20
$(\frac{\pi D}{\lambda} u_2)$

Fig. 32

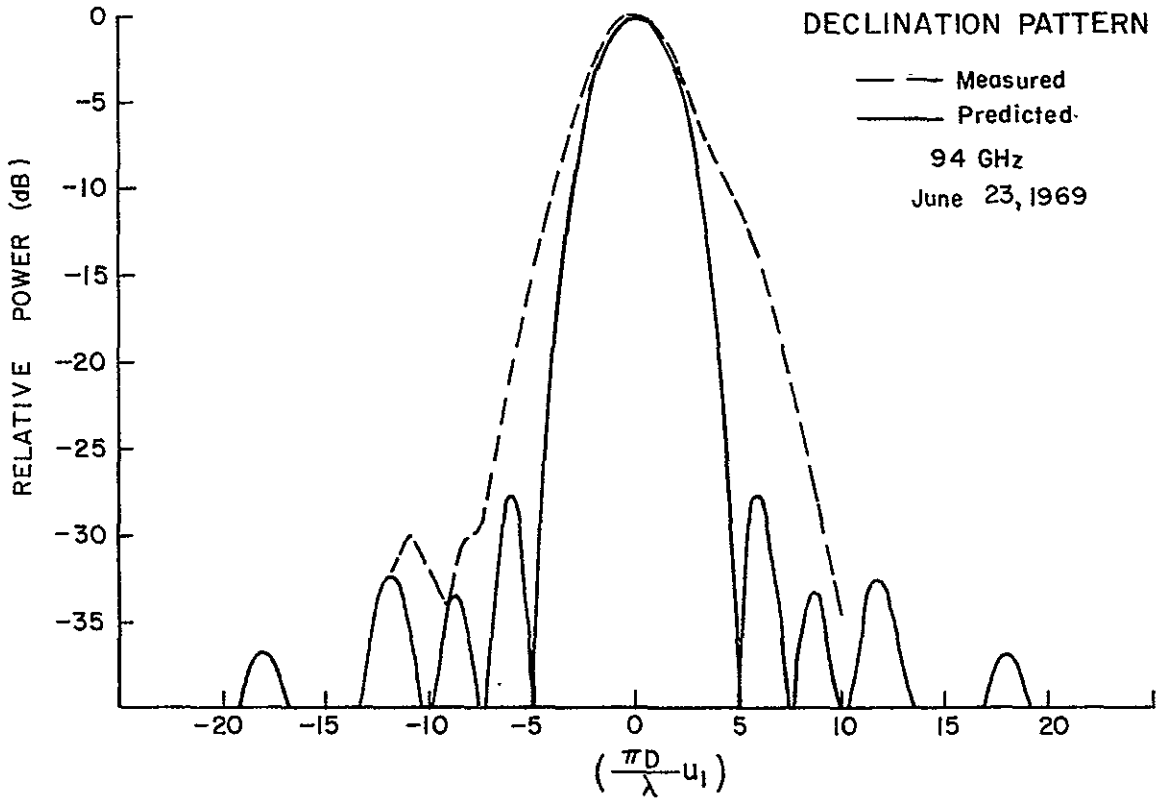
DECLINATION PATTERN
Measured
Predicted
94 GHz
June 23, 1969
RELATIVE POWER (dB)
0
-5
-10
-15
-20
-25
-30
-35
-20
-15
-10
-5
0
5
10
15
20
$(\frac{\pi D}{\lambda} u_1)$

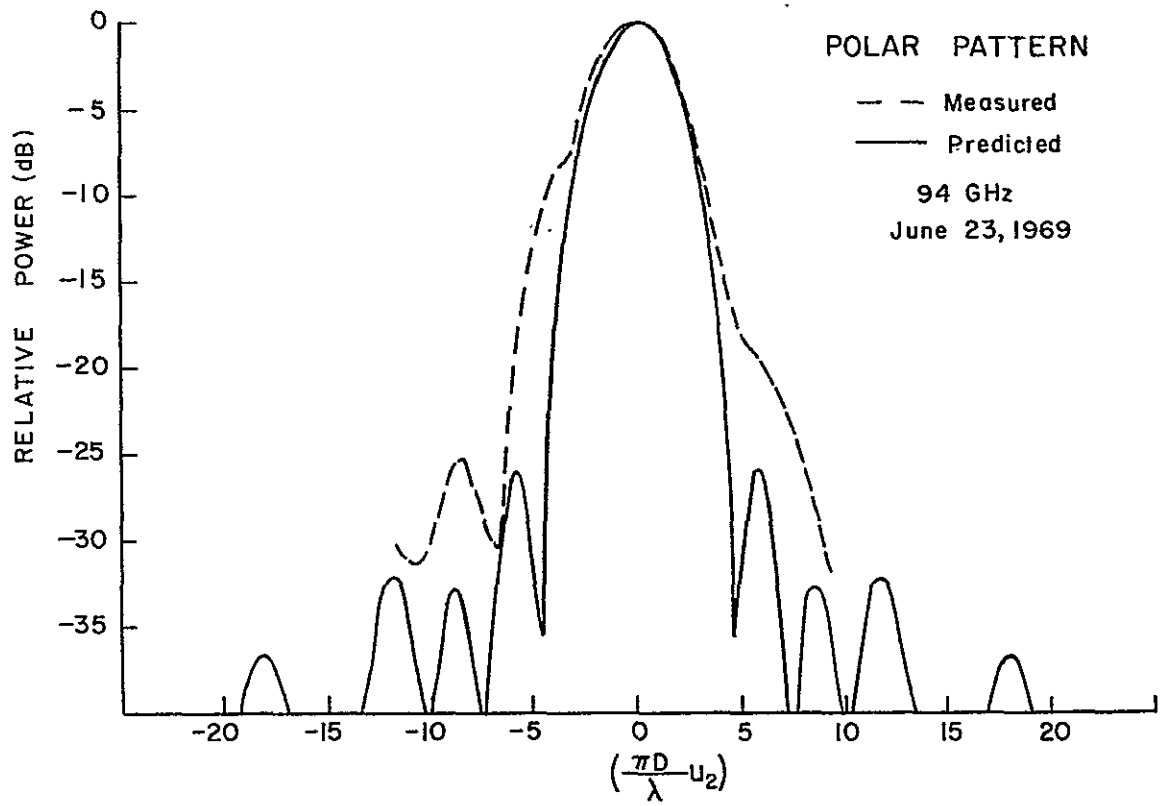
POLAR PATTERN
Measured
Predicted
94 GHz
June 23, 1969
RELATIVE POWER (dB)
0
-5
-10
-15
-20
-25
-30
-35
-20
-15
-10
-5
0
5
10
15
20
$(\frac{\pi D}{\lambda} u_2)$

Fig. 33

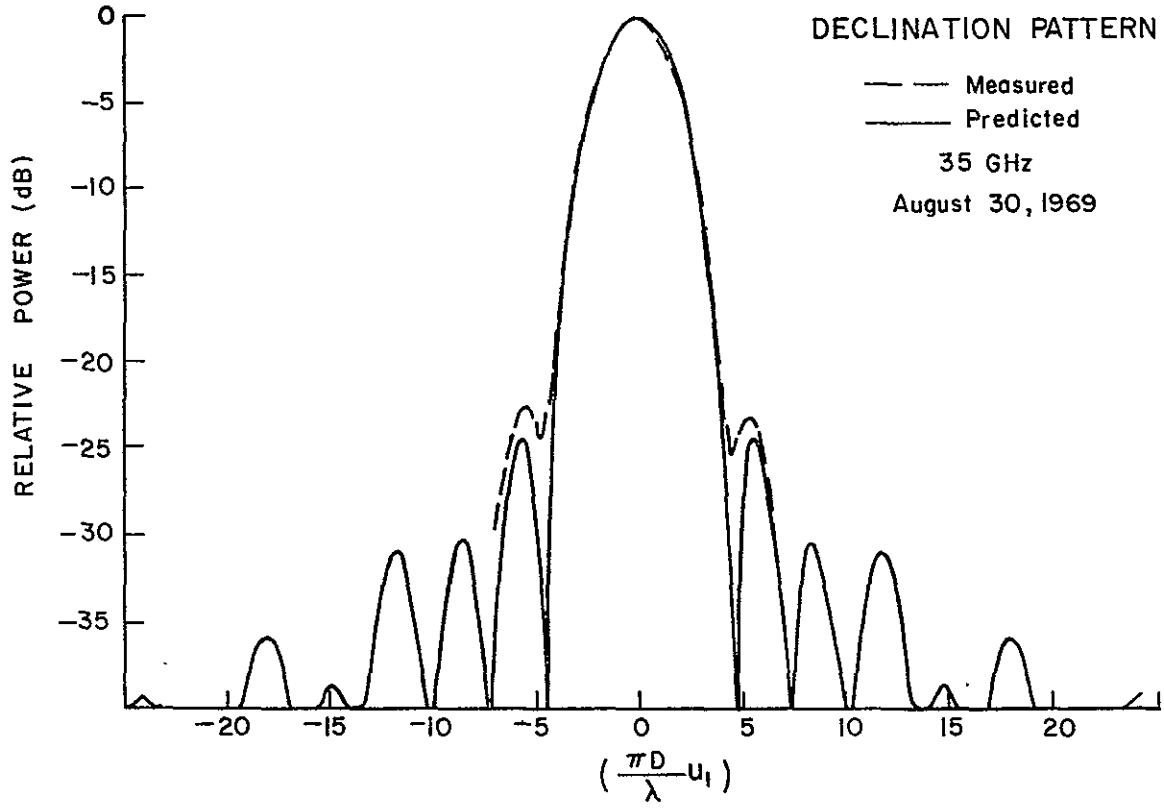
DECLINATION PATTERN
Measured
Predicted
35 GHz
August 30, 1969
RELATIVE POWER (dB)
0
-5
-10
-15
-20
-25
-30
-35
-20
-15
-10
-5
0
5
10
15
20
$(\frac{\pi D}{\lambda} u_1)$

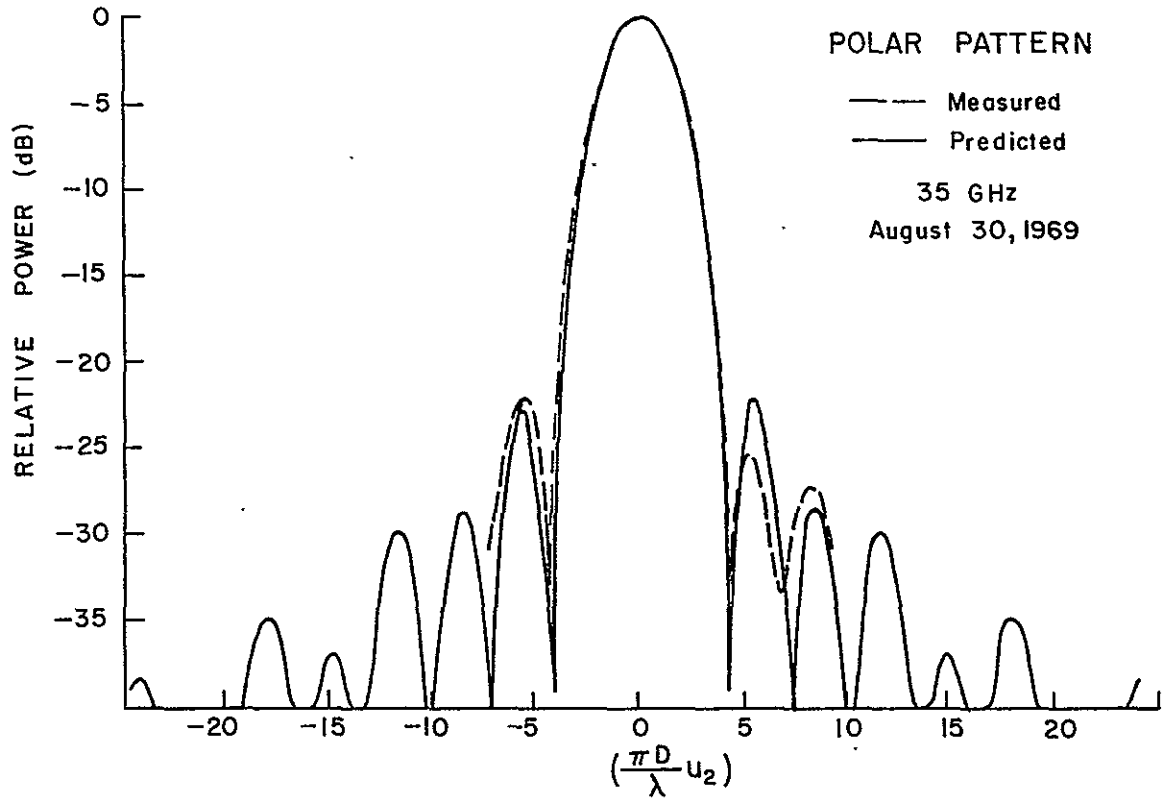
POLAR PATTERN
Measured
Predicted
35 GHz
August 30, 1969
RELATIVE POWER (dB)
0
-5
-10
-15
-20
-25
-30
-35
-20
-15
-10
-5
0
5
10
15
20
$(\frac{\pi D}{\lambda} u_2)$

Fig. 34

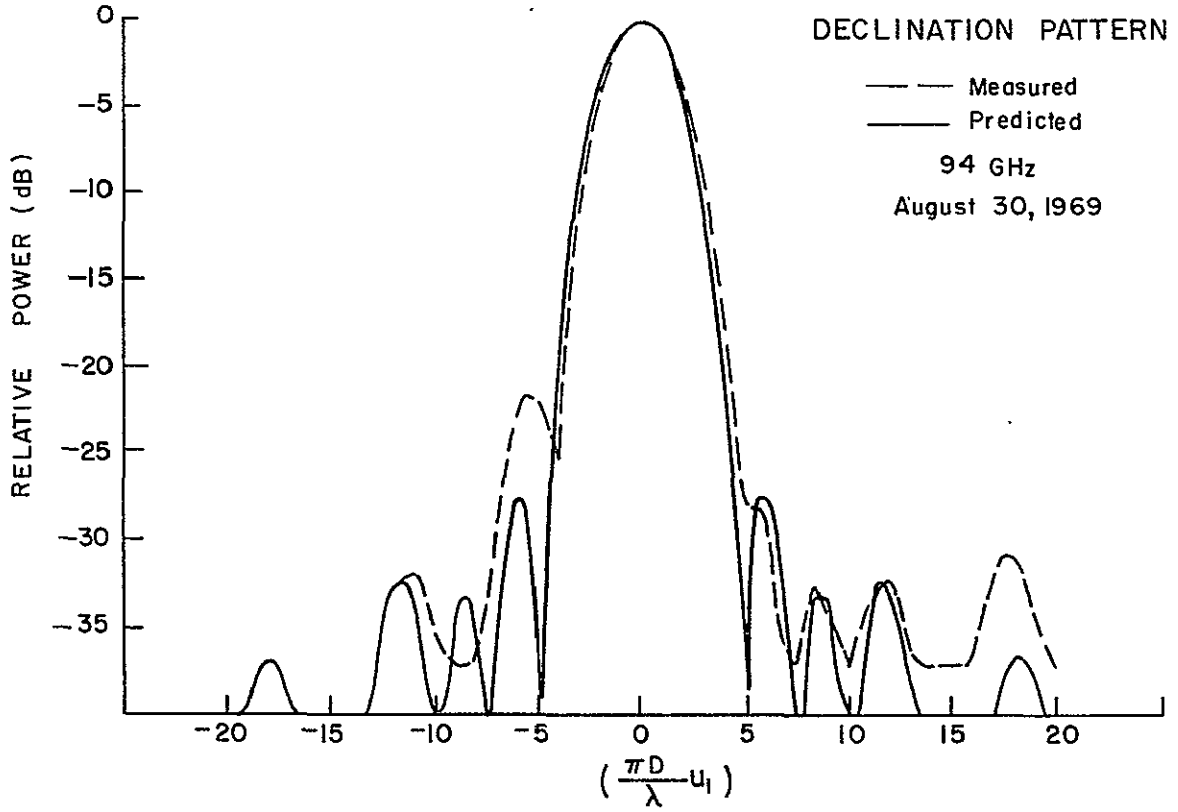
DECLINATION PATTERN
Measured
Predicted
94 GHz
August 30, 1969
RELATIVE POWER (dB)
0
-5
-10
-15
-20
-25
-30
-35
-20
-15
-10
-5
0
5
10
15
20
$(\frac{\pi D}{\lambda} u_1)$

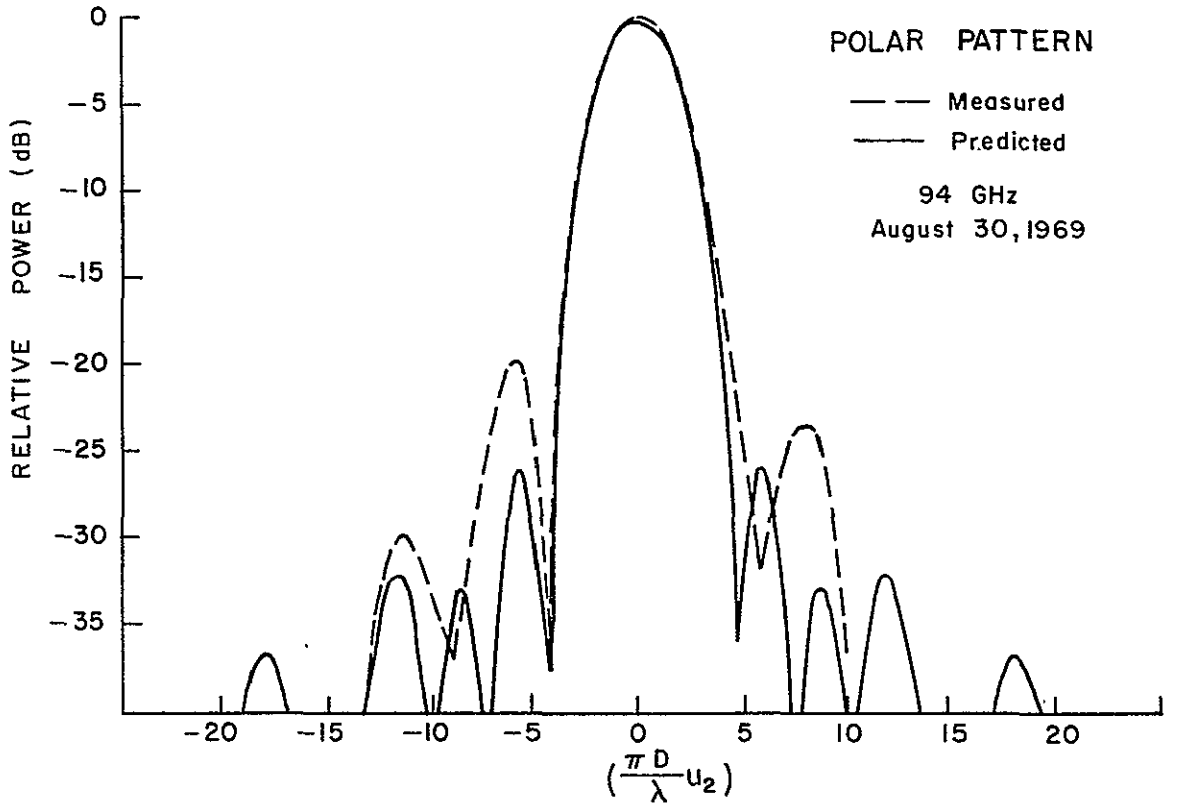
POLAR PATTERN
Measured
Predicted
94 GHz
August 30, 1969
RELATIVE POWER (dB)
0
-5
-10
-15
-20
-25
-30
-35
-20
-15
-10
-5
0
5
10
15
20
$(\frac{\pi D}{\lambda} u_2)$

Fig. 35

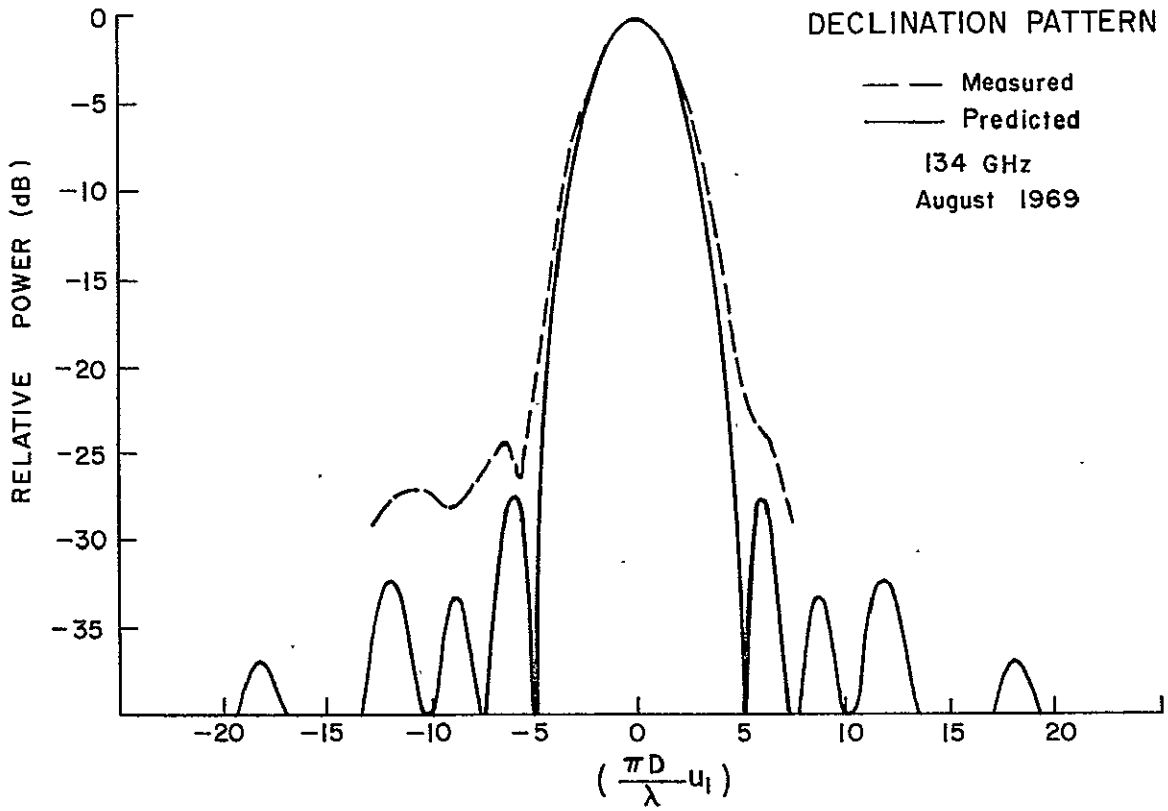
DECLINATION PATTERN
Measured
Predicted
134 GHz
August 1969
RELATIVE POWER (dB)
0
-5
-10
-15
-20
-25
-30
-35
-20
-15
-10
-5
0
5
10
15
20
$(\frac{\pi D}{\lambda} u_1)$

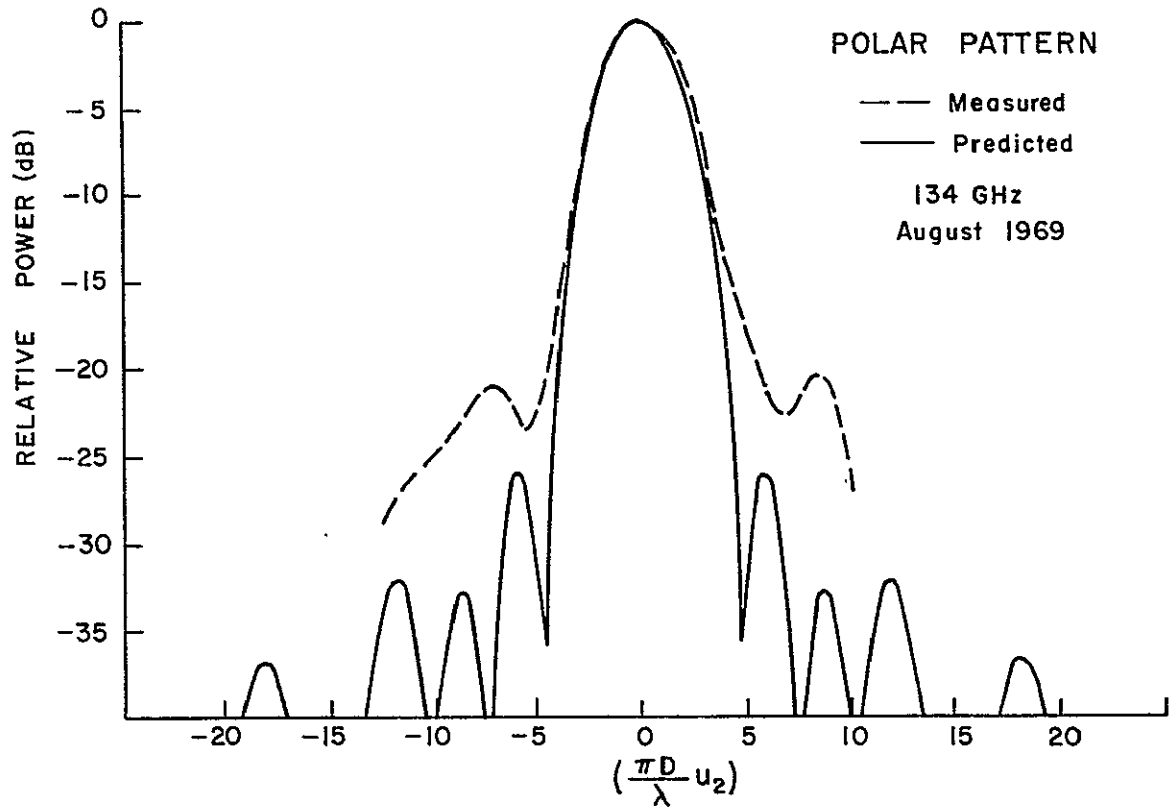
POLAR PATTERN
Measured
Predicted
134 GHz
August 1969
RELATIVE POWER (dB)
0
-5
-10
-15
-20
-25
-30
-35
-20
-15
-10
-5
0
5
10
15
20
$(\frac{\pi D}{\lambda} u_2)$

Fig. 36

of pattern degeneration. Figure 31 shows the 95 GHz pattern. It is clear that from this figure that the observed pattern is much broader than it should be. The first sidelobes are greatly enhanced while the sidelobes after the first are relatively lower. As discussed in Chapter III this sidelobe arrangement is evidence that the phase errors decorrelate over distances comparable to the diameter of the antenna.

Figures 34, 35, and 36 show the antenna patterns after the adjustment discussed in the previous section. Figure 34 is the observed pattern at 35 GHz plotted in the same scale with the predicted pattern. These two patterns agree very well. This means that there is very little phase error at 35 GHz. In addition, the excellent agreement of the observed and predicted pattern in the sidelobe regions at a frequency where there is little phase error means that the feed theory describes the illumination function very well. Figure 35 is the observed and predicted patterns at 94 GHz. In comparison to Figure 33 this pattern shows that the phase error was much reduced by the adjustment.

Figure 36 is the observed and predicted pattern at 134 GHz. At 134 GHz the performance has deteriorated but the antenna is still very good. For some applications the overall efficiency of the radio telescope is not as important as the main beam efficiency. Since the beamwidths are broader than the design beamwidths by about ten percent in each plane, the energy that is lost from the peak direction is scattered near the main lobe. Consequently, the main beam efficiency is still quite high at this frequency.

C. Efficiency Measurement

The efficiency of the antenna has been measured at 134 GHz, which is near the highest frequency of operation at the present time. As was shown in Chapter V this one measurement is sufficient to define the efficiency at all lower frequencies. Since the error bars scale down with the frequency squared, the inferred efficiencies at 15 and 35 GHz have extremely close tolerances. This opens the possibility of making extremely accurate radio astronomical measurements at these frequencies.

1. Measurement Technique

The efficiency measurement was carried out by comparing the gain of the 16-foot antenna to a conical standard gain horn. The comparison was accomplished by disconnecting the feed from the radiometer input flange and connecting the standard gain horn to it. Thus, the measured gain is relative to the receiver input flange.

The circuit that was used for the comparison is shown in Figure 37. One begins by finding the peak radiation level of the conical horn by taking the pattern of the horn in two orthogonal planes. Then with the horn pointed in the peak direction, a level was established on the recorder. After a few minutes, the receiver was switched to the 16-foot antenna. Sufficient attenuation was then inserted on the precision IF attenuator to make the levels agree. The reading of the IF attenuator is the difference in gain between the horn and the 16-foot antenna. Subsequently the standard gain horn was reconnected to check for drift.

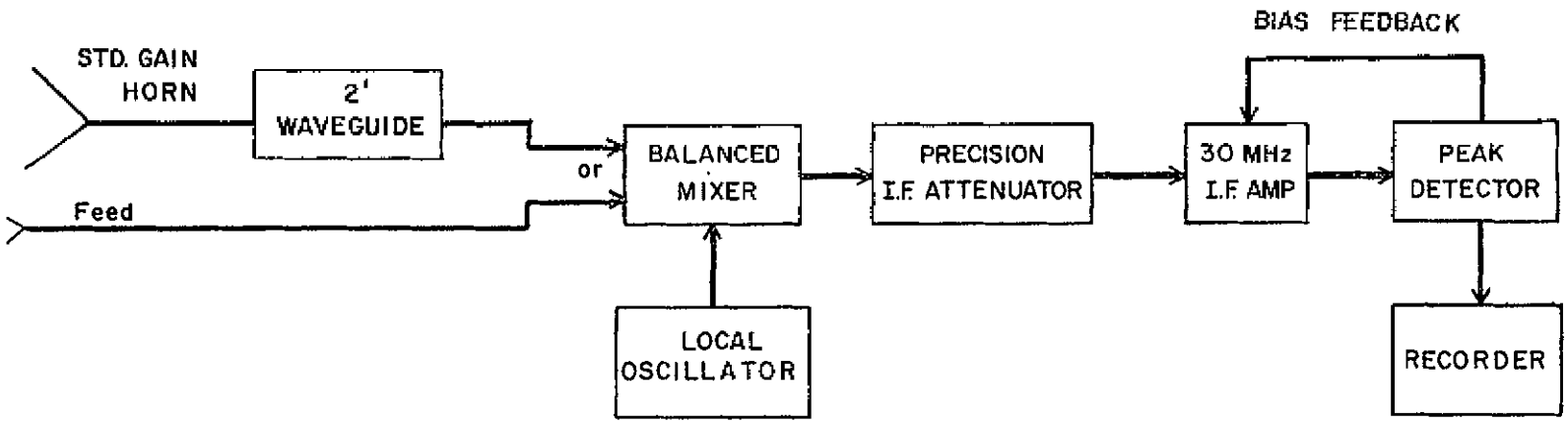

GAIN COMPARISON CIRCUIT

Fig. 37

This circuit and procedure is believed by the author to be the best available for the gain comparison measurements. The principle advantage of this method is that the gain difference between the standard gain horn and the large antenna is determined very accurately through the precision IF attenuator. The only disadvantage to this circuit is that it assumes linearity of the mixer over a 40 dB range. However, the mixer has been checked experimentally for saturation with negative results. The saturation effects begin at least 20 dB higher than the highest level encountered in the gain comparison measurements.

The only reasonable alternative to this circuit is to use RF attenuation at the transmitter sight. This method also requires some mixer linearity because the RF attenuator must be calibrated by the IF substitution method. In addition, it has proved impossible to repeat calibrations of the RF attenuator at 134 GHz. This is consistent with a history of unreasonable efficiency measurements given by the RF attenuator method. Thus, the RF attenuation method was discarded as unuseable.

The calibration of the standard gain horn is another crucial consideration in the overall accuracy of the measurement. The value used for the directivity is a value calculated by a method given by Cogdell[91]. This method gives values which are in excellent agreement with several horns of varying dimensions measured experimentally by King.[92] Some had considerably larger flare angles than standard gain horn used for this measurement. The major shortcomings of Cogdell's

method is in accounting for the effects of the non-zero horn flare angle[93]. Thus, it is felt that the calculated value for the horn gain is very close to the actual value since Cogdell's theory seems to work well under considerably more demanding circumstances.

It is difficult to put error bars on a measurement of this kind because all errors tend to be systematic, so repreating the measurement does not increase accuracy. The procedure that has been adopted is to give the accuracy of each step in the measurement. Then the total error is computed by assuming the errors are random variables and the error limits given are values of $2\sigma(\epsilon)$ where ϵ is the error. This procedure is not really justifiable as pointed out by Ludwig[94], but it is the customary procedure.[95]

2. Results

The results of the efficiency measurements are given in Table 3. All of the values are given in dB. The 16-foot antenna gain is simply the gain of the horn plus the difference in gain registered on the IF attenuator. The gain of the standard horn at the receiver input flange is the directivity of the horn minus the omic loss in the horn and the loss in the 2 foot waveguide connecting section.

The efficiency is the gain of the 16-foot antenna minus the gain for 100% efficiency. The tolerance loss which is the loss from phase errors is the directivity of the antenna minus the design directivity. The directivity is higher than the design gain by the omic loss in the feed.

Table 4 gives the efficiencies at other frequencies calculated from the Cassegrain antenna version of Theorem 1 given in Chapter V. It is necessary to use this extended version of Theorem 1 because the actual feeds which are used are not perfectly scaled. The theoretical efficiencies were calculated with the program given in Appendix A using the feed dimensions given in the table. The feed omic loss factor becomes appreciable at higher frequencies. Since this loss does not scale with frequency, it was taken out before the scaling was done. Subsequently, the feed omic loss was reinserted to calculate the total efficiency which is relative to the receiver input flange.

D. Antenna Stability

The observed patterns and gain measurement in the previous sections were taken in the hours from 2 a.m. until sunrise. This time period has been found to be best because the atmospheric induced signal fluctuations are smallest during these hours. Since these measurements were done under more or less ideal thermal conditions, it is mandatory that the antenna stability be tested under less favorable conditions.

There are two main effects that might occur. One of these is differential gravity loading. The antenna is always pointed in the direction of the transmitter site to make gain and pattern measurements. Thus as pointed out before gravity loading might cause astigmatism in the antenna when it is pointed in another direction.[96]

Temperature effects are the other possible source of instability. Strong temperature gradients, especially, might affect the antenna

Summary of Gain Measurement of the

16-Foot Antenna at 134 GHz

Item	Value (dB)	2σ (dB)
A. Gain Difference	40.55	0.10
B. Gain of Conical Horn	32.55	0.27
1. Directivity of Horn[+]	34.98	0.25
2. Omic Loss in Horn[*]	0.1	0.1
3. Loss in Waveguide[x]	2.33	0.05
C. Gain of 16-Foot Antenna at 134 GHz	73.10	0.28
D. Gain for 100% Efficiency at 134 GHz	76.71	----
E. Efficiency of Antenna at 134 GHz	-3.61 (43.6%)	0.27 (±2.8%)
F. Design Gain	74.55	0.1
1. Design Directivity (65.02%)	74.85	----
2. Feed Omic Loss[*]	0.3	0.1
G. Tolerance Loss	-1.45	0.29

[+]Calculated by Cogdell's method as discussed in text.

[*]Estimated

[x]Measured radiometrically

Table 3

EFFICIENCY CHARACTERISTICS OF THE U.T. 16 FOOT ANTENNA

JANUARY 1969

FREQUENCY (GHz)	FEED DIMENSIONS				FEED LOSS (dB)	DESIGN EFFICIENCY (%)	EFFICIENCY WITHOUT FEED LOSS (%)	TOTAL EFFICIENCY (%)	TOTAL GAIN (dB)	TOTAL EFFECTIVE AREA (m^2)
	a (inches)	a/λ	b (inches)	b/λ						
15.0^{O}	0.986	1.25	0.709	0.900	0.01	65.02	64.73±0.09^{X}	64.58±0.09	55.79± 0.01	12.06± 0.02
35.0^{O}	0.422	1.25	0.304	0.900	0.03	65.02	63.50± 0.46^{X}	63.06± 0.46	63.04±0.03	11.78 ± 0.09
35.0^{R}	0.400	1.18	0.285	0.844	0.03	64.57	63.05± 0.47^{X}	62.61 ± 0.46	63.01±0.03	11.70 ± 0.09
70.0^{O}	0.211	1.25	0.152	0.900	0.10	65.02	59.2 ± 1.7^{X}	57.8 ± 1.6	68.69±0.11	10.80 ± 0.30
94.0^{R}	1.164	1.30	0.113	0.899	0.15	64.92	55.0±2.5^{X}	53.1 ± 2.4	70.88±0.19	9.92 ± 0.44
100.0^{R}	0.164	1.39	0.113	0.957	0.17	64.06	53.0±2.6^{X}	50.9 ± 2.5	71.23±0.21	9.51 ± 0.47
134.0^{R}	0.104	1.18	0.076	0.862	0.30	64.68	46.6 ±3.1	43.6 ± 2.9	73.10±0.28*	8.13 ± 0.53
140.0^{O,R}	0.104	1.24	0.076	0.901	0.30	65.02	45.7 ±3.6^{X}	42.6 ± 3.3	73.38±0.33	7.96 ± 0.62

All confidence levels are 2σ levels in the same units as the quantity.

^{O} Feed designed for maximum forward gain

^{R} Feed on Rathion radiometer

* Measured

^{X} Based on Theurem 1, Chapter V

TABLE 4.

structure. A strong temperature gradient is produced, for example, by the sun shining on part of the antenna and the other part is in shadow.

The first experiment performed was an experiment to check for temperature gradient effects. Just before sunrise the antenna was pointed at the transmitter with the chart recorder calibrated on a rather sensitive scale. Then the system was left untouched for about an hour. During this time the sun shone on more of the antenna. The experiment was terminated when the sun shone on about half the antenna. The record showed no evidence of gain deterioration.

This experiment is significant because it exposes the antenna to the worst possible conditions of differential heating. The first effects of differential thermal loading of the structure is to steer the beam away from the equilibrium position. Since no significant gain reduction occurred there is apparently no significant thermal loading.

As mentioned earlier differential gravity loading should produce astigmatism. It was known that there was no astigmatism when the antenna was pointed toward the transmitter sight, but there could well be astigmatism at some other pointing. Thus, the second experiment was designed to detect astigmatism at other pointings. This was done by the solar limb crossing experiment discussed in Chapter IV. From this data one can deduce the beamwidth of the antenna in the direction the antenna crosses the limb. Then as discussed in Chapter IV the astigmatism can be determined from plotting the beamwidth vs focus position.

For this experiment, thirty-six polar and thirty-six declination scans were made of the sun. Figure 38 shows a typical scan. The experimental procedure was to make two polar and two declination scans. Then, the axial feed position was changed and another set of scans were taken. Three feed positions were used, with twelve scans in each direction for each feed position.

Table 5 shows the results of this study. This table shows no significant astigmatism. In addition, the beamwidths at the shim position nearest the optimum agree very well with the value measured on the pattern range. This occurs even at an hour angle of +42° and a declination of -20°. This is a very different pointing from the transmitter site which is at an hour-angle of -69° and a declination of -34°. From this data it was concluded that there was no significant gravity loading of the antenna structure.

E. Summary

This chapter illustrates the theory that has been developed in Chapters IV and V. It is a detailed account of how this theory was put into practice. The work was successful in substantially improving the performance of the 16-foot antenna and establishing its stability in all pointing directions. In addition, the efficiency of the antenna has been accurately measured at 134 GHz, and the efficiencies at other frequencies of interest inferred by the method given in Chapter V.

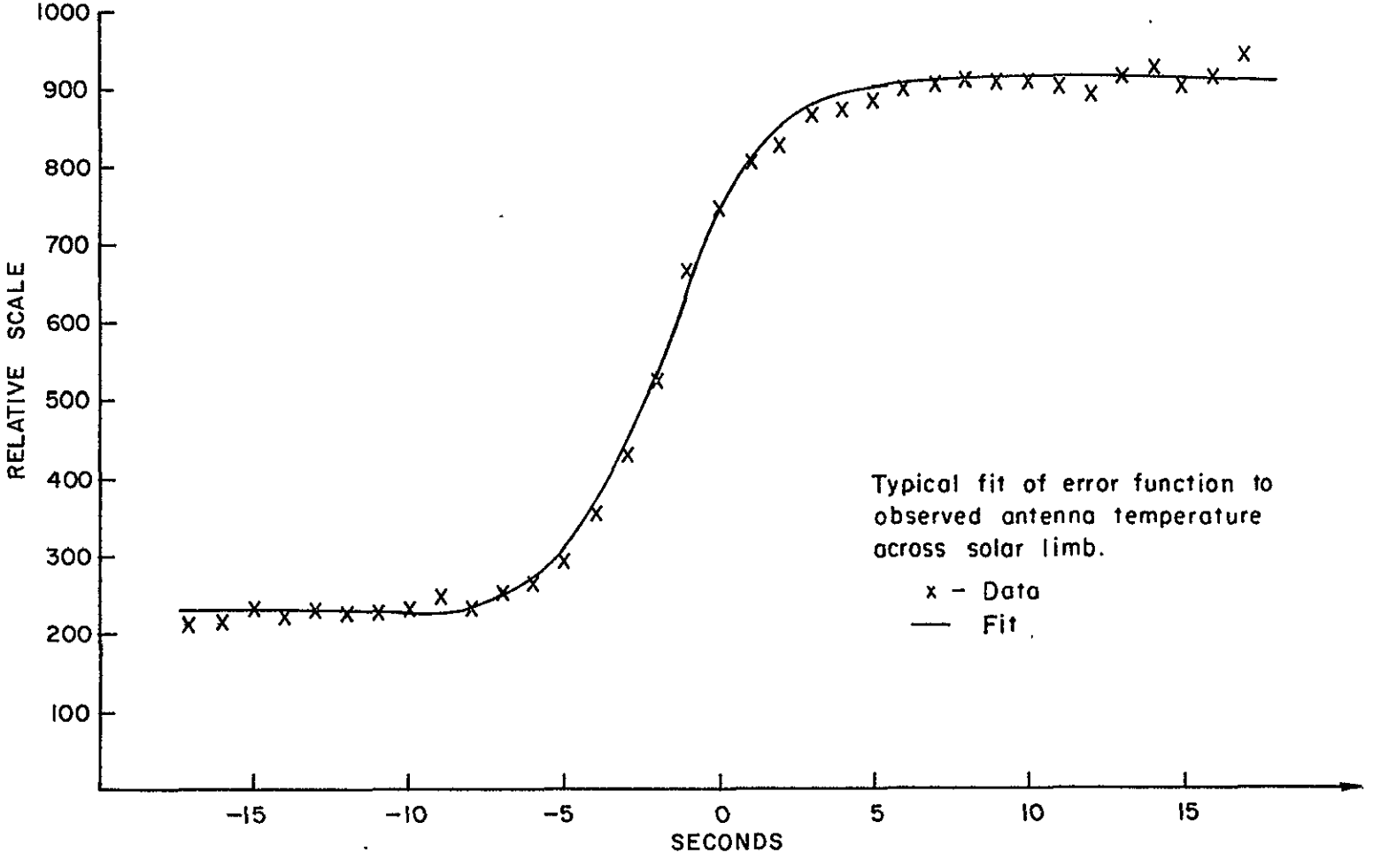
1000
900
800
700
600
500
400
300
200
100
RELATIVE SCALE
-15
-10
-5
0
5
10
15
SECONDS
Typical fit of error function to observed antenna temperature across solar limb.
x - Data
— Fit

Fig. 38

Declination and Hour Angle Beamwidths in Milli-Degrees

	Hour Angle in Degrees ($\times 10^{-3}$)			
	335	12	42	Pattern
HA	33.2	33.0	32.3	33.5
DEC	34.5	33.3	34.5	32.5

$\Gamma/\lambda = 0.23$

	Hour Angle in Degrees ($\times 10^{-3}$)			
	312	354	21	Pattern
HA	37.6	36.0	36.0	----
DEC	38.4	35.0	34.6	----

$\Gamma/\lambda = 0.68$

	Hour Angle in Degrees ($\times 10^{-3}$)			
	320	2	31	Pattern
HA	----	46.8	45.0	----
DEC	40.2	43.9	46.0	----

$\Gamma/\lambda = 1.13$

Declination of sun -20°

All values except the pattern range measurements are ±1.5 milli-degrees (2σ)

Table 5

Appendix A

An Antenna Radiation Pattern Program

Using the Fast Fourier Transform

A. Introduction

Calculating the far field radiation pattern of a reflector antenna from the aperture fields is a problem which has attracted considerable interest. With ordinary analytical methods one is restricted to a very small class of aperture illuminations and phase functions. For example, one can calculate the radiation pattern of a circular uniform phase aperture[97] with illumination proportional to

$$\left[1 - \left(\frac{r}{r_o}\right)^2\right]^p .$$

where r_o is the radius of the aperture. This form is convenient because its Fourier transform is a Bessel function. This aperture distribution is also useful for tutorial studies of the general effects of tapering on reflector antennas[98].

The engineer involved in the evaluation of a large reflector antenna has a need to calculate the radiation pattern in a much more general context. Spencer[99] has given an infinite series expression (later corrected by Fagot[100]) for the radiation pattern of an antenna with phase errors. However, this series has two disadvantages. The first is that it requires one to calculate the derivatives of the design pattern with respect to the angular coordinates. The second is that no convergence criterion is given for the series. In order to treat realistic problems Ludwig[101],

Dion[102], Bao[103], and others have turned to numerical methods. By calculating the radiation pattern numerically one is not restricted to any specific tapering or phase error function

As Dion[104] and Bao[105] have pointed out the computation required is enormous. Suppose one wanted the radiation pattern calculated at an (NXN) grid of points. This requires the calculation of N^2 two dimensional integrals. If each integral is approximated by an NXN sum then one must carry out approximately N^4 additions and multiplications. This is too large to be practical. For example, with N = 128 on the CDC 6600 this procedure would take over one hour.

In this Appendix a computer program will be presented that takes advantage of the efficiency of the Fast Fourier Transform (FFT)[106]. The FFT can be used to perform the same calculation as outlined above by using the FFT 2N times. The FFT itself requires approximately $N \log_2 N$ additions and multiplications[107]. Thus, the time savings factor is

$$r = \frac{2N \cdot N \log_2 N}{N^4} = \frac{\log_2 N^2}{N^2}$$

If N = 128 then $r < 10^{-3}$. Thus the FFT method is more than a factor of one thousand more efficient than the direct method. This efficiency makes possible the model fitting discussed in Chapter III. This method also uses storage very efficiently because only a single N x N complex array is required.

A program similar to this one has been developed by Pratt and Andrews[108]. Their program calculates the defraction pattern of light from an arbitrarily shaped aperture in a plane screen. However, it would be difficult to use this program to calculate an antenna pattern because of the blockage problem which will be discussed later. In addition, the program given here allows more flexibility in choosing the grid size for both the aperture plane and the far zone angular coordinates.

In the following section the mathematical development of the program is given. In Section C the program itself is discussed and a listing is given. In Section D the computed results for a uniformly illuminated aperture are compared with the exact results. This program will calculate the radiation pattern of a circular aperture excited by electric field with arbitrary amplitude and phase. It assumes linear polarization of the aperture fields. The program allows one to account for central circular blockage and the blockage of two spars at arbitrary angles to the reference coordinate system. The spars are, however, assumed to pass through the origin of the reference coordinate system. This assumption and the assumption of a circular aperture are not required by the mathematical development, but they are reasonable assumptions and simplify the program coding.

B. Mathematical Development

As shown in Chapter I the far field gain function can be written as

$$G(u_1, u_2) = \frac{k^2}{\pi} \left| I(u_1, u_2) \right|^2 \tag{A1}$$

where

$$I(u_1, u_2) = \iint_{-\infty} T(x_1, x_2)\, e^{jkL(x_1, x_2)}\, e^{jk(u_1 x_1 + u_2, x_2)}\, dx_1 dx_2 \tag{A2}$$

The tapering function $T(x_1, x_2)$ is defined as the electric field in the aperture plane normalized by the square root of the input power and the free space impedance, i.e.

$$T(x_1, x_2) = \frac{E(x_1, x_2)}{\sqrt{P_{in}\, z_o}}\, e^{jk\ell(x_1, x_2)} = \sqrt{\frac{G_f(\theta', \varphi')}{4\pi(f + \frac{r^2}{4f})^2}}\, e^{jk\ell(x_1, x_2)}$$

Equation (A2) is particularly convenient for computer calculation because the feed characteristics can be thought of as an input and the far field gain pattern of the reflector as the output. In the case where the feed is an extended source, as it is in a Cassegrain feed, one must take explicit account of the phase shift, $k\ell(x_1, x_2)$, caused by the feed system. For a point source feed there is no phase shift caused by the feed, so ℓ may be set to zero.

A typical tapering function is shown in Figure A1. These functions are gradually changing, well behaved functions, except where the antenna feed system blocks the aperture. In these blocked areas the functional value is zero. The blocked regions are characterized by having at least one dimension much smaller than the diameter of the antenna.

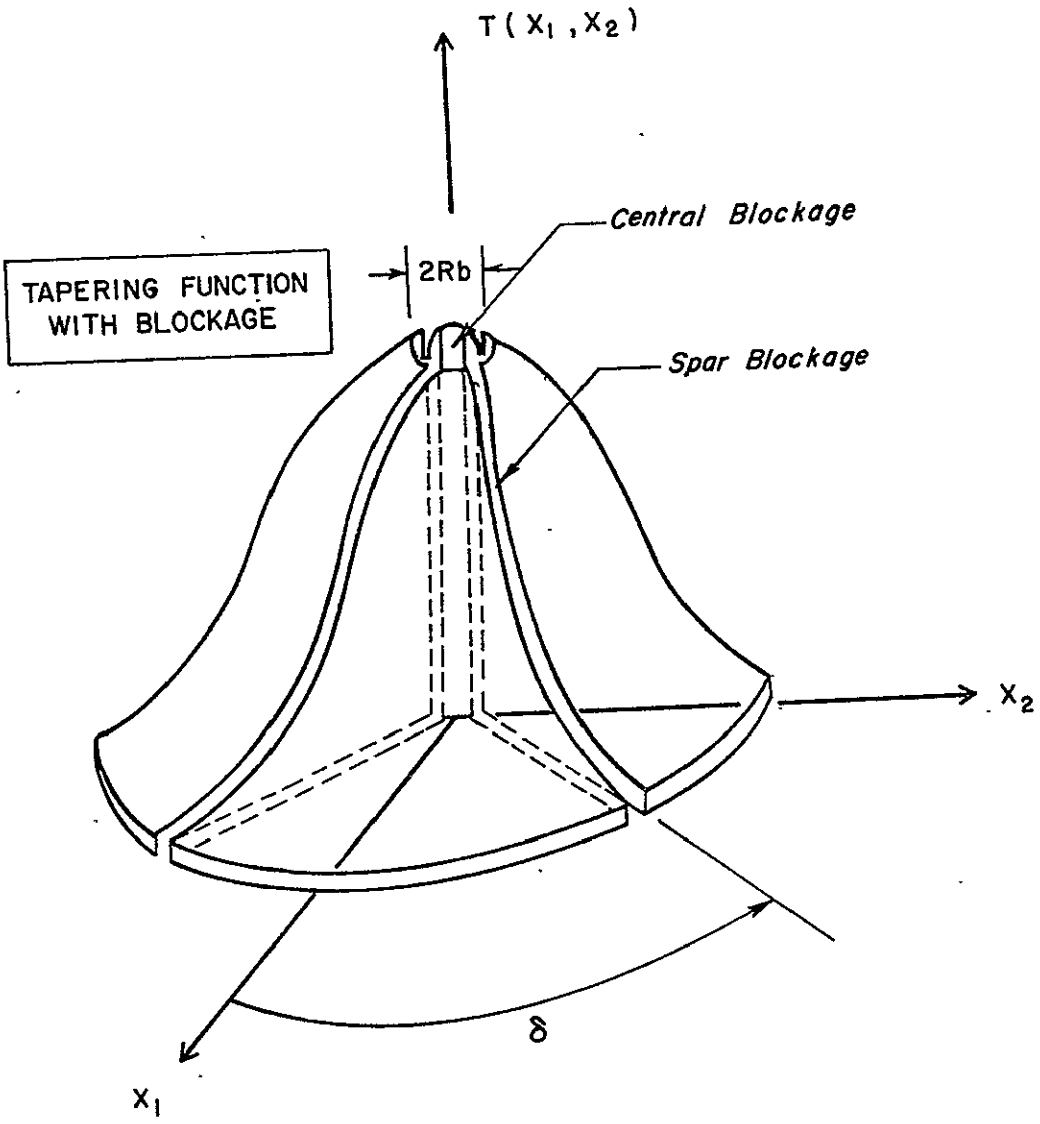
T (X1 , X2)
TAPERING FUNCTION
WITH BLOCKAGE
2Rb
Central Blockage
Spar Blockage
X2
δ
X1

Fig. A.1

This latter fact leads to a rather fundamental problem in choosing the integration grid size for the integral, I. If the grid size is chosen appropriate to an unblocked antenna, it will be much too course to account for the blocked areas effectively. On the other hand if the grid size is chosen small enough for the smallest blocked area, then the core storage and time required to calculate the integral is exorbitantly large.

A solution to this problem is to break the tapering function into several parts so that it is written as the unblocked tapering function plus several corrections. Then the contribution of each component is calculated separately and the results totaled. This method takes advantage of the linearity of the integral, and it may be thought of as the engineering method of "superposition." The tapering function is written

$$T(\underline{x}) = T_{ub}(\underline{x}) - T_c(\underline{x}) - T_{s1}(\underline{x}) - T_{s2}(\underline{x})$$

The function T_{ub} is the tapering function the antenna would have without blockage. The functions T_c, T_{s1}, T_{s2} are the blockage functions to account for the central blockage and the blockage of two spars. These functions have a value of zero outside the area to which they refer and the value of T_{ub} inside this area. This process of decomposition is illustrated in Figure A1.

The components of the integral I that correspond to each of the tapering functions will be written I_{ub}, I_c, I_{s1}, and I_{s2} after their respective tapering functions. The technique used in the program is to calcuate the unblocked integral, I_{ub}, which is by far the dominant

contribution. The others are accumulated as corrections. This is a standard digital computer technique and conserves a great deal of storage.

Calculation of the Unblocked Integral

The three basic steps in calculating the unblocked integral, I_{ub}, are the calculation of the tapering function on an array of points, the introduction of a linear phase grading, and the performance of a row-wise and column-wise transformation of the array with the FFT. The result of this transformation is that $I_{ub}(u_1, u_2)$ appears in the array at a grid of points. The tapering function is an input to the program and may be put in as a table of laboratory measurements. It may also be calculated from a theory for the feed system. The introduction of linear phase grading merely translates the points in the transformed array. This is done for convenience so the axial gain will be in the center of the array. The remainder of this section is devoted to the mathematical development of the FFT method of calculating this integral.

The integral that must be calculated is

$$I_{ub}(u_1, u_2) = \int_{-\infty}^{\infty}\int T(x_1, x_2)\, e^{jkL(x_1, x_2)}\, e^{jk(u_1 x_1 + u_2 x_2)}\, dx_1 dx_2.$$

The (x_1, x_2) - coordinate system is the natural coordinate system for the reflector, but it proves inconvenient for Fortran programming. Thus, let us introduce a (y_1, y_2) - coordinate system as

$$y_1 = x_1 + h_1$$

$$y_2 = x_2 + h_2$$

The purpose of this translation is to shift all of the non-zero values of T into the first quadrant. Figure A2 shows these two coordinate systems. In (y_1, y_2) - coordinates the integral above can be written

$$I_{ub}(u_1, u_2) = e^{-jk(u_1 h_1 + u_2 h_2)} \int_{-\infty}^{\infty} \int T(y_1 - h_1, y_2 - h_2)\, e^{jkL(y_1 - h_1, y_2 - h_2)}$$

$$e^{jk(u_1 y_1 + u_2 y_2)}\, dy_1 dy_2 .$$

The computer calculation of an integral requires that it be approximated by a sum. A uniform grid of points that are Δy_1 and Δy_2 apart in the two coordinates are used, so that the integral may be approximated as

$$I_{ub}(u_1, u_2) = e^{-jk(u_1 h_1 + u_2 h_2)}\, \Delta y_1 \Delta y_2 \sum_{m=1}^{K} \sum_{n=1}^{K} T(m\Delta y_1 - h_1,\ n\Delta y_2 - h_2)$$

$$e^{jkL(m\Delta y_1 - h_1,\ m\Delta y_2 - h_2)}\, e^{jk(u_1 m\Delta y_1 + u_2 n\Delta y_2)} \qquad \text{(A4)}$$

In the following, the explicit form of T and L will not be written out, but will be written as T(m, n) and L(m, n). It will be understood that the indices (m, n) stand for the appropriate place on the aperture plane. Thus, Equation (A4) can be written as

$$I_{ub}(u_1, u_2) = e^{-jk(u_1 h_1 + u_2 h_2)} \Delta y_1 \Delta y_2 \sum_{m=1}^{K} \sum_{n=1}^{K} T(m, n)\, e^{jkL(m, n)}$$

$$e^{jk(u_1 m \Delta y_1 + u_2 n \Delta y_2)} \qquad \text{(A5)}$$

All of the non-zero values of $T(m, n)\, e^{jkL(m, n)}$ are placed in an N x N complex array which is stored as a real array, PR, and an imaginary array, PI, in PAT. N and K are unequal in general with $N \leq K$. It will usually prove convenient to choose K a factor of two to four larger than N. For the FFT routine used here N and K must also be powers of two. The reason for this will become apparent later.

It is convenient to choose h_1 and h_2 so that the value of T and L at the center of the aperture appear in the center of the array. This may be accomplished by choosing $h_1 = N/2\ \Delta y_1$, and $h_2 = N/2\ \Delta y_2$.

The u-variables in Equation A5 are continuous variables, so they must be rewritten as discrete indexed variables. Let u_1 and u_2 be defined as

$$\begin{aligned} u_1 &= \Delta u_1\, s \qquad & s &= \pm 1, 2, \ldots. \\ u_2 &= \Delta u_2\, t \qquad & t &= \pm 1, 2, \ldots. \end{aligned} \qquad \text{(A6)}$$

where

$$\Delta u_1 = \frac{2\pi}{K\, k\, \Delta y_1}$$

and

$$\Delta u_2 = \frac{2\pi}{K\, k\, \Delta y_2} .$$

The grid size for the u-array is chosen so that the integration grid size and the wavenumber fall out of the second phase term in Equation (A5). This normalized form is required by the FFT. Substituting the values discussed for h_1, h_2, u_1, and u_2 in Equation A5, one has

$$I_{ub}(s,t) = e^{-j\frac{N}{K}\pi(s+t)} \Delta y_1 \Delta y_2 \sum_{m=1}^{K} \sum_{n=1}^{K} T(m,n)\, e^{jkL(m,n)}\, e^{j\frac{2\pi}{K}(ms+nt)} \tag{A7}$$

the indices s and t represent a point in the angular coordinates u_1 and u_2 just as m and n represent a point on the aperture plane.

Half of the s and t indices are negative, and since negative subscripts are not allowed in Fortran programming, s and t must be biased so that the only positive indices are used. This may be done by introducing a linear phase grading into the input which shifts the axial direction (s = t= 0) to the middle of the array. Let

$$s' = s + \frac{N}{2}$$

and

$$t' = t + \frac{N}{2} .$$

With these translations Equation A7 becomes

$$I_{ub}(s',t') = e^{-j\frac{N}{K}\pi(s'+t')} \Delta y_1 \Delta y_2 \sum_{m=1}^{K}\sum_{n=1}^{K} T(m,n)\, e^{jkL(m,n)}$$

$$e^{-j\pi\frac{N}{K}(m+n)}\, e^{j\frac{2\pi}{K}(ms'+nt')} \qquad \text{(A8)}$$

Equation (A8) may be regrouped as follows:

$$I_{ub}(s',t') = e^{-j\frac{N}{K}\pi(s'+t')} \Delta y_1 \Delta y_2 \left\{ \sum_{m=1}^{K} e^{j\frac{2\pi}{K}ms'} \left(\sum_{n=1}^{K} e^{j\frac{2\pi}{K}nt'} P(m,n) \right) \right\} \qquad \text{(A9)}$$

where

$$P(m,n) = T(m,n)\, e^{jkL(m,n)}\, e^{-j\pi\frac{N}{K}(m+n)}$$

The Fast Fourier Transform is a program that replaces an array, say B(n), with its discrete transform, i.e.,

$$B(n) \rightarrow \sum_{m=1}^{K} B(m)\, e^{j\frac{2\pi}{K}mn}$$

One can see that the calculations indicated in Equation (A9) can be done by first applying the FFT to each row of P(m, n) and replacing the results in that row. This procedure gives an array P(m, t′). Then the FFT is applied to each column of P(m, t′) and the result replaced in that column. The result of this is the desired integral except for a phase shift factor.

Correction for Central Circular Blockage

The central blockage correction can be written

$$I_{cb}(u_1, u_2) = \int_{\substack{\text{central} \\ \text{region}}} \int T_{ub}(x_1, x_2)\, e^{jkL(x_1, x_2)}\, e^{jk(u_1 x_1 + u_2 x_2)}\, dx_1\, dx_2$$

The region of the central blockage is small compared with the variations in T and L, so T and L will be assumed constant for this calculation.

$$I_{cb}(u_1, u_2) = T(0,0)\, e^{jkL(0,0)} \int_{\substack{\text{central} \\ \text{region}}} \int e^{jk(u_1 x_1 + u_2 x_2)}\, dx_1 dx_2.$$

Changing variables to r and ξ such that

$$x_1 = r \cos \xi$$

$$x_2 = r \sin \xi$$

and

$$u_1 = \theta \cos \varphi$$

$$u_2 = \theta \sin \varphi,$$

one has

$$I_{cb}(u_1, u_2) = T(0,0)\, e^{jkL(0,0)} \int_0^{R_b} \int_0^{2\pi} e^{jk\theta r \cos(\varphi - \xi)}\, r\, dr\, d\xi,$$

where R_b is the radius of the blocked area. The integral in ξ is just the zero order Bessel function, so one can write

$$I_{cb}(u_1, u_2) = T(0, 0\ e^{jkL(0, 0)}\ 2\pi\ R_b^{\ 2} \int_0^1 J_o(k\theta\ R_b\ z)\ z\ dz.$$

This last integral is also a Bessel function, i.e.

$$I_{cb}(u_1, u_2) = T(0, 0)\ e^{jkL(0, 0)}\ 2\pi R_b^{\ 2}\ \frac{J_1(k\ R_b\ \theta)}{k\ R_b \theta}\ , \qquad \text{(A10)}$$

where θ may be calculated as the Pathagorian sum of u_1 and u_2

$$\theta = \sqrt{u_1^{\ 2} + u_2^{\ 2}}\ .$$

When written in terms of the indices s' and t', Equation (A10) becomes

$$I_{cb}(s', t') = T(0, 0)\ e^{jkL(0, 0)}\ \pi R_b^{\ 2}\ \frac{J_1(F)}{F} \qquad \text{(A11)}$$

where

$$F = \frac{2\pi}{K} \sqrt{\left(\frac{R_b}{\Delta x_1}\right)^2 \left(s' - \frac{N}{2}\right)^2 + \left(\frac{R_b}{\Delta x_2}\right)^2 \left(t' - \frac{N}{2}\right)^2}\ .$$

Spar Blockage

The spar blockage correction may be written, using vector notation, as

$$I_s(u_1, u_2) = \int\int_{\text{spar}} T_{ub}(x_1, x_2)\ e^{jkL(x_1, x_2)}\ e^{jk\ \underline{u}^T\ \underline{x}}\ dx_1 dx_2 \qquad \text{(A12)}$$

Let us transform coordinates so that the primed coordinates agree with the direction of the spar as shown in Figure A2. The primed coordinates are given by

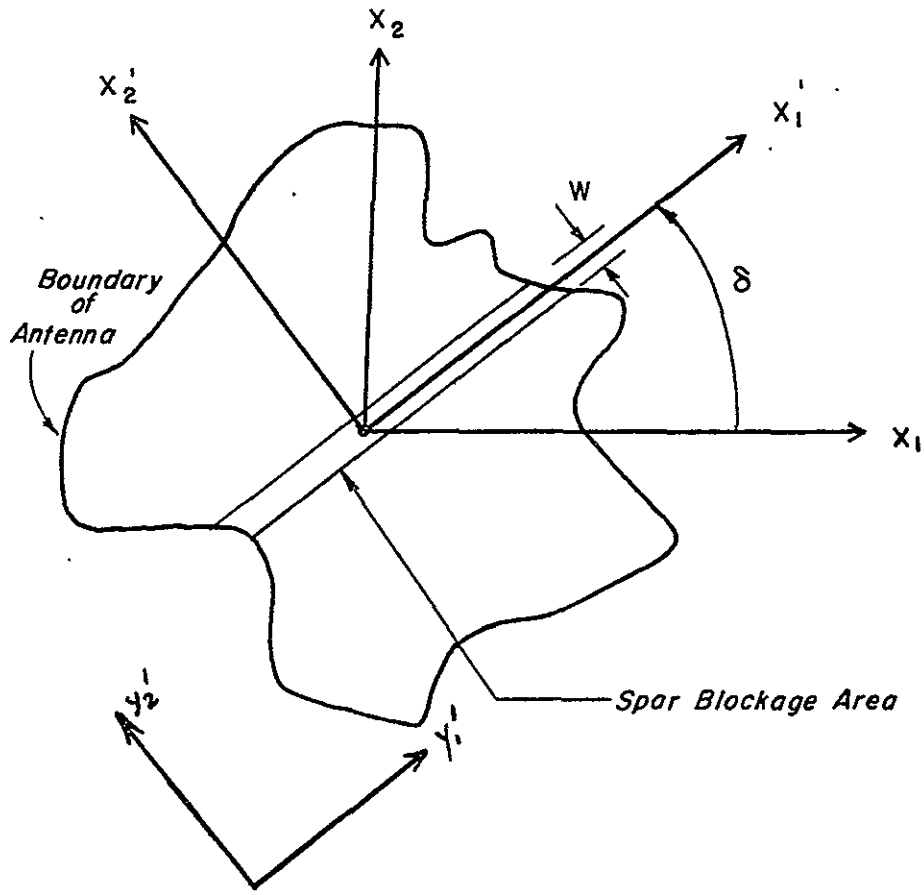

SPAR BLOCKAGE

Fig. A.2

$$\underline{x}' = \underline{R}\underline{x}$$

where

$$\underline{R} = \begin{bmatrix} \cos\delta & -\sin\delta \\ \sin\delta & \cos\delta \end{bmatrix} .$$

Also let us define the primed angular coordinates as

$$\underline{u}' = \underline{R}\underline{u}$$

$$I_s(u_1', u_2') = \iint_{spar} T_{ub}(x_1, x_2)\, e^{jkL(x_1, x_2)}\, e^{jk(u_1'x_1' + u_2'x_2')}\, dx_1' dx_2' . \tag{A13}$$

The x_2' integration is now trivial since I and L do not vary much over the small extent of x_2'. Thus Equation (A13) may be written

$$I_s(u_1', u_2') = w \int_{x_1'=-\infty}^{\infty} T_{ub}(x_1, x_2)\, e^{jkL(x_1, x_2)}\, e^{jk\,u_1'\,x_1'}\, dx_1' \tag{A14}$$

Now we need to change variables to y so that all of the non-zero values of T_{ub} are to the right of the origin. Let

$$x_1' = y - h,$$

so Equation (A14) becomes

$$I_s(u_1', u_2') = w\, e^{-jk\,u_1'\,h} \int_{-\infty}^{\infty} z(y)\, e^{jku_1'\,y}\, dy$$

where z(y) is a complex quantity given by

$$z(y) = T_{ub}(x_1, x_2)\, e^{jkL(x_1, x_2)}$$

where

$$x_1 = (y - h) \cos \delta$$

$$x_2 = (y - h) \sin \delta .$$

Approximating the integral by a sum of k terms one has

$$I_s(u_1', u_2') = w\, \Delta y\, e^{-jk\, u_1' h} \sum_{m=1}^{K} z(m\Delta y)\, e^{jk\, u_1' m\Delta y} \qquad \text{(A15)}$$

Let

$$u_1' = v\, \Delta u_1' \qquad v = \pm 1, 2, 3, \ldots . \qquad \text{(A16)}$$

where

$$\Delta u_1' = \frac{2\pi}{K\, k\, \Delta y} .$$

Substituting Equation (A16) into Equation (A15) and letting $h = \frac{K}{2} \Delta y$, one obtains

$$I_s(v) = w\, \Delta y\, e^{-j\pi v} \sum_{m=1}^{K} z(m)\, e^{j\frac{2\pi}{K} mv}, \qquad \text{(A17)}$$

where it is understood that $I_s(v)$ is $I_s(u_1', u_2')$ where $u_1' = v\, \Delta u_1'$. In addition, $z(m)$ stands for $z(m\Delta y)$.

Some of the v's of interest are negative. This is inconvenient for Fortran programming so let

$$v' = v + K/2.$$

Thus Equation A17 becomes

$$I_s(v') = w\,\Delta y\, e^{-j\pi (v' - \frac{K}{2})} \sum_{m=1}^{K} z(m)\, e^{-j\pi m}\, e^{j\frac{2\pi}{K} mv'} \qquad \text{(A18)}$$

The sum in Equation (A18) may be calculated with a single application of the FFT. The array z(m) is calculated first. Second one modifies z(m) with the linear phase grading $e^{-j\pi m}$. Third, z(m) is transformed with FFT, and finally the transformed array is multiplied by the required constant factors and linear phase grading.

The value of v′ that corresponds to s′ and t′ will now be calculated. The angles u_1 and u_2 are given by

$$u_1 = \frac{2\pi}{K\, k\, \Delta y_1}\, s$$

$$u_2 = \frac{2\pi}{K\, k\, \Delta y_2}\, t.$$

The value of u_1' is then

$$u_1' = \frac{2\pi}{K\, k\, \Delta y_1}\, s \cos\delta - \frac{2\pi}{K\, k\, \Delta y_2}\, t \sin\delta.$$

Substituting Equations (A16) for u_1' into the equation above and cancelling the common terms, one obtains

$$v = s\frac{\Delta y}{\Delta y_1} \cos\delta - E\frac{\Delta y}{\Delta y_2} \sin\delta.$$

Now substituting v', s', and t' for v, s, t, one obtains

$$v' = (s' - H)\frac{\Delta y}{\Delta y_1}\cos\delta - (t' - H)\frac{\Delta y}{\Delta y_2}\sin\delta + K/2.$$

A slight problem arises in that the values of v' needed for the blockage correction are not necessarily integers. However since this correction is a small one, it is felt that interpolating linearly between integer values is sufficiently accurate.

C. The Program

The first input to the program is a card that has the diameter of the antenna in feet in the first field and the wavelength in meters in the second. All fields are E 10.3. The next card specifies the angle between the far field pattern grid points in degrees. If this card is left blank the program calculates its own increment to optimize accuracy. This latter mode of operation is recommended unless the grid interval must be specified, as when it is being compared to measured data. The third card specifies the radius of the central blockage circle in inches. The fourth card specifies the width of the two spars in the first field in inches. It also specifies the angle the two spars make with the (x_1, x_2)-coordinates in the second and third fields.

The subroutine MAG(X1,X2) calculates the magnitude of the tapering function. The tapering function is assumed to be real in this program.

The subroutine PHASE (X1, X2, Z, NX, PH) calculates the phase function $kL(\underline{x})$. The phase in radians is returned as PH. The Z vector

is a parameter vector. The number NX is the maximum number of parameters.

The internal program parameters KEXP and NEXP determine the grid spacings, accuracy, and storage requirements of the program. The unblocked integral is carried out over an N X N array of points with spacing Δy_1 and Δy_2, where

$$N = 2^{NEXP}.$$

The grid spacing of the points in angle space is given by Equation (A6) as

$$\Delta u_1 = \frac{2\pi}{K\, k\, \Delta y_2} \tag{A19}$$

and

$$\Delta u_2 = \frac{2\pi}{K\, k\, \Delta y_2},$$

where

$$K = 2^{KEXP}.$$

If the grid spacing in angle space are left unspecified, then Δy_1 and Δy_2 are calculated to just fill up the N X N array. If Δu_1 and Δu_2 are specified, on the other hand, Δy_1 and Δy_2 are calculated from Equation (A19). Since K and N may be different, the grid intervals may be adjusted somewhat for the particular application. Increasing N makes the program more accurate while increasing K makes the grid in angle space finer. Increasing N, however, increases the program storage requirements.

One detail of the coding differs from the mathematical development given in the previous sections. The FFT routine used here actually shifts one grid spacing as well as transforming. That is, if B(m) is a complex array being transformed, then

$$B(K) \rightarrow \sum_{m=1}^{K} B(m)\, e^{j\frac{2\pi}{K}(m-1)(k-1)}$$

D. Verification

The calculation of the unblocked integral was checked by setting the blockage corrections to zero and calculating the pattern of a uniformly illuminated constant phase aperture. This was done by substituting another subroutine for FEED. FEED normally calculates the gain of the horn feed. This subroutine calculates the gain of the point source feed required to give a uniform aperture illumination, Silver[109]. For this test N = 128, K = 512, D = 16 feet, λ = 3.2 mm, and f = 8 feet. The result was an efficiency of unity to more than five significant figures and a normalized pattern given in Table A1.

The central blockage and spar blockage corrections were checked by setting the tapering function to unity everywhere and printing out these corrections separately. Then several points were checked by hand.

angle °(x10^{-3})	Patterns (dB)	
	Calculated	Exact
0	0.00	0.00
10	-0.77	-0.77
20	-3.23	-3.23
30	-8.06	-8.06
40	-18.32	-18.31
50	-24.05	-23.98
60	-17.64	-17.59
70	-19.68	-19.61
80	-30.50	-30.27
90	-28.56	-28.72
100	-23.83	-23.91
110	-26.45	-26.56
120	-30.96	-30.74
130	-27.98	-27.86
140	-31.87	-31.81

Table A1

Verification of Program

E. Listing

```
      PROGRAM PAT(INPUT, OUTPUT)
C
C       DIMENSION PR AND PI TO NXN.
C
      DIMENSION PR(128, 128), PI(128, 128)
C
C       DIMENSION A AND B TO K.
C
      DIMENSION A(1024), B(1024)
C
C       DIMENSION D AND E TO N.
      DIMENSION D(128), E(128)
      DIMENSION Z(15)
      DIMENSION SIG(2)
      DIMENSION MM(2), IDEC(2)
      DIMENSION IX(5), JX(5), MX(5)

        DIMENSION XX AND YY TO 2K.

      COMMON/SCRFFT/ XX(2048)/FFF/YY(2048)
      INTEGER H
      INTEGER HK
      REAL LAMDA
      REAL MAG
      RES1 = 0.5
      RES2 = -0.5**4
      RES3 = 0.5**7/3.
      RES4 = -0.5**7/3./2./4./3./2.
      I0 = 3H  0
      I5 = 3H -5
      I10 = 3H-10
      I15 = 3H-15
      I20 = 3H-20
      I25 = 3H-25
      I30 = 3H-30
      I35 = 3H-35
      JX(1) = 10HTICK MARKS
      JX(2) = 10H ARE 5PI*D
      JX(3) = 10H/LAMDA
      MM(1) = 10HCONTOUR MA
      MM(2) = 1HP
      I3DB = 4H 3DB
      I10DB = 4H10DB
      I20DB = 4H20DB
      I30DB = 4H30DB
```

```
      IPOL = 5H U2
      IPAT = 7HPATTERN
      IDEC(1) = 10H     U1
      PIE = 3.1415926535897932384
      NEXP = 7
      KEXP = 10
      N = 2**NEXP
      K = 2**KEXP
      H = N/2+1
      READ 28, DIAMF, LAMDA
      DIAM = DIAMF*0.0254*12.
      SCALE = PIE*DIAM/LAMDA
      WAVENR = 2.*PIE/LAMDA
      READ 28, DD1, DD2
C
C       IF DD1 IS ZERO THE PROGRAM
C       CALCULATES ITS OWN DD1 AND DD2.
C
      IF (DD1.NE. 0.0) GO TO 1
      DU1 = 2.*PIE/K/WAVENR/DIAM*(N-2)
      DU2 = DU1
      DD1 = DU1*180./PIE
      DD2 = DU2*180./PIE
1     CONTINUE
      DU1 = DD1*PIE/180.
      DU2 = DD2*PIE/180.
      READ 28, RB
      READ 28, W, SIG(1), SIG(2)
      PRINT 29
      PRINT 30, DIAMF, LAMDA
      PRINT 31, NEXP, KEXP
      PRINT 32, DD1, DD2
      PRINT 33, DU1, DU2
      PRINT 34, RB
      RB = RB*0.0254
      PRINT 35, SIG(1), SIG(2)
      DO 2 I = 1, 2
2     SIG(I) = SIG(I)*PIE/180.
      PRINT 36, W
      W = W*0.0254
      DY1 = 2.*PIE/K/WAVENR/DU1
      DY2 = 2.*PIE/K/WAVENR/DU2
      EXT1 = DIAM/DY1
      EXT2 = DIAM/DY2
      PRINT 37, EXT1
```

```
      PRINT 38, EXT 2
      IF (EXT1 .GR. (N-1)) STOP 1
      IF (EXT2 .GT. (N-1)) STOP 2
C
C       THIS COMPLETES THE INITILIZATION PROCEDURE.
C
C
C       CALCULATION OF THE UNBLOCKED INTEGRAL FOLLOWS.
C
      CALL SECOND (QT)
      CONST = PIE*N/K
      DO 3 I = 1, N
      DO 3 J = 1, N
      X1 = (I-H)*DY1
      X2 = (J-H)*DY2
      TMAG = MAG(X1, X2)
      CALL PHASE (X1, X2, Z, NX, PH)
      PH = PH-(I-H+J-H)*CONST
      PR(I, J) = TMAG*COS(PH)
      PI(I, J) = TMAG*SIN(PH)
3     CONTINUE
      CALL SECOND (QT1)
      Q = QT1 - QT
      QT = QT1
      PRINT 51
      PRINT 39, Q
      CALL XTD (PR, PI, NEXP, KEXP)
      FACTOR = DY1*DY2
      DO 4 I = 1, N
      DO 4 J = 1, N
      PH = - (I-H+J-H)*CONST
      COSINE = COS(PH)
      SINE = SIN(PH)
      RE = PR(I, J)*COSINE-PI(I, J)*SINE
      XM - PR(I, J)*SINE+PI(I, J)*COSINE
      PR(I, J) = RE*FACTOR
      PI(I, J) = XM*FACTOR
4     CONTINUE
      CALL SECOND (QT1)
      Q = QT1-QT
      QT = QT1
      PRINT 40, Q
C
C       THIS COMPLETES THE CALCULATION OF THE UNBLOCKED
C       INTEGRAL.
C
C
C       CALCULATE THE CENTRAL BLOCKAGE CORRECTION.
```

```
C
      CALL PHASE (0., 0., Z, NX, PH)
      TMAG = 2.0*PIE*MAG(0., 0.)*RB*RB
      RE = TMAG*COS(PH)
      XM = TMAG*SIN(PH)
      FAC1 = RB/DY1
      FAC2 = RB/DY2
      DO 5 I = 1, N
      DO 5 J = 1, N
      F = 2.0*PIE/K*SQRT((FAC1*(I-H)**2+(FAC2*(J-H))**2)
      F = F*F
      FACTOR = ((BES4*F+BES3)*F+BES2)*F+BES1
      PR(I, J) + PR(I, J)-RE*FACTOR
      PI(I, J) = PI(I, J)-XM*FACTOR
5     CONTINUE
      CALL SECOND (QT1)
      Q = QT1-QT
      QT = QT1
      PRINT 41, Q
C
C       THIS COMPLETES THE CENTRAL BLOCKAGE CALCULATION.
C
C
C       CALCULATE THE SPAR CORRECTIONS.
C       JJ=1 FOR FIRST SPAR, AND
C       JJ=2 FOR SECOND SPAR.
C
      DO 9 JJ = 1, 2
      DUP = DU1
      IF (DUP.GT. DU2) DUP = DU2
      FAC1 = COS(SIG(JJ))
      FAC2 = SIN(SIG(JJ))
      DY = 2.*PIE/K/WAVENR/DUP
      CONST = PIE
      HK = K/2+1
      DO 6 I = 1, K
      X1P = (I-HK)*DY
      X1 = X1P*FAC1
      X2 = X1P*FAC2
      CALL PHASE (X1, X2, Z, NX, PH)
      PH = PH-(I-HK)*CONST
      A(I) = MAG(X1, X2)*COS(PH)
      B(I) = MAG(X1, X2)*SIN(PH)
6     CONTINUE
      CALL FETR (A, B, K, 0)
C
```

```
C         APPLY PHASE TERM
C
      DO 7 I = 1, K
      PH = -COST*(I-HK)
      COSINE = COS(PH)
      SINE = SIN(PH)
      RE = A(I)*COSINE-B(I)*SINE
      XM = A(I)*SINE+B(I)*COSINE
      A(I) = RE*W*DY
      B(I) = XM*W*DY
7     CONTINUE
C
C         THIS COMPLETES THE SPAR CORRECTION
C         IN THE PRIMED CORDINATES.
C
C
C         APPLY SPAR CORRECTION.
C
      DO 8 I = 1, N
      DO 8 J = 1, N
      COSINE = COS(SIG(JJ))
      SINE = SIN(SIG(JJ))
      S = I-H
      T = J-H
      XV = S*DY/DY1*COSINE-T*DY/DY2*SINE+HK
      IV = XV
      IVP1 = IV+1
      RE = (A(IVP1)-A(IV))*XV+A(IVP1)-(A(IVP1)-A(IV))*IVP1
      XM = (B(IVP1)-B(IV))*XV+B(IVP1)-(B(IVP1)-B(IV))*IVP1
      PR(I, J) = PR(I, J)-RE
      PI(I, J) = PI(I, J)-XM
8     CONTINUE
9     CONTINUE
      CALL SECOND (QT1)
      Q = QT1-QT
      PRINT 42, Q
C
C         THIS COMPLETES THE SPAR CORRECTION.
C
C
C         CALCULATE THE FAR FIELD GAIN.
      AGEO = PIE*DIAM*DIAM/4.
      FACTOR = WAVENR*WAVENR/PIE
      DO 10 I = 1, N
```

```
      DO 10 J = 1, N
      PR(I, J) = FACTOR*(PR(I, J)**2+PI(I, J)**2)
10    CONTINUE
      GAIN = PR(H, H)
      F = 10.*ALOG10(GAIN)
      AF = LAMDA*LAMDA*GAIN/4./PIE
      EFF = AF*100./AGEO
C
C       PRINT AXIAL GAIN PARAMETERS.
C
      PRINT 29
      PRINT 43, GAIN
      PRINT 44, AE
      PRINT 45, F
      PRINT 46, EFF
      DO 12 I = 1, N
      DO 12 J = 1, N
      IF (PR(I, J) .NE. 0.0) GO TO 11
      PR(I, J) = -40.
      GO TO 12
11    PR(I, J) = 10.*ALOG10(PR(I, J))-F
12    CONTINUE
      DO 13 I = 1, N
      DO 13 J = 1, N
      IF (PR(I, J) .LE. -40.) PR(I, J) = -40.
13    CONTINUE
C
C       THIS COMPLETES THE CALCULATION OF
C       THE FAR FIELD GAIN.
C
C
C       IN THE FOLLOWING A CONTAINS THE U1 PATTERN
C       AND B CONTAINS THE U2 PATTERN.
C
      DO 14 I = 1, N
      A(I) = PR(I, H)
      B(I) = PR(H, I)
      D(I) = (I-H)*DU1*SCALE
      E(I) = (I-H)*DU2*SCALE
14    CONTINUE
C
C       CALCULATE BEAM WIDTHS.
C
      D1 = DD1*1000.
```

```
      CALL WIDTH (A, -03., D1, D3, N)
      CALL WIDTH (A, -10., D1, D10, N)
      CALL WIDTH (A, -15., D1, D15, N)
      CALL WIDTH (A, -20., D1, D20, N)
      CALL WIDTH (A, -25., D1, D25, N)
      CALL WIDTH (A, -30., D1, D30, N)
      DT = DD2*1000.
      CALL WIDTH (B, -03., DT, P3, N)
      CALL WIDTH (B, -10., DT, P10, N)
      CALL WIDTH (B, -15., DT, P15, N)
      CALL WIDTH (B, -20., DT, P20, N)
      CALL WIDTH (B, -25., DT, P25, N)
      CALL WIDTH (B, -30., DT, P30, N)
C
C           PRINT BEAM WIDTHS.
C
      PRINT 51
      PRINT 47
      PRINT 48
      PRINT 49, D3, D10, D15, D20, D25, D30
      PRINT 48
      PRINT 50, P3, P10, P15, P20, P25, P30
C
C           PRINT PATTERNS.
C
      PRINT 51
      PRINT 52
      PRINT 54, (A(I), I = 1, N)
      PRINT 51
      PRINT 53
      PRINT 54, (B(I), I = 1, N)
C
C           PRINT PATTERN MAP.
C
      PRINT 29
      PRINT 55
      JJ = -15
15    JJ = JJ+16
      KK = JJ+15
      DO 16 J = 1, N
      II = N-J+1
      PRINT 54, (PR(I, II), I = JJ, KK)
16    CONTINUE
      PRINT 29
      IF (KK .NE. N) GO TO 15
```

```
      PLOT PATTERNS.

 XPLUS = H*DU1*SCALE
 YPLUS = H*DU2*SCALE
 XMINUS = -XPLUS
 YMINUS = -YPLUS
 CALL AXES (6., XMINUS, XPLUS, -1., 4., -40., 0., 5., 5.,
132, 50)
 CALL PLOTITL (JX, 26, 4, 2, 0., -0.5)
 CALL PLOTITL (I0, 3, 0, 2, -.395, 3.94)
 CALL PLOTITL (I5, 3, 0, 2, -.395, 3.44)
 CALL PLOTITL (I10, 3, 0, 2, -.395, 2.94)
 CALL PLOTITL (I15, 3, 0, 2, -.395, 2.44)
 CALL PLOTITL (I20, 3, 0, 2, -.395, 1.94)
 CALL PLOTITL (I25, 3, 0, 2, -.395, 1.44)
 CALL PLOTITL (I30, 3, 0, 2, -.395, 0.94)
 CALL PLOTITL (I35, 3, 0, 2, -.395, 0.44)
 CALL PLOTITL (IDEC, 6, 0, 2, 4.625, 3.69)
 CALL PLOTITL (IPAT, 7, 0, 2, 4.805, 3.44)
 CALL PLOT (D, A, N, -8)
 CALL AXTERM (1)
 CALL AXES (6., YMINUS, YPLUS, -1., 4., -40., 0., 5., 5.,
132, 50)
 CALL PLOTITL (JX, 26, 4, 2, 0., -0.5)
 CALL PLOTITL (I35, 3, 0, 2, -.395, 0.44)
 CALL PLOTITL (I30, 3, 0, 2, -.395, 0.94)
 CALL PLOTITL (I25, 3, 0, 2, -.395, 1.44)
 CALL PLOTITL (I20, 3, 0, 2, -.395, 1.94)
 CALL PLOTITL (I15, 3, 0, 2, -.395, 2.44)
 CALL PLOTITL (I10, 3, 0, 2, -.395, 2.94)
 CALL PLOTITL (I5, 3, 0, 2, -.395, 3.44)
 CALL PLOTITL (I0, 3, 0, 2, -.395, 3.94)
 CALL PLOTITL (IPAT, 7, 0, 2, 4.805, 3.44)
 CALL PLOTITL (IPOL, 5, 0, 2, 4.95, 3.69)
 CALL PLOT (E, B, N, -8)
 CALL AXTERM (1)
 IF (YPLUS .GT. XPLUS) XPLUS = YPLUS
 XMINUS = -XPLUS

      PLOT MAP.

 CALL AXES (6., XMINUS, XPLUS, -1., 6., XMINUS, XPLUS, 5.,
15., 32, 1000)
 CALL PLOTITL (JX, 26, 4, 2, 0., -0.5)
 CALL PLOTITL (MM, 11, 0, 2, 4.5, 5.75)
```

```
      CALL PLOTITL (I3DB, 4, 0, 2, 4.86, 5.50)
      CALL PLOTITL (I10DB, 4, 0, 2, 4.86, 5.25)
      CALL PLOTITL (I20DB, 4, 0, 2, 4.86, 5.0)
      CALL PLOTITL (I30DB, 4, 0, 2, 4.86, 4.75)
      DO 27 JJ = 1, 4
      GO TO (17, 18, 19, 20), JJ
17    C = -3.
      GO TO 21
18    C = -10.
      GO TO 21
19    C = -20.
      GO TO 21
20    C = -30.
21    NN = 0
      KUP = N-1
      DO 25 I = 1, KUP
      XI = I
      DO 25 J = 1, KUP
      XJ = J
      IF ((PR(I, J) .GT. C) .AND. (PR(I, J+1) .LT. C) .OR. (PR(I, J) .LT.
     1C) .AND. (PR(I, J+1) .GT. C)) GO TO 22
      GO TO 23
22    XJ = J
      XJ1 = J+1
      XM = PR(I, J+1)-PR(I, J)
      P = PR(I, J)-XM*XJ
      NN = NN+1
      IF (NN .GE. 2045) GO TO 26
      YY(NN) = ((C-B)/XM-H)*DU2*SCALE
      XX(NN) = (XI-H)*DU1*SCALE
23    CONTINUE
      IF((PR(I, J) .GT. C) .AND. (PR(I+1, J) .LT. C) .OR. (PR(I, J) .LT.
     1C) .AND. (PR(I+1, J) .GT. C)) GO TO 24
      GO TO 25
24    XI1 = XI+1
      XM = PR(I+1, J)-PR(I, J)
      B = PR(I, J)-XM*XI
      NN = NN+1
      IF (NN .GE. 2045) GO TO 26
      XX(NN) = ((C-B)/XM-H)*DU1*SCALE
      YY(NN) = (XJ-H)*DU2*SCALE
25    CONTINUE
26    CONTINUE
      CALL PLOT (XX, YY, NN, JJ)
27    CONTINUE
      CALL AXTERM (1)
```

```
      CALL AXTERM (0)
C
28    FORMAT (8F10.3)
29    FORMAT (1H1)
30    FORMAT (//10X. *THE DIAMETER OF THE ANTENNA=*F6.5*
     1FEET*//10X*LAMDA=*F10.3* METERS*)
31    FORMAT (//10X, *NEXP=*I3, 5X, *KEXP=*I3)
32    FORMAT (//10X, *DELTA U1=*F8.6* DEGREES*5X*DELTA U2=
     1*F8.6* DEGREES*)
33    FORMAT (//10X, *DELTA U1=*E10.3* RADIANS*5X*DELTA U2=
     1*E10.3* RADIANS*)
34    FORMAT (//10X, *THE RADIUS OF THE BLOCKED AREA=*F8.3*
     1INCHES*)
35    FORMAT (//10X*THE ANGLE OF SPAR 1=*F6.1* DEGREES*//
     110X*THE ANGLE OF SPAR 2=*F6.1* DEGREES*)
36    FORMAT (//10X*THE WIDTH OF THE SPARS=*F8.6* INCHES*)
37    FORMAT (//10X*THE EXTENT OF THE NONZERO APERTURE IN
     1THE Y1 DIRECTION=*F6.1* POINTS*)
38    FORMAT (//10X*THE EXTENT OF THE NONZERO APERTURE IN
     1THE Y2 DIRECTION=*F6.1* POINTS*)
39    FORMAT (10X*THE TIME FOR INITILIZING ARRAY=*F16.7* SECONDS*)
40    FORMAT (10X*THE TIME FOR FFT=*F16.7* SECONDS*)
41    FORMAT (10X*THE TIME FOR THE BLOCKAGE CORRECTION=
     1*E16.7* SECONDS*)
42    FORMAT (10X*THE TIME FOR THE SPAR CORRECTION=*E16.7*
     1 SECONDS*)
43    FORMAT (//10X*GAIN=*E16.7)
44    FORMAT (//10X*THE EFFECTIVE AREA=*F8.3* SQ. METERS*)
45    FORMAT (//10X*GAIN=*F8.3* DB*)
46    FORMAT (//10X*EFFICIENCY=*F8.3* PERCENT*)
47    FORMAT (*WIDTHS (M-DEG) 3DB 10DB 15DB 20DB 25DB 30DB*)
48    FORMAT (/)
49    FORMAT (*    U1    *6F7.1)
50    FORMAT (*    U2    *6F7.1)
51    FORMAT (/////)
52    FORMAT (*    THE U1PATTERN FOLLOWS*)
53    FORMAT (*    THE U2PATTERN FOLLOWS*)
54    FORMAT (2X16F7.1)
55    FORMAT (*    PRINT MAP OF PATTERN*)
      END
```

SUBROUTINE XTD (PR, PI, NEXP, KEXP)

```
      SUBROUTINE XTD (PR, PI, NEXP, KEXP)
      DIMENSION PR(128, 128), PI(128, 128)
      DIMENSION A(1024), B(1024)
      IF (NEXP .GE. KEXP) STOP
      N = 2**NEXP
      K = 2**KEXP
      JH = N+1
      DO 3 I = 1, N
      DO 1 J = 1, N
      A(J) = PR(J, I)
1     B(J) = PI(J, I)
      DO 2 J = JH, K
      A(J) = 0.0
2     B(J) = 0.0
      CALL FFTR (A, B, K, 0)
      DO 3 J = 1, N
      PR(J, I) = A(J)
3     PI(J, I) = B(J)
      DO 6 I = 1, N
      DO 4 J = 1, N
      A(J) = PR(I, J)
4     B(J) = PI(I, J)
      DO 5 J = JH, K
      A(J) = 0.0
5     B(J) = 0.0
      CALL FFTR (A, B, K, 0)
      DO 6 J = 1, N
      PR(I, J) = A(J)
6     PI(I, J) = B(J)
      RETURN
      END
```

SUBROUTINE FFTR (X, Y, N, IFWD)

```
      SUBROUTINE FFTR (X, Y, N, IFWD)
      DIMENSION X(1), Y(1)
      COMMON/SCRFFT/ F(1024), G(1024)/FFF/S(512), C(512), IBR(1024)
      MASK = 0000777777777777777B
      NREM = NREM.AND.MASK
      IF (NREM-N) 1,7,1
1     PI = 3.1415926535897932384
      N2 = N/2
      RN = N$PIR = 2.*PI/RN
      NEXP = ALOG10(RN)/ALOG10(2.)
      NEXP1 = NEXP-1
C GENERATE SIN COS ARRAY S, C
      N4 = N/4$S(N4+1) = C(1) = 1.$C(N4+1) = S(1) = 0.0
      N42 = N4+2$N22 = N2+2
      DO 2 I = 2, N4
      CC = COS(PIR*(I-1))
      C(I) = CC$C(N22-I) = -CC$S(N42-1) = CC
2     S(N4+I) = CC
C GENERATE BIT REVERSAL ARRAY IBR
      N1 = N-1$N21 = N2-7
      DO 4 I = 1, N21, 8
      J = I-1$II = 0$ISH = -NEXP-1$MASK = 1
      DO 3 L = 1, NEXP
      ISH = ISH+2
      NEW = LSHIFT(J, ISH)
      NEW = NEW.AND.MASK
      II = II+NEW
3     MASK = LSHIFT(MASK, 1)
      IBR(I) = 1+II
4     IBR(I+N2) = IBR(I)+1
      IBR(3) = N4+1$IBR(5) = N4/2+1$IBR(7) = 3*N4/2+1
      N7 = N-7
      DO 5 I = 9, N7, 8
      IDIF = IBR(I)-IBR(I-8)
      DO 5 J = 2, 6, 2
5     IBR(I+J) = IBR(I+J-8)+IDIF
      DO 6 I = 1, N1, 2
      JJ = N-I+1
6     IBR(JJ) = N-IBR(I)+1
C ADD UP 1ST ROW
7     NREM = N
      IF (IFWD) 8, 8, 10
```

```
8       DO 9 I = 1, N2
        IN2 = I+N2$F(I) = X(I)+X(IN2)
        G(I) = Y(I)+Y(IN2)$G(IN2) = Y(I)-Y(IN2)
9       F(IN2) = X(I)-X(IN2)
        GO TO 12
10      DO 11 I = 1, N2
        IN2 = I+N2$F(I) = X(I)+X(IN2)
        G(I) = -Y(I) - Y(IN2)$G(IN2) = - Y(I)+Y(IN2)
11      F(IN2) = X(I)-X(IN2)
COMPUTE TREE
12      JN = 2
        IF (N-4) 16, 16, 13
13      DO 15 K = 2, NEXP1
        IE = N2/JN$NJN = N/JN$KK = -1
        DO 14 J = 1, JN
        KK = KK+2$IA = IBR(KK)$IS1 = (J-1)*NJN
        DO 14 I = 1, IE
        IS = IS1+I
        ISS = IS+IE
        SAVE = F(IS)$SAVER = G(IS)
        SAVEM = F(ISS)*C(IA)-G(ISS)*S(IA)$SAVES = F(ISS)*S(IA)+G(ISS)*C(IA1)
        F(IS) = SAVEM+SAVE$G(IS) = SAVES+SAVER
        F(ISS) = - SAVEM+SAVE$G(ISS) = -SAVES+SAVER
14      CONTINUE
15      JN = JN*2
C BIT REVERSE AND LAST ROW
16      IF (IFWD) 17, 17, 19
17      DO 18 I = 1, N1, 2
        II = I+1$J = IBR(I)$JJ = IBR(II)
        SAVE = F(II)*C(J)-G(II)*S(J)$SAVER = F(II)*S(J)+G(II)*C(J)
        X(J) = F(I)+SAVE$X(JJ) = F(I)-SAVE
        Y(J) = G(I)+SAVER
18      Y(JJ) = G(I)-SAVER
        RETURN
19      DO 20 I = 1, N1, 2
        II = I+1$J = IBR(I)$JJ = IBR(II)
        SAVE = F(II)*C(J)-G(II)*S(J)$SAVER = F(II)*S(J)+G(II)*C(J)
        X(J) = (F(I)+SAVE)/RN$X(JJ) = (F(I)-SAVE)/RN
        Y(J) = (-G(I)-SAVER)/RN
20      Y(JJ) = (-G(I)+SAVER)/RN
        RETURN
        END
```

SUBROUTINE WIDTH (A, C, DT, W, N)

```
      SUBROUTINE WIDTH (A, C, DT, W, N)
C
C       THIS ROUTINE CALCULATES THE WIDTH AT
C       LEVEL C OF A WITH DISTANCE DT BETWEEN POINTS.
C
      DIMENSION A(128)
      INTEGER H
      H = N/2+1
      DO 2 I = H, N
      IF ((A(I) .GT. C) .AND. (A(I+1) .LE. C)) GO TO 1
      GO TO 2
1     XM = A(I+1)-A(I)
      B = A(I)-XM*I
      HW = ((C-B)/XM-H)*DT
      GO TO 3
2     CONTINUE
3     CONTINUE
      DO 5 I = 1, H
      IF ((A(I) .LE. C) .AND. (A(I+1) .GT. C)) GO TO 4
      GO TO 5
4     XM = A(I+1)-A(I)
      B = A(I)-XM*I
      HW2 = (H-(C-B)/XM)*DT
5     CONTINUE
      W = HW+HW2
      RETURN
      END
```

FUNCTION MAG (X, Y)

```
      FUNCTION MAG (X, Y)
C
C       THIS ROUTINE CALCULATES THE TAPERING
C       FUNCTION FOR A 2RO METER ANTENNA WITH A FOCAL
C       LENGTH FO.
C       GAIN IS THE GAIN OF THE FEED SYSTEM.
C
      COMPLEX G
      REAL MAG
      G = (0., 0.)
      PIE = 3.1415926535
      FO = 8.*12.*2.54/100.
      RO = FO
      RSQ = X**2+Y**2
      R = SQRT(RSQ)
      IF (R.GT.RO) GO TO 1
      Z1 = RSQ/4./FO
      PS = ATAN(R/(FO-Z1)
      SC = -3.1415926535/2.
      IF (Y .GE. 0.0) XC = 3.1415926535/2.
      IF (X .NE. 0.0) XC = ATAN(Y/X)
      A = 1.0
      B = 0.66
      CALL FEED (GAIN, PS, XC, A, B, G)
      MAG = GAIN/4./PIE/(FO+R*R/4./FO)**2
      MAG = SQRT(MAG)
      RETURN
      CONTINUE
      MAG = 0.0
      RETURN
      END
```

SUBROUTINE FEED (GAIN, TH, PH, A, B, G)

```
      SUBROUTINE FEED (GAIN, TH, PH, A, B, G)
C
C       THIS ROUTINE CALCULATES THE DIRECTIVITY OF A
C       HORN ANTENNA IN DIRECTION TH=THETA
C       AND PH=PHI.  THE DIMENSIONS OF THE HORN ARE
C       A/LAMDA AND B/LAMDA.
C
      COMPLEX CT1, CT2, CT3, CT4, G
      PI = 3.1415926535
      G2 = 1.0-CABS(G)*CABS(G)
      X = PI*PI*PI/2./G2
      U = SQRT(1.-.25/A/A)
      S = SIN(TH)
      P   COS(PH)
      T1 = PI*A*S*P
      F1 = COS(T1)/(T1*T1-PI*PI*.25)
      F1 = F1*F1
      SP = SIN(PH)
      T2 = PI*B*S*SP
      F2 = 1.0
      IF (T2 .NE. 0.0) F2 = SIN(T2)/T2
      F2 = F2*F2
      CT = COS(TH)
      T1 = 1.+U*CT
      CT1 = T1*(1.0, 0.0)
      CT2 = CT1+G*CT1
      T3 = CABS(CT2)
      T4 = SP*SP*T3*T3
      T1 = CT+U
      CT1 = T1*(1.0, 0.0)
      T2 = CT-U
      CT2 = T2*(1.0, 0.0)
      CT3 = CT1+G*CT2
      T3 = CABS(CT3)
      F3 = T4+P*P*T3*T3
      GAIN = X*A*B*F1*F2*F3/U
      RETURN
      END
```

SUBROUTINE PHASE (X1, X2, Z, NX, PH)

```
SUBROUTINE PHASE (X1, X2, Z, NX, PH)
PH=0.0
RETURN
END
```

APPENDIX B

A. Introduction

This Appendix gives the proofs of the astigmatic phase error properties. The phase error in the aperture plane under this model is given by Equation (25),

$$L(\underline{x}) = \left[\alpha x_1^2 + \beta x_1 x_2 - \alpha x_2^2 + \Gamma K(x_1^2 + x_2^2)\right]/R_o^2.$$

All of these properties take advantage of the fact that $L(\underline{x})$ is even, i.e.

$$L(\underline{x}) = L(-\underline{x}).$$

B. Property 1

If the illumination function $E(\underline{x})$ is symmetric about the origin, i.e. $E(\underline{x}) = E(-\underline{x})$, then any contour map is symmetric about the origin for all feed positions and reflector errors. That is

$$G(\underline{u}) = G(-\underline{u}). \text{ for all } \alpha, \beta, \text{ and } \Gamma.$$

Proof of Property 1

The gain is given by Equation (7) as

$$G(u_1, u_2, \alpha, \beta, \Gamma) = \frac{\eta k^2}{4\pi z_o P_{in}} \left| \int_{\underline{x}} E(\underline{x})\, e^{j k L(\underline{x})}\, e^{j k \underline{u} \cdot \underline{x}}\, d\underline{x} \right|^2.$$

Now by the assumptions of the property

$$E(\underline{x}) = E(-\underline{x})$$

and

$$L(\underline{x}) = L(-\underline{x}).$$

Making use of these assumptions and changing variables to $\underline{y}$, $\underline{y} = -\underline{x}$, one has

$$G(u_1, u_2, \alpha, \beta, \Gamma) = \frac{\eta k^2}{4\pi z_o P_{in}} \left| \int_{\underline{y}} E(\underline{y})\, e^{j k L(y)}\, e^{j k (-\underline{u}) \cdot \underline{y}}\, d\underline{y} \right|^2$$

$$= G(-u_1, -u_2, \alpha, \beta, \Gamma).$$

This completes the proof of property 1.

C. Property 2

If the illumination function $E(\underline{x})$ is only a function of r, the radius from the center of the aperture, when a contour map of the pattern is symmetric about the lines

$$\tan 2\varphi = \frac{-\beta}{2\alpha}$$

for all feed positions.

Proof of property 2

In order to prove this property it is sufficient to show that

$$G(u_1', u_2', \alpha, \beta, \Gamma) = G(-u_1', u_2', \alpha, \beta, \Gamma)$$

and

$$G(u_1', u_2', \alpha, \beta, \Gamma) = G(u_1', -u_2', \alpha, \beta, \Gamma)$$

in a coordinate system $\underline{u}'$ which is at an angle φ to the $\underline{u}$ coordinates. Only the first of these equalities will be shown.

The $\underline{u}'$ coordinates are related to the $\underline{u}$ coordinates by the well known rotation

$$\underline{u}' = \underline{R}\underline{u},$$

where

$$\underline{R} = \begin{bmatrix} \cos\varphi & -\sin\varphi \\ \sin\varphi & \cos\varphi \end{bmatrix}$$

Also let us define the $\underline{x}'$ coordinates by the same rotation

$$\underline{x}' = \underline{R}\underline{x}.$$

Substituting $\underline{u}'$ into Equation (7), one has

$$G(u_1', u_2', \alpha, \beta, \Gamma) = \frac{\eta\, k^2}{4\pi z_o P_{in}} \left| \int_{\underline{x}} E(r) \cdot e^{j\,k\,L(\underline{x})}\, e^{j\,k[\underline{R}^{-1}\,\underline{u}']^T \cdot \underline{x}}\, d\underline{x} \right|^2$$

Changing variables to $\underline{x}'$ in the above, one has

$$G(u_1', u_2', \alpha, \beta, \Gamma) = \frac{\eta\, k^2}{4\pi z_o P_{in}} \left| \int_{\underline{x}'} E(r) e^{jk\{\alpha'(x_1'^2 - x_2'^2)} \right.$$

$$\left. + \Gamma(x_1'^2 + x_1'^2)\}/R_o^2}\, e^{jk\{u_1'x_1' + u_2'x_2'\}}\, dx_1' dx_2' \right|^2,$$

where $\alpha' = \alpha \sec 2\varphi.$

Changing variables once again so that $y = -x_1$, it follows that:

$$G(u_1', u_2', \alpha, \beta, \Gamma) = \frac{\eta\, k^2}{4\pi z_o P_{in}} \left| \int_{x_2} \int_{y} E(r)\, e^{jk\{(y^2 - x_2'^2) + \Gamma(y^2 + x_2'^2)\}/R_o} \right.$$

$$\left. e^{jk\{(-u_1')\,y + u_2'\,x_2\}}\, dy\, dx_2 \right|^2 = G(-u_1', u_2', \alpha, \beta, \Gamma)$$

This completes the proof of property 2.

D. Property 3

If the illumination function $E(\underline{x})$ is symmetric about the origin, i.e. $E(\underline{x}) = E(-\underline{x})$, then the gain is an even function of α, β, and Γ taken together. That is

$$G(u_1, u_2, \alpha, \beta, \Gamma) = G(u_1, u_2, -\alpha, -\beta, -\Gamma).$$

Proof of Property 3

The gain function may be written by Equation (7) as:

$$G(u_1, u_2, \alpha, \beta, \Gamma) = \frac{\eta k^2}{4\pi z_o P_{in}} \left| \int_{\underline{x}} E(\underline{x}) \, e^{jk\{\alpha x_1^2 + \beta x_1 x_2 - \alpha x_2^2 + \Gamma(x_1^2 + x_2^2)\}/R_o^2} \, e^{jk\{u_1 x_1 + u_2 x_2\}} \, d\underline{x} \right|^2.$$

The magnitude of a complex number is the magnitude of its complex conjugant, so

$$G(u_1, u_2, \alpha, \beta, \Gamma) = \frac{\eta k^2}{4\pi z_o P_{in}} \left| \int_{\underline{x}} E(\underline{x}) \, e^{jk\{(-\alpha) x_1^2 - \beta x_1 x_2 - (-\alpha) x_2^2 + (-\Gamma)(x_1^2 + x_2^2)\}/R_o^2} \, e^{jk\{-u_1 x_1 - u_2 x_2\}} \, d\underline{x} \right|^2$$

$$= G(-u_1, -u_2, -\alpha, -\beta, -\Gamma) = G(u_1, u_2, -\alpha, -\beta, -\Gamma).$$

The last equality follows from property 1. This completes the proof of property 3.

E. Property 4

If the illumination function $E(\underline{x})$ is only a function of r, then the angular coordinates which are aligned with the φ direction, $\tan 2\varphi = \frac{\Gamma\beta}{2\alpha}$, change roles when α and β change sign. That is

$$G(u_1', u_2', \alpha, \beta, \Gamma) = G(u_2', u_1', -\alpha, -\beta, \Gamma),$$

where

$$\begin{bmatrix} u_1' \\ u_2' \end{bmatrix} \begin{bmatrix} \cos\varphi & -\sin\varphi \\ \sin\varphi & \cos\varphi \end{bmatrix} \begin{bmatrix} u_1 \\ u_2 \end{bmatrix}.$$

Proof of Property 4

From property 3, one has

$$G(u_1', u_2', \alpha, \beta, \Gamma) = G(u_1', u_2', -\alpha, -\beta, -\Gamma).$$

Then from property 5 to be proved subsequently, it follows that:

$$G(u_1', u_2', -\alpha, -\beta, -\Gamma) = G(u_2', u_1', -\alpha, -\beta, +\Gamma).$$

This completes the proof of property 4.

F. Property 5

If the illumination function $E(\underline{x})$ is only a function of r, then the angular coordinates which are aligned with the φ direction, $\tan 2\varphi = \frac{-\beta}{2\alpha}$, change roles when Γ changes sign. That is

$$G(u_1', u_2', \alpha, \beta, \Gamma) = G(u_2', u_1', \alpha, \beta, -\Gamma).$$

Proof of Property 5

Referring to the proof of property 2, one has

$$G(u_1', u_2', \alpha, \beta, \Gamma) = \frac{\eta k^2}{4\pi z_o P_{in}} \left| \int_{\underline{x}'} E(r) e^{jk\{\alpha' (x_1'^2 - x_2'^2)} \right.$$

$$\left. + \Gamma(x_1'^2 + x_2'^2)\}/R_o^2 \; e^{jk\{u_1' x_1' + u_2' x_2'\}} \, dx_1' \, dx_2 \right|^2.$$

Once again observing that the magnitude of a complex number is the magnitude of its complex conjugant, one can rewrite the above equation as

$$G(u_1', u_2', \alpha, \beta, \Gamma) = \frac{\eta k^2}{4\pi z_o P_{in}} \left| \int_{\underline{x}'} E(r) e^{jk\{\alpha' (x_2'^2 - x_1'^2)} \right.$$

$$\left. - \Gamma(x_1'^2 + x_2'^2)\}/R_o^2 \; e^{-jk\{u_1' x_1' + u_2' x_2'\}} \, dx_1' \, dx_2' \right|^2.$$

Now changing variables to

$$y_1 = -x_2$$

$$y_2 = -x_1,$$

it follows that:

$$G(u_1', u_2', \alpha, \beta, \Gamma) = \frac{\eta k^2}{4\pi z_o P_{in}} \left| \int_{\underline{y}} E(r) e^{jk\{\alpha' (y_1^2 - y_2^2)} \right.$$

$$\left. - \Gamma(y_1^2 + y_2^2)\}/R_o^2 \; e^{jk\{u_1' y_2 + u_2' y_1\}} \, d\underline{y} \right|^2$$

$$= G(u_2', u_1', \alpha, \beta, -\Gamma).$$

This completes the proof of property 5.

APPENDIX C

This appendix gives two theorems which concern the frequency dependence of reflector antenna efficiency. Theorem 1 and 2 concern prime focus instruments with simple point source feed systems. Theorem 1, however, is extended to apply to a Cassegrain antenna system.

Theorem 1 requires as input data the design efficiency, η_o, the measured efficiency at some frequency, $\eta'(f_m) \pm B_m$, and an estimate of the peak reflector phase error in radians, $K(f_m)$. From this information Theorem 1 predicts both an upper and lower bound at another frequency, f_e.

Theorem 1 may be stated as follows:

Theorem 1

If the feed system of a prime focus reflector antenna at a frequency f_e is a scale model of the feed system at f_m, and

$$\left| \eta'(f_m) - \eta(f_m) \right| \leq B_m$$

and

$$\left| \delta(f_m, \underline{x}) - \delta(f_m, \underline{y}) \right| \leq K(f_m), \text{ all } \underline{x} \text{ and } \underline{y},$$

then the bounds

$$\eta(f_e) \leq \eta_o - P\left[\eta_o - \eta'(f_m)\right]\left(\frac{f_e}{f_m}\right)^2 + \eta_o \sup S + P\, B_m \left(\frac{f_e}{f_m}\right)^2, \text{ for all } P$$

and

$$\eta(f_e) \geq \eta_o - P\left[\eta_o - \eta'(f_m)\right]\left(\frac{f_e}{f_m}\right)^2 + \eta_o \inf S - P\, B_m \left(\frac{f_e}{f_m}\right)^2, \text{ for all } P$$

hold. The set S is defined as

$$S = \left\{z : z = U\left(\frac{f_e}{f_m}\right) - P\left(\frac{f_e}{f_m}\right)^2 U(x);\ 0 \leq x \leq K(f_m)\right\}.$$

The function U(x) is given by

$$U(\underline{x}) = \cos(\underline{x}) - 1.$$

Proof of Theorem 1

Recall from the text that the efficiency of a reflector antenna can be expanded into an infinite series in even powers of frequency. This series is given in Equation (31) as

$$\eta(f) = \sum_{n=0}^{\infty} f^{2n} A_{2n}$$

Denote by A_2' the estimate of A_2 based upon the true efficiency at f_m, i.e.

$$A_2' = \frac{1}{f_m^2}\left[\eta(f_m) - \eta_o\right].$$

Let us define the estimate of the efficiency at frequency f_e as

$$\eta_e(f_e) = \eta_o + P\, A_2'\, f_e^2$$

where P is a free parameter. Now one has

$$\eta(f_e) - \eta_e(f_e) = \sum_{n=0}^{\infty} A_{2n} f_e^{2n} - \eta_o - P[\eta(f_m) - \eta_o] \left(\frac{f_e}{f_m}\right)^2.$$

Substituting of the series expression for $\eta(f_m)$ into the above equation and using straightforward manipulation, one obtains

$$\eta(f_e) - \eta_e(f_e) = \sum_{n=2}^{\infty} A_{2n} f_e^{2n} + (1 - P) A_2 f_e^2 - P\left(\frac{f_e}{f_m}\right)^2 \sum_{n=2}^{\infty} A_{2n} f_m^{2n}.$$

Making use of a remainder function $R[x]$ defined as $R[x] = \cos(x) + x^2/2 - 1$, one has

$$\eta(f_e) = \eta_o - P[\eta_o - \eta(f_m)] \left(\frac{f_e}{f_m}\right)^2 + F \int_{\underline{\tau}} \int_{\underline{x}}$$

$$E(\underline{x})\, E(\underline{x} + \underline{\tau}) \left\{R[u] - (1 - P)\, u^2/2 - P\left(\frac{f_e}{f_m}\right)^2 R\left[\frac{f_m}{f_e} u\right]\right\} d\underline{x}\, d\underline{\tau},$$

where

$$u = \delta(f_e, \underline{x}) - \delta(f_e, \underline{x} + \underline{\tau}),$$

and δ is the reflector phase error function. The proportionality factor, F, is defined in the text.

The integral above is the mathematical error of approximation. It may be possible to actually perform the integral with $\delta(x)$ being obtained from a STAIR program or mechanical measurement of the reflector surface. The result of this calculation would be a small correction to the efficiency estimate. The purpose here, however, is to bound this error.

Using the mean value theorem, one has

$$\eta(f_e) \leq \eta_o - P[\eta_o - \eta(f_m)]\left(\frac{f_e}{f_m}\right)^2 + \eta_o \sup S$$

and

$$\eta(f_e) \geq \eta_o - P[\eta_o - \eta(f_m)]\left(\frac{f_e}{f_m}\right)^2 + \eta_o \inf S$$

where S is a set defined as

$$S = \left\{z : z = R[u] - (1 - P)u^2/2 - P\left(\frac{f_e}{f_m}\right)^2 R\left[\frac{f_m}{f_e} u\right] ; 0 \leq u \leq K(f_e)\right\}.$$

This definition for S is equivalent to the one given in the text. One must now take the measurement errors into account. Thus,

$$\eta(f_e) \leq \eta_o - P[\eta_o - \eta'(f_m)]\left(\frac{f_e}{f_m}\right)^2 + \eta_o \sup S + P\left(\frac{f_e}{f_m}\right)^2 B_m, \text{ for all } P$$

and

$$\eta(f_e) \geq \eta_o - P[\eta_o - \eta'(f_m)]\left(\frac{f_e}{f_m}\right)^2 + \eta_o \inf S - P\left(\frac{f_e}{f_m}\right)^2 B_m, \text{ for all } P$$

This completes the proof of Theorem 1.

Theorem 2 is similar to Theorem 1. It uses a measurement at two frequencies to imply bounds at a third frequency. Theorem 2 may be stated as follows:

Theorem 2

If the feed system of a prime focus reflector antenna is scaled at frequencies f_e, f_1, and f_2, and

$$|\eta'(f_1) - \eta(f_1)| \leq B_1$$

$$|\eta'(f_2) - \eta(f_2)| \leq B_2,$$

$$|\delta(f_e, \underline{x}) - \delta(f_e, \underline{y})| \leq K(f_e) \text{ all } \underline{x} \text{ and } \underline{y},$$

and A_2'' and A_4'' are roots of the equations

$$\eta_o + A_2'' f_1^2 + A_4'' f_2^4 = \eta'(f_1)$$

$$\eta_o + A_2'' f_2^2 + A_4'' f_2^4 = \eta'(f_2).$$

Then,

$$\eta(f_e) \leq \eta_o + PA_2'' f_e^2 + QA_4'' f_e^4 + |F_1| B_1 + |F_2| B_2 + \eta_o \sup S,$$

for all P and Q

and

$$\eta(f_e) \geq \eta_o + PA_2'' f_e^2 + QA_4'' f_e^4 - |F_1| B_1 - |F_2| B_2 + \eta_o \inf S,$$

for all P and Q,

where

$$S = \left\{z: z = F_2 T\left[\frac{f_2}{f_e} u\right] - F_1 T\left[\frac{f_1}{f_e} u\right] + T[u] - (1 - P) u^2/2!\right.$$

$$\left. +(1 - Q) u^4/4!;\ 0 \leq u \leq K(f_e)\right\}$$

Proof of Theorem 2

The proof of Theorem 2 differs from that of Theorem 1 in that three terms of the cosine series are used instead of two. Define $\eta_e(f_e)$ as

$$\eta_e(f_e) = \eta_o + P\, A_2'' f_e^2 + Q\, A_4'' f_e^4,$$

where P and Q are free parameters. Now one has

$$\eta(f_e) - \eta_e(f_e) = \sum_{n=0}^{\infty} f_e^{2n} A_{2n} - \eta_o - P\, A_2'' f_e^2 - Q\, A_4'' f_e^4.$$

Let us define A_2' and A_4' as the values A_2'' and A_4'' would have were there no measurement errors. A sequence of straightforward manipulations yields

$$\eta(f_e) - \eta_e(f_e) = P(A_2 - A_2') f_e^2 + Q(A_4 - A_4') f_e^4$$

$$+(1 - P) A_2 f_e^2 + (1 - Q) A_4 f_e^4 + \sum_{n=3}^{\infty} f_e^{2n} A_{2n}$$

$$+ P(A_2' - A_2'') f_e^2 + Q(A_4' - A_4'') f_e^4. \qquad (C1)$$

The first five terms are errors in approximation while the last two are caused by measurement errors. Clearly the summation term is

$$\sum_{n=3}^{\infty} f_e^{2n} A_{2n} = F \int_{\tau} \int_{x} f(\underline{x})\, f(\underline{x} + \underline{\tau})\, T[\delta(f_e, \underline{x}) - \delta(f_e, \underline{x} + \underline{\tau})]\, d\underline{x}\, d\underline{\tau},$$

where

$$T[x] = \cos x - 1 + x^2/2! - x^4/4!.$$

One can now obtain expressions for $A_2 - A_2'$ and $A_4 - A_4'$. The definitions for A_2' and A_4' may be written as

$$\eta_o + A_2' f_1^2 + A_4' f_1^4 = \eta(f_1)$$

$$\eta_o + A_2' f_2^2 + A_4' f_2^4 = \eta(f_2).$$

Rewriting this set of equations in matrix form, one has

$$\begin{bmatrix} f_1^2 & f_1^4 \\ f_2^2 & f_2^4 \end{bmatrix} \begin{bmatrix} A_2' \\ A_4' \end{bmatrix} = \begin{bmatrix} f_1^2 & f_1^4 \\ f_2^2 & f_2^4 \end{bmatrix} \begin{bmatrix} A_2 \\ A_4 \end{bmatrix} + \begin{bmatrix} \sum_{n=3}^{\infty} f_1^{2n} A_{2n} \\ \sum_{n=3}^{\infty} f_2^{2n} A_{2n} \end{bmatrix}.$$

By inverting the square matrix above, it can be seen that A_2 and A_4 are A_2' and A_4' respectively, plus error times. Thus

$$\begin{bmatrix} A_2' - A_2 \\ A_2' - A_4 \end{bmatrix} = \frac{1}{(f_1 f_2)^2 (f_2^2 - f_1^2)} \begin{bmatrix} f_2^4 - f_1^4 \\ -f_2^2 \quad f_1^2 \end{bmatrix} \begin{bmatrix} \sum_{n=3}^{\infty} f_1^{2n} A_{2n} \\ \sum_{n=3}^{\infty} f_2^{2n} A_{2n} \end{bmatrix}$$

and calculating at each error term individually one has

$$A_2' - A_2 = \frac{1}{(f_1 f_2)^2 (f_2^2 - f_1^2)} \left[f_2^4 \sum_{n=3}^{\infty} f_1^{2n} A_{2n} - f_1^4 \sum_{n=3}^{\infty} f_2^{2n} A_{2n} \right]$$

and

$$A_4' - A_4 = \frac{1}{(f_1 f_2)^2 (f_2^2 - f_1^2)} \left[f_1^2 \sum_{n=3}^{\infty} f_2^{2n} A_{2n} - f_2^2 \sum_{n=3}^{\infty} f_1^{2n} A_{2n} \right].$$

Rewriting once again, one has

$$A_2 - A_2' = \frac{f_1^2}{f_2^2 (f_2^2 - f_1^2)} F \int_{\tau} \int_{x} E(\underline{x}) E(\underline{x} + \tau) \left\{ T[\delta(f_2, \underline{x}) - \delta(\underline{x} + \underline{\tau})] \right.$$

$$- \left(\frac{f_2}{f_1}\right)^4 T[\delta(f_1 \underline{x}) - \delta(f_1, \underline{x} + \underline{\tau})]\Big\} \, d\underline{x} \, d\underline{\tau} \qquad \text{(C2)}$$

and

$$A_4 - A_4' = - \frac{1}{f_2^2 (f_2^2 - f_1^2)} F \int_{\tau} \int_{x} E(x) \, E(x + \tau) \Big\{ T[\delta(f_2, \underline{x}) - \delta(f_2, \underline{x} + \underline{\tau})]$$

$$- \left(\frac{f_2}{f_1}\right)^2 T[\delta(f_1, \underline{x} + \underline{\tau})]\Big\} \, d\underline{x} \, d\underline{\tau}. \qquad \text{(C3)}$$

Now one needs an expression for the measurement errors $A_2' - A_2''$ and $A_4' - A_4''$. This may be accomplished by subtracting the defining relations for A_2'', and A_4'' from the defining equations for A_2' and A_4', i.e.

$$(A_2' - A_2'') f_1^2 + (A_4' - A_4'') f_1^4 = \eta(f_1) - \eta'(f_1) = \epsilon_1$$

$$(A_2' - A_2'') f_2^2 + (A_4' - A_4'') f_2^4 = \eta(f_2) - \eta'(f_2) = \epsilon_2,$$

where ϵ_1 and ϵ_2 are the measurement errors. Inverting this pair of equations one obtains

$$A_2' - A_2'' = \left(\frac{f_2}{f_1}\right)^2 \frac{\epsilon_1}{f_2^2 - f_1^2} - \left(\frac{f_1}{f_2}\right)^2 \frac{\epsilon_2}{f_2^2 - f_1^2} \qquad \text{(C4)}$$

and

$$A_4' - A_4'' = \frac{\epsilon_2}{f_2^2 (f_2^2 - f_1^2)} - \frac{\epsilon_1}{f_1^2 (f_2^2 - f_1^2)} . \qquad \text{(C5)}$$

Substitution of Equations (C2), (C3), (C4), and (C5) into Equation (C1) gives

$$\eta(f_e) - \eta_e(f_e) = F \int\int E(\underline{x})\, E(\underline{x} + \underline{\tau}) \left\{ F_2\, T\left[\frac{f_2}{f_e}\, u\right] - F_1\, T\left[\frac{f_1}{f_e}\, u\right] \right.$$

$$\left. + T[u] - (1 - P)\, u^2/2! + (1 - Q)\, u^4/4! \right\} d\underline{x}\, d\underline{\tau} + F_1\, \epsilon_1 - F_2\, \epsilon_2,$$

where

$$u = \delta(f_e, \underline{x}) - \delta(f_e, \underline{x} + \underline{\tau}),$$

and

$$F_2 = \frac{f_e^{\,2}\,(P\, f_1^{\,2} - Q\, f_e^{\,2})}{f_2^{\,2}\,(f_2^{\,2} - f_1^{\,2})}$$

$$F_1 = \frac{f_e^{\,2}\,(P\, f_2^{\,2} - Q\, f_e^{\,2})}{f_1^{\,2}\,(f_e^{\,2} - f_1^{\,2})}.$$

Thus, since $|\epsilon_1| \le B_1$ and $|\epsilon_2| \le B_2$

$$\eta(f_e) \le \eta_e(f_e) + \eta_o \sup S + |F_1|\, B_1 + |F_2|\, B_2, \text{ for all } P \text{ and } Q$$

and

$$\eta(f_e) \ge \eta_e(f_e) + \eta_o \inf S - |F_1|\, B_1 - |F_2|\, B_2, \text{ for all } P \text{ and } Q.$$

This completes the proof of Theorem 2.

Theorem 1, Cassegrain Antenna Version

The extension of Theorem 1 to the case of a Cassegrain antenna depends upon considering only the most significant terms in an expansion of the efficiency. A Cassegrain system in general has a slightly different illumination function at two different frequencies. The fractional change

in the illumination at the two frequencies will be given by $e(\underline{x})$, i.e.

$$E(f_e, \underline{x}) = E(f_m, \underline{x} + \tau)\,[1 + e(\underline{x})],$$

where f_e is the frequency of estimation and f_m is the frequency of measurement. In addition the feed system of a Cassegrain antenna system usually introduces a small phase error. This error will be denoted by $k\ell(\underline{x})$.

With these definitions and the assumptions listed in the text the stated bounds can be derived. These added assumptions are as follows:

1. Integrals involving the sine of the reflector phase error differences between two points in the aperture are negligible. The Ruze model for the reflector error predicts that the expectation of these integrals are identically zero. In addition the Ruze model will be used explicitly to evaluate one term.
2. Fourth order terms and above in $e(\underline{x})$, $\ell(\underline{x})$, and $\delta(\underline{x})$ can be eliminated. The $\delta^4(\underline{x})$ terms are retained, however.

The efficiency at frequency f_e is

$$\eta(f_e) = F \int_{\tau} \int_{\underline{x}} E(f_e, \underline{x})\, E(f_e, \underline{x} + \underline{\tau}) \cos [S_e + T_e]\, d\underline{x}\, d\underline{\tau}$$

where $E(f_e, \underline{x})$ is the magnitude of the electric field in the aperture plane at the frequency f_e. The functions S_e and T_e are

$$S_e = \ell(f_e, \underline{x}) - \ell(f_e, \underline{x} + \underline{\tau})$$

and

$$T_e = \delta(f_e, \underline{x}) - \delta(f_e, \underline{x} + \underline{\tau}).$$

Expanding the cosine of a sum factor, the above expression becomes

$$\eta(f_e) = F \int_{\underline{\tau}} \int_{\underline{x}} E(f_e, \underline{x})\, E(f_e, \underline{x} + \underline{\tau}) \cos S_e \cos T_e \, d\underline{x}\, d\underline{\tau}$$

$$- F \int_{\underline{\tau}} \int_{\underline{x}} E(f_e, x)\, E(f_e, \underline{x} + \underline{\tau}) \sin S_e \sin T_e \, d\underline{x}\, d\underline{\tau}.$$

The second integral in this expression is zero under assumption 2 above. It is felt that this term should be very small for any reasonable phase function δ.

One can now expand the cosine of T_e term in the first integral so that

$$\eta(f_e) = \eta_o(f_e) - F \int_{\underline{\tau}} \int_{\underline{x}} E(f_e, \underline{x})\, E(f_e, \underline{x} + \underline{\tau})\, T_e^{\,2}/2! \, d\underline{x}\, d\underline{\tau}$$

$$+ F \int_{\tau} \int_{\underline{x}} E(f_e, \underline{x})\, E(f_e, \underline{x} + \underline{\tau})\, R[T_e] \, d\underline{x}\, d\tau$$

where $R[x]$ is defined as

$$R[x] = \cos x - 1 + x^2/2! \, .$$

The $\cos S_e$ term has been eliminated from the second integral by assumption 2. The leading term is by definition the design efficiency, $\eta_o(f_e)$, the

efficiency without phase errors in the primary reflector.

Inserting the free parameter P and taking advantage of the fact that the reflector errors scale, one has

$$\eta(f_e) = \eta_o(f_e) - P\left(\frac{f_e}{f_m}\right)^2 F \int_{\underline{\tau}} \int_{\underline{x}} E(f_e, \underline{x})\, E(f_e, \underline{x} + \underline{\tau})\, T_m{}^2/2!\, d\underline{x}\, d\underline{\tau}$$

$$+ F \int_{\underline{\tau}} \int_{\underline{x}} E(f_e, \underline{x})\, E(f_e, \underline{x} + \underline{\tau}) \left\{(P - 1)\, T_e{}^e/2! + R[T_e]\right\} d\underline{x}\, d\underline{\tau}.$$

Substituting the fractional change in illumination into this expression, it follows that

$$\eta(f_e) = \eta_o(f_e) - P\left(\frac{f_e}{f_m}\right)^2 F \int_{\underline{\tau}} \int_{\underline{x}} E(f_m, \underline{x})\, E(f_m, \underline{x} + \underline{\tau})\, T_m{}^2/2!\, d\underline{x}\, d\underline{\tau}$$

$$-P\left(\frac{f_e}{f_m}\right)^2 F \int_{\underline{\tau}} \int_{\underline{x}} [e(\underline{x}) + e(\underline{x} + \underline{\tau}) + e(\underline{x})\, e(x + \tau)]\, E(f_m, \underline{x})\, E(f_m, \underline{x} + \underline{\tau})$$

$$T_m{}^2/2!\, d\underline{x}\, d\underline{\tau}$$

$$+F \int_{\underline{\tau}} \int_{\underline{x}} E(f_e, \underline{x})\, E(f_e, \underline{x} + \underline{\tau}) \left\{(P - 1)\, T_e{}^2/2! + R[T_e]\right\} d\underline{x}\, d\underline{\tau}.$$

The second integral is now evaluated by the Ruze model after fourth and higher order terms are dropped so that the expansion becomes

$$\eta(f_e) = \eta_o(f_e) - P\left(\frac{f_e}{f_m}\right)^2 F \int_{\underline{\tau}} \int_{\underline{x}} E(f_m, \underline{x})\, E(f_m, \underline{x} + \underline{\tau})\, T_m^2/2!\, d\underline{x}\, d\underline{\tau}$$

$$+ P\left(\frac{f_e}{f_m}\right)^2 \sigma^2 (f_m) [\eta_o(f_m) - \eta_o(f_e)]$$

$$+ F \int_{\tau} \int_{x} E(f_e, \underline{x})\, E(f_e, \underline{x} + \underline{\tau}) \left\{(P - 1)\, T_e^2/2! + R[T_e]\right\} d\underline{x}\, d\underline{\tau}.$$

The task now is to determine an expression for the first integral above in terms of the efficiency at the measurement frequency. This can be done by taking the difference between the true efficiency, $\eta(f_m)$, at f_m and the design efficiency at f_m, $\eta_o(f_m)$:

$$\eta(f_m) - \eta_o(f_m) = F \int_{\underline{\tau}} \int_{\underline{x}} E(f_m, \underline{x})\, E(f_m, \underline{x} + \underline{\tau}) \cos S_m \cos T_m$$

$$- F \int_{\underline{\tau}} \int_{\underline{x}} E(f_m, \underline{x})\, E(f_m, \underline{x} + \underline{\tau}) \cos S_m.$$

In the first integral the sin T_m terms were eliminated by assumption 1 as before. Expanding the cosine terms in a power series and applying assumption 2, one obtains

$$\eta'(f_m) - \eta_o(f_m) = - F \int_{\underline{\tau}} \int_{\underline{x}} E(f_m, \underline{x})\, E(f_m, \underline{x} + \underline{\tau})\, T_m^2/2!\, d\underline{x}\, d\underline{\tau}$$

$$+ F \int_{\underline{\tau}} \int_{\underline{x}} E(f_m, \underline{x})\, E(f_m, \underline{x} + \underline{\tau})\, R[T_m]\, d\underline{x}\, d\underline{\tau}.$$

Solving for the first integral and substituting the result into Equation one has

$$\eta(f_e) = \eta_o(f_e) - P\left(\frac{f_e}{f_m}\right)^2 [\eta_o(f_m) - \eta(f_m)]$$

$$+ P\,\sigma^2(f_e)\,[\eta_o(f_m) - \eta_o(f_e)]$$

$$- F \int_{\underline{\tau}} \int_{\underline{x}} E(f_m, \underline{x})\, E(f_m, \underline{x} + \underline{\tau}) \left\{P\left(\frac{f_e}{f_m}\right)^2 R[T_m]\right\} d\underline{x}\, d\underline{\tau}$$

$$+ F \int_{\underline{\tau}} \int_{\underline{x}} E(f_e, \underline{x})\, E(f_e, \underline{x} + \underline{\tau}) \left\{(P - 1)\, T_e^2/2! + R[T_e]\right\} d\underline{x}\, d\underline{\tau}.$$

Once again making use of the fractional change in illumination and eliminating fourth and higher terms, one has

$$\eta(f_e) = \eta_o(f_e) - P\left(\frac{f_e}{f_m}\right)^2 [\eta_o(f_m) - \eta(f_m)]$$

$$+ \sigma^2(f_e)\,[\eta_o(f_m) - \eta_o(f_e)]$$

$$+ F \int_{\underline{\tau}} \int_{\underline{x}} E(f_m, \underline{x})\, E(f_m, \underline{x} + \underline{\tau}) \left\{(P - 1)\, T_e^2/2! + R[T_e] - P\left(\frac{f_e}{f_m}\right)^2 R[T_m]\right\}$$

$$d\underline{x}\, d\underline{\tau}.$$

The bounds given in the text now follow from the mean value theorem:

$$\eta(f_e) \leq \eta_o(f_e) - P\left(\frac{f_e}{f_m}\right)^2 [\eta_o(f_m) - \eta'(f_m)] + P\left(\frac{f_e}{f_m}\right)^2 B$$

$$+ \sigma^2 (f_e) [\eta_o(f_m) - \eta_o(f_e)] + \eta_o(f_m) \sup S, \text{ for all } P$$

and

$$\eta(f_e) \geq \eta_o(f_e) - P\left(\frac{f_e}{f_m}\right)^2 [\eta_o(f_m) - \eta'(f_m)] - P\left(\frac{f_e}{f_m}\right)^2 B$$

$$+ \sigma^2(f_e) [\eta_o(f_m) - \eta_o(f_e)] + \eta_o(f_m) \inf S, \text{ for all } P.$$

The set S is given by

$$S = \left\{z : z = (P - 1)\, u^2/2! + R[u] - P\left(\frac{f_e}{f_m}\right)^2 R[u];\ 0 \leq u \leq K(f_m)\right\}.$$

This definition for S is equivalent to the one given in the text.

References

[1] Born, M. and E. Wolf, Principles of Optics, Pergamon Press, Inc., London, 1965, p. 468.

[2] Ruze, J., "The Physical Limitations on Antennas," Sc. D. Thesis, Massachusetts Institute of Technology, Cambridge, Massachusetts, 1952.

[3] Tolbert, C., A. Straiton, and L. Krause, "A 16-foot Diameter Millimeter Wavelength Antenna System, Its Characteristics and Applications," T-AP, Vol. AP-13, No. 2, March 1965, pp. 225-9.

[4] Silver, S., Microwave Antenna Theory and Design, Rad. Lab. Series, Vol. 12, McGraw-Hill Book Co., New York (1949), p. 174.

[5] Spencer, R. and G. Hyde, "Studies of the Focal Region of a Spherical Reflector: Geometric Optics," T-AP, May 1968, p. 317.

[6] Herbison-Evans, D., "Optimum Paraboloid Aerial and Feed Design," Proc. IEE, Vol. 115, No. 1, January 1968, p. 87.

[7] Shimizu. J., "Octave Bandwidth Feed Horn for Paraboloid," T-AP, March 1961, p. 223.

[8] Silver, S., op. cit., ref. 4, p. 169.

[9] Silver, S., op. cit., ref. 4, p. 158.

[10] Cogdell, J., unpublished class notes.

[11] Silver, S., op. cit., ref. 4, p. 158.

[12] Ibid, p. 160.

[13] Sancer, M., "An Analysis of the Vector Kirchoff Equations and the Associated Boundary-line Charge," Radio Science, Vol. 3, (New Series), No. 2, Feb. 1968, p. 141-4.

[14] Cogdell, J., unpublished class notes.

[15] Bracewell, R., "Tolerance Theory of Large Antennas," IRE Trans. on Antennas and Propagation, Vol. AP-9, January 1961, p. 49-48.

[16] Ludwig, A., "Antenna Feed Efficiency," Supporting Research and Advanced Development, Space Programs Summary 37-26, Vol. IV, JPL, Pasadena, Calif., April 30, 1964, p. 200-8.

[17] Herbison-Evans, D., op. cit, ref. 6, p. 88.

[18] Dragone, C. and D. Hogg, "Wide-Angle Radiation Due to Rough Phase Fronts," Bell Systems Technical Journal, September 1963, p. 2285-96.

[19] Silver, S., op. cit., Ref. 4, p. 186.

[20] Spencer, R., "Fourier Integral Methods of Pattern Analysis," Radiation Lab. Report No. 761-1. M.I.T., January 21, 1946.

[21] Fagot, W., "Antenna Pattern Perturbations for a Quadratic Phase Error," T-AP, July 1964, p. 506.

[22] Ruze, J., op. cit, Ref. 2.

[23] Bao, V., "Influence of Correlation Interval and Illumination Taper in Antenna Tolerance Theory," Proc. IEE, Vol. 116, No. 2, February 1969, p. 195.

[24] Shifrin, Y., "The Statistics of the Field of a Linear Antenna," Radio Engrg. Electronic Phys., Vol. 8, March 1963, p. 351-358.

[25] Davenport, W. and W. Root, An Introduction to the Theory of Random Signals and Noise, McGraw-Hill, New York, 1958, p. 153.

[26] Ruze, J., "Antenna Tolerance Theory-A Review," Proc. IEEE, Vol. 54, No. 4, April 1966, p. 633-40.

[27] Zarghamee, M., "A Note on the Prediction of Antenna Tolerance from Efficiency Measurements," T-AP, May 1969, p. 354.

[28] Mezger, P., "An Experimental Check of Antenna Tolerance Theory Using the NRAO 85-Foot and 300-Foot Telescopes," 1964 International Symp. on Antennas and Propagation, p. 181-5.

[29] Zarghamee, M., op. cit., ref. 27.

[30] Ruze, J., op. cit., ref. 26, p. 637.

[31] Bao, V., "Nonconstant Correlation Interval in Antenna Tolerance Theory," T-AP, January 1970, p. 118.

[32] Zucker, H., "Gain of Antennas with Random Surface Deviations," Bell System Tech. Journal, October 1968, p. 1637-51.

[33] Bao, V., op. cit., ref. 23, p. 195-200.

[34] Scheffler, H., "Uber die Genauigkeitsforderungen bei der kerstelung optischer flachen fur astronomische teleskope," Z. Astrophys. (Germany), Vol. 55, 1962, p. 1-20.

[35] Zucker, H., op. cit., ref. 32, p. 1644.

[36] Ruze, J., "The Effects of Aperture Errors on Antenna Radiation Patterns," Supplemento al Nuovo Cimento, Vol. 9, N. 3, 1952, p. 365.

[37] Zucker, H., op. cit., ref. 32, p. 1644.

[38] Schraml, J., "Pointing and Focus Calibration of the 36-Foot Telescope," NRAO Internal Report, Sept. 1969, p. A1.

[39] Cogdell, J., "Calibration Program for the 16-Foot Antenna," Technical Report No. NGL-006-69-1, Electrical Engineering Research Laboratory, The University of Texas at Austin, January 1969, p. 23.

[40] Bathker, D., "Radio Frequency Performance of an 85-Foot Ground Antenna X-Band," JPL, Technical Report 32-1300, July 1968, p. 32.

[41] Bathker, D., "Radio Frequency Performance of a 85-ft. Ground Antenna; X-Band," JPL, Technical Report 32-1300, July 1968, p. 32.

[42] Bathker, D., "Radio Frequency Performance of a 210-ft. Ground Antenna; X-Band," JPL, Technical Report 32-1417, Dec. 1969, p. 9.

[43] Cogdell, J, "The Use of Gaussian Functions in Radio Astronomy Source Measurements," Electrical Engineering Research Laboratory, The University of Texas at Austin, Technical Report No. NGL-006-69-2, May 1969, p. 9.

[44] Ruze, J., op. cit., ref. 26, p. 635.

[45] Bathker, D., op. cit., ref. 40, p. 32.

[46] Stuart, D., "Haystack Antenna Reflector Surface Improvement Program," TN1968-7, Lincoln Laboratory, M.I.T., Jan. 1968, p. 12.

[47] Cogdell, J., op. cit., ref. 39, p. 21

[48] Jacobs, E., and H. King, "2.8-minute Beamwidths, Millimeter-wave Antenna-measurement and Evaluation," IEEE Intern. Conv. Record, Pt. 5, p. 92.

[49] Bathker, D., op. cit., ref. 40, p. 25.

[50] Bathker, D., op. cit., ref. 42, p. 15.

[51] Dion, A., Investigation of Effects of Surface Deviations on Haystack Antenna Radiation Pattern," Technical Report No. 324, Lincoln Laboratory, M.I.T., July 1963, p. 9.

[52] Bracewell, R., op. cit., ref. 15, p. 58.

[53] Silver, S., op. cit., ref. 4, p. 186.

[54] Cogdell, J., op. cit., ref. 39, p. 22.

[55] Bathker, D., op. cit., ref. 40, p. 32.

[56] Jacobs, E., H. King, op. cit., ref. 48, p. 98.

[57] Ibid, p. 99.

[58] Bracewell, R., "Aerial Smoothing in Radio Astronomy," Australian J. Phys., Vol. 7, Dec. 1954, p. 615-640.

[59] Silver, S., op. cit., ref. 4, p. 193.

[60] Bracewell, R., op. cit., ref. 15, p. 49-58.

[61] Ruze, J., op. cit., ref. 26, p. 633-40.

[62] Levy, G., D. Bathker, A. Ludwig, "Efficient Antenna Systems: Gain Measurements of the Advanced Antenna System Using Surveyor I Signals," J.P.L. Space Programs Summary, 37-44, Vol. III, March 1967, p. 100.

[63] Mezger, P., op. cit., ref. 28, p. 184

[64] Ruze, J., op. cit., ref. 2, p. 81.

[65] Stuart, D., op. cit., ref. 46.

[66] Katow, G., "85-Foot Az-el Antenna Structure Deformation from Gravity Loads," JPL-Space Programs Summary, 33-44, Vol. III, May 1968, p. 106-111.

[67] Spencer, R., "A Least-Square Analysis of the Effect of Phase Errors on Antenna Gain," Air Force Cambridge Research Center, Bedford, Massachusetts, AFCRC Report E5025, January 1949.

[68] Ruze, J., "The Effect of Aperture Errors on the Antenna Radiation Pattern," Supplemento al Nuovo Cemento, Vol. 9, No. 3, pp. 364-380, 1952.

[69] Bathker, D., op. cit., ref. 40, p. 22-29.

[70] Cogdell, J., op. cit., ref. 39, p. 29.

[71] Mezger, P., op. cit., ref. 28, p. 181-4.

[72] Cogdell, J., unpublished data.

[73] Bathker, D., op. cit., ref. 40, p. 1-4.

[74] Bathker, D., op. cit., ref. 40, p. 30.

[75] Katow, op. cit., ref. 66, p. 106-111.

[76] Bathker, D., Private Communication.

[77] Bathker, D., op. cit., ref. 40, p. 8.

[78] Bathker, D., op. cit., ref. 40, p. 29.

[79] "S-Band Antenna Gain and Pattern Calibration," JPL Space Programs Summary, No. 37-22, Vol. III, July 1963, p. 11-15.

[80] Cogdell, J., op. cit., ref. 39, p. 29.

[81] Jelks, E., "A Measurement of the Blackbody Disc Temperature of Jupiter at 8.6 mm Wavelength," M.S. Thesis, The University of Texas at Austin, 1968.

[82] Ibid.

[83] Bathker, D., op. cit., ref. 40, p. 29.

[84] Cogdell, J., op. cit., ref. 39, p. 29.

[85] Ludwig, A., "Antenna Feed Efficiency," JPL Space Programs Summary, No. 37-42, Vol. IV., 1964, p. 200-7.

[86] Ibid.

[87] Ludwig, A., "Efficient Antenna Systems: Calculated Gain of the Advanced Antenna System", JPL Space Programs Summary, No. 37-32, Vol. III, 1966, p. 37-40.

[88] Cogdell, J., op. cit., ref. 39.

[89] Cogdell, J., op. cit., ref. 39, p. 25-28.

[90] Cogdell, J., op. cit., ref. 39, p. 16-21.

[91] Cogdell, J., op. cit., ref. 39, p. 28-30.

[92] King, A., "The Radiation Characteristics of Conical Horn Antennas", Proc. IRE, Vol. 38, March, 1950, p. 249-251.

[93] Cogdell, J., op. cit., ref. 39, p. 45-51.

[94] Ludwig, A., op. cit., ref. 85.

[95] Ibid.

[96] Katow, G., op. cit., ref. 66.

[97] Silver, S., op. cit., ref. 4, p. 194.

[98] Silver, S., op. cit., ref. 4, p. 195.

[99] Spencer, R., op. cit., ref. 20.

[100] Fagot, W., op. cit., ref. 21.

[101] Ludwig, A., "Calculation of Scattered Patterns from Asymmetric Reflectors", JPL, Technical Report 32-1430, Feb. 1970.

[102] Dion. A., op. cit., ref. 51.

[103] Bao, V., op. cit., ref. 23.

[104] Dion, A., op. cit., ref. 51.

[105] Bao, V., op. cit., ref. 23.

[106] Brigham, E., and Morrow, R., "The Fast Fourier Transform", IEEE Spectrum, Dec. 1967, p. 63-70.

[107] Ibid.

[108] Pratt, W., and Andrews, H., "Computer Calculated Diffraction Patterns", Applied Optics, Vol. 7, No. 2, Feb. 1968, p. 378-389.